Empirical Analysis of Molecular Modeling and Evolution of Respiratory Syncytial Virus Fusion Glycoprotein Antibody Escape Variants

A Dissertation

Presented in Partial Fulfillment of the Requirements for the

Degree of Doctor of Philosophy

with a

Major in Microbiology, Molecular Biology and Biochemistry

in the

College of Graduate Studies

University of Idaho

by

Sierra S. Beach

Approved by:

Major Professor: Tanya A. Miura, Ph.D.

Committee Members: Paul Rowley, Ph.D., Craig Miller, Ph.D., Santanu Bose, Ph.D.

Department Administrator: Tanya A. Miura, Ph.D.

August 2022

Abstract

Respiratory syncytial virus (RSV) is an important pathogen that causes severe lower respiratory infections in young infants, the immunocompromised, and the elderly. There are no vaccines or targeted anti-viral drugs for active RSV infection and only supportive care for hospitalized patients. The only approved treatment by the FDA is the prophylactic monoclonal antibody, palivizumab, given exclusively to high-risk infants during cold and flu season. The consequence of using monoclonal antibodies to prevent or treat viral infection is that it puts selective pressure on a specific epitope, which can result in a phenomenon called antibody escape. Current identification of antibody escape variants relies on patient samples or passage experiments. In this project, we aimed to use molecular modeling to identify antibody escape variants. We used molecular modeling to predict single mutations in RSV fusion glycoprotein (F protein) that would disrupt the binding of the palivizumab derivative, motavizumab, but not disrupt the folding of the F protein monomer. We accurately predicted eight F protein variants that propagated new virus. Six of our eight mutations were identified as monoclonal antibody resistant mutants (MARMs) that had reduced neutralization and binding by motavizumab. Surface plasmon resonance revealed a reduced on-rate for motavizumab for K272E, L258K, and S275H. We then examined the evolutionary pathway of RSV F protein using passage and fitness experiments to understand the likelihood and relevance of our predicted MARMs. We directed the evolution of RSV and derived a novel escape variant from passage experiments. This study empirically tested and validated the accuracy of our molecular modeling approach. We accurately predicted viral resistance to a monoclonal antibody and established a methodology that can be used to monitor the emergence of resistant viruses.

Acknowledgements

I would like to give my greatest appreciation to my major professor, Dr. Tanya Miura. Thank you for taking a chance on a liberal arts student and giving me the opportunity to grow and develop as a scientist. It has been an honor and privilege to learn from you. I am grateful for the time I have spent in your lab and for all the skills I have moving forward in my career.

I would like to thank the entire EPSCoR Geno2Pheno team (National Science Foundation EPSCoR Research Infrastructure Improvement Program: Track-2, award number OIA-1736253) for the funding and collaborations it has supported. Thank you to Dr. Jagdish Patel for the molecular modeling work, my research would not exist without it. I would like to thank Dr. Paul Rowley for his excellent guidance and enthusiasm during MoVIES meetings. Also, thank you to the Rowley Lab for allowing me to continually invade their space to set up PCRs. I would also like to thank Dr. F. Marty Ytreberg as the PI of the entire EPSCoR Geno2Pheno grant and for never turning down a request for funding to go to a conference for my professional development. Thank you to Dr. Mandar Naik for his guidance on biochemistry.

Thank you to Dr. Craig Miller for all his contributions on anything evolution related to my project. Your insight has been paramount in a field that I am still getting comfortable in. I would also like to thank Dr. Santanu Bose for his expansive knowledge of respiratory syncytial virus and excellent feedback on my research. The responses I have received from the both of you has given me ideas and helped guide my research.

I would like to thank the Optical Imaging Core and Dr. Onesmo Balemba. Thank you for allowing me to add to my professional development by creating a position for me to maintain and train users on the flow cytometer.

Dedication

First and foremost, I would like to thank Herb and Carol Fuller for their love, support, and mentorship over the years. Thank you for bringing me into your family. I would not be here today without you and I am devastated that you will not see it all come to fruition.

Thank you to my best friends: Jennifer and Matthew. My trips home to Olympia were always a welcomed break from the nonstop work life of a graduate student.

Thank you to my family for their support. Thank you to my mom and grandma for their continued support and for the rest and relaxation at home in Maui.

Thank you to all the women scientists and mentors that I have had over the years:
Dr. Carolyn Prouty, Dr. Paula Schofield, Dr. Lydia McKinstry, Dr. Clarissa Dirks,
Dr. Jennifer Kyle, and Dr. Brenda Rubenstein. Representation matters and I have been fortunate in my career path to have had your guidance and mentorship.

I would like to thank all the former Miura Lab members for their support and laughter over the years. McKenna, thank you for being equally sarcastic. Frankie, thank you for being the eternal optimist with the sunniest of dispositions. Kevin and Laura, thank you for all the trivia nights. Andy, thank you for all the insights on life and science.

Finally, thank you to my partner, Tomislav. Your insight as a scientist and support as a partner have been immeasurable.

Table of Contents

List of Tables

List of Figures

CHAPTER 1
Introduction

1.1 Respiratory Syncytial Virus

Human respiratory syncytial virus (RSV) is an enveloped single-stranded negative sense RNA virus of the *Pneumoviridae* family and consists of two subtypes, A and B. Both subtypes are present during RSV season, although RSV A is more prevalent and causes more severe symptoms (1–6). RSV was first discovered in chimpanzees in 1956 and later isolated from infants in 1957 (7, 8). The dominant circulating strain of RSV A is ON1, identified in Ontario, Canada, in 2006 (9). However, the predominant strain used in laboratory settings and for drug and vaccine development is RSV A2, first described in 1961(10). RSV particles have been observed in three morphologies: spherical, asymmetric, and filamentous, but a study has demonstrated that the filamentous morphology is the most infectious (11) (Figure 1A). The genome contains ten genes that encode eleven proteins, including surface proteins (fusion glycoprotein (F protein), small hydrophobic (SH) protein, and attachment (G) protein), structural proteins (matrix (M) protein and nucleoprotein (N)), proteins for genome replication (polymerase (L), phosphoprotein (P), M2 proteins 1 and 2 (M2-1 and M2-2)), and immune evasion proteins (nonstructural proteins 1 and 2 (NS1 and NS2)) (12) (Figure 1B).

RSV infects at the apical cell surface of the airway epithelium (13). The G and F proteins are involved in the attachment and entry of the virion into the host cell. The attachment receptor for G protein has been identified as CX3CR1 in primary airway human epithelium cells and heparan sulfate in immortalized cell lines (14–17). After the G protein attaches to its cell receptor, the F protein mediates fusion of the viral membrane with the host cell membrane. The F protein receptor *in vivo* is thought to be nucleolin (18–20) with multiple co-receptor candidates, including TLR-4 (21, 22), EGRF (23), ICAM-1 (24), IGRF-1 (25), and collectins (26). In cell culture, F protein has been associated with heparan sulfate (27). G and SH proteins are not required for cell entry *in vitro* (28, 29). However, virus produced in primary bronchial epithelial cultures has a larger G protein and demonstrated reduced infection in immortalized cell lines (30). It could be that the findings of the *in vitro* studies were just artifacts of cell culture, given that the cell receptors are not the same and that the virus produced from primary cells was less infectious in cell culture. After the viral and host membrane fuse, the helical
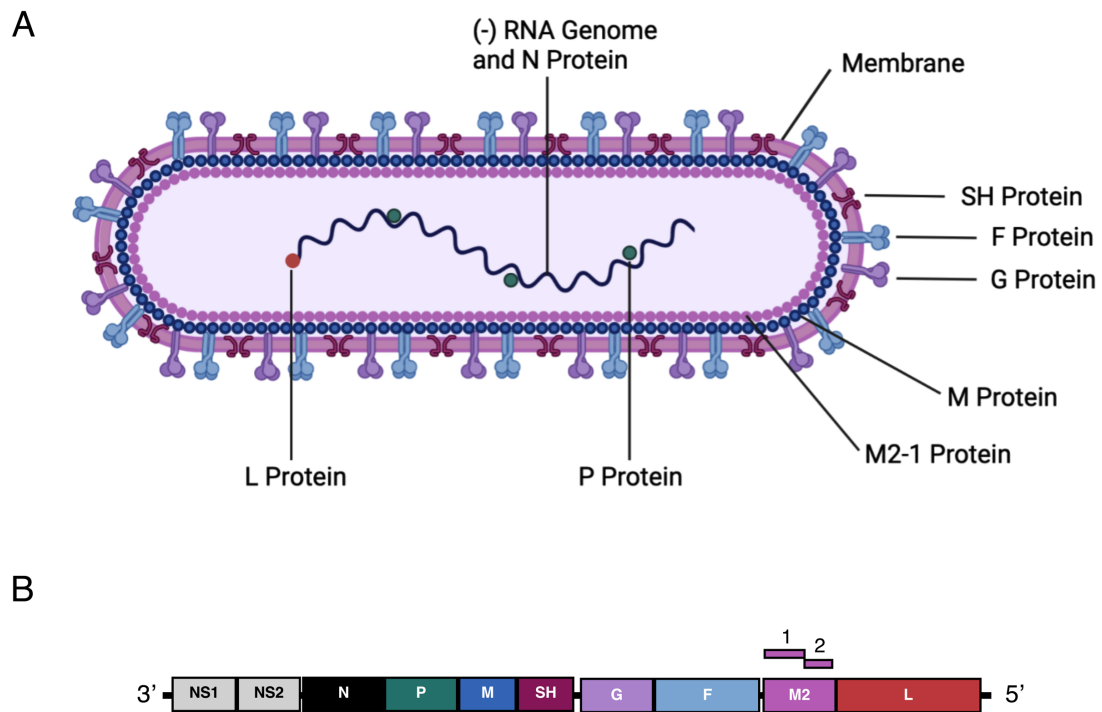
Figure 1. Filamentous morphology of respiratory syncytial virus and diagram of the genome.
(A) The fusion glycoprotein (F protein), attachment (G), and small hydrophobic (SH) proteins are located on the surface of the virus. RSV is an enveloped virus with a membrane that has a layer of matrix (M) protein and interacts with M2-1 protein. The negative sense RNA genome is encased in nucleoprotein (N protein). The large polymerase (L protein) and phosphoprotein (P protein) are associated with the N protein. (B) The RSV genome contains 10 genes coding for 11 proteins. The M2 gene encodes for two proteins, M2-1 and M2-2. The genes are ordered from most transcribed to least transcribed. Cartoon image generated in Biorender.

ribonucleoprotein complex enters the cell cytoplasm. Transcription and replication occur in viral inclusion bodies in the cell cytoplasm (31–33)

RSV has an RNA-dependent RNA polymerase, L protein, with no proofreading capabilities that allow for replication errors and generation of single nucleotide polymorphisms (SNP) with an estimated substitution rate between 5.27×10^{-3} and 3.382×10^{-3} (34, 35). L protein transcribes viral mRNA, intermediate positive sense RNA for genome replication, and negative genome copies (31). Genes closer to the 3' end—essential for viral assembly and host immune regulation—are transcribed at a higher rate than the genes at the 5' end. M2-1 is an essential elongation factor needed to produce complete viral genomes (36, 37), and M2-2 induces the change from transcription to replication of the genome (38). Viral assembly occurs
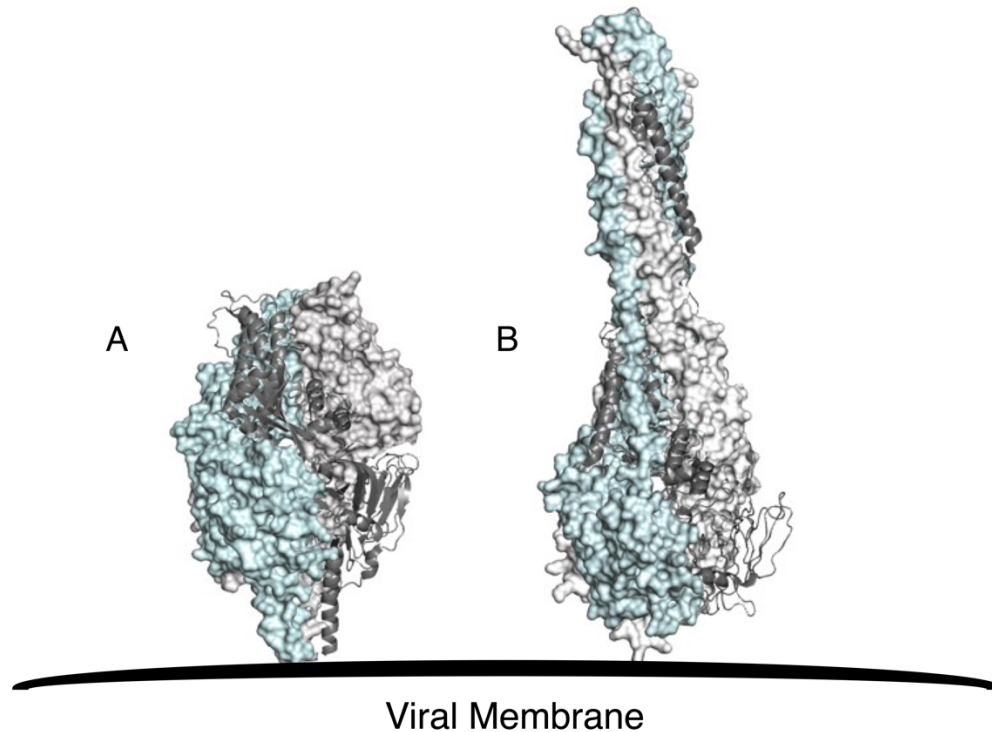
Figure 2. RSV F protein in pre-fusion and post-fusion conformation.
The F protein consists of three monomers shown in molecular surfaces (blue and white) and ribbon structure (grey). The protein mediates fusion between the virus and host cell membranes. (A) Pre-fusion F protein (PDB ID: 4ZYP). (B) Post-fusion F protein (PDB ID:3RRT).

at or near the plasma membrane (11, 39). F protein associates with cholesterol-rich lipid rafts in the cell membrane and starts recruiting M protein that then starts filament formation by actin-dependent outward membrane deformation (40–43). The viruses bud and detach from the cell membrane.

1.2 Viral Fusion Proteins and RSV Fusion Glycoprotein

Class I fusion proteins are non-covalently linked homotrimer proteins made up primarily of α-helices with the fusion peptide held within the interface of the homotrimers and can be triggered by low pH or interaction with host cell receptors (44, 45). In contrast, class II fusion proteins are composed mainly of β-sheets and rearrange from an inactive homodimer to a fusion-active homotrimer in low pH conditions (45, 46). The fusion peptide in class II fusion proteins is masked in the trimer interface after reassembly from the dimer. In class I fusion proteins, the fusion peptide is located near the N-terminus in the primary sequence, and in class
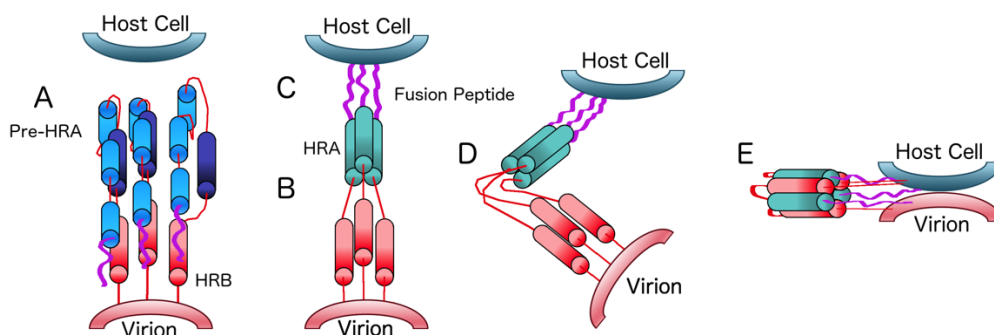
Figure 3. RSV F protein mediates the fusion between viral and host membrane.
F protein exists in a metastable state and is triggered by an unknown mechanism. The fusion peptide is inserted into the host membrane by the assembly of pre-heptad A (pre-HRA) into heptad repeat A (HRA). The protein jackknifes and heptad repeat B (HRB) and HRA are brought together to form a six-helix bundle that brings the host and viral membranes in contact with each other. Diagram based on McLellan et al. (2013) (47).

II, the fusion peptide is located internally within the protein sequence rather than near the N- or C-terminus (45). Class I and II fusion proteins are found on the surface of the virus, but class I are perpendicular to the virus surface and class II are parallel (45). After fusion, both class I and II form a trimer of hairpins, except that class I forms a six-helix bundle and class II forms stacks of β-sheets(45). The F protein is a class I fusion glycoprotein synthesized as a 574 amino acid precursor, F_0 (Figure 2) (48, 49). The trimeric F protein is assembled as three F_0 monomers and trafficked through the Golgi, where the monomers are activated by a furin-like host protease (50, 51). The F_0 monomer is cleaved twice, resulting in F_1, F_2, and pep27, and F_1 and F_2 are covalently linked by two disulfide bonds (52, 53). Pep27 disassociates from F_1 and F_2 after cleavage (54). The F_1 subunit contains one glycosylation site essential for membrane fusion (55).

F protein exists in a metastable state, and the trigger from pre- to post-fusion for F protein remains unknown. However, it is known to be pH independent and insensitive to lysosome acidification (56, 57). One proposed mechanism is that the basal conversion rate between pre and post-fusion F is sufficient for infection once the virus is brought close to the cell surface by attachment of G or F protein (40, 57). The provocateur model has also been proposed where the binding of G protein causes a conformational change that allows for association with F protein and subsequent triggering from prefusion to post-fusion (58). RSV may fuse directly at the plasma membrane or through micropinocytosis, followed by fusion in

endosomes (59, 60). Each F monomer consists of a fusion peptide, pre-heptad repeat A (pre-HRA), heptad repeat B (HRB), and transmembrane domain from C-terminus to N-terminus (Figure 3) (47, 48). Once F protein is triggered, PHRA refolds into a single long heptad repeat A (HRA) and inserts the fusion peptide into the host membrane (Figure 3)(47). The HRA from each monomer trimerize with each other, and the protein folds in half where the HRA and HRB interlock to form a 6-helix bundle (Figure 3)(47, 61). The folding of the protein brings the host cell and viral membranes together to allow for fusion (Figure 3).

The RSV F gene is conserved across A and B subtypes with 90% amino acid sequence identities, including the conservation of some antigenic sites (47, 62). The high conservation of the F gene, the role of F protein in cell entry, and the response of the host immune system to F protein make it an ideal candidate for anti-viral treatments (3, 47, 62–65).

1.3 RSV Demographics and Immunity

Nearly every child is infected with RSV by age 2 (66), and it is a leading cause of infant death in developing nations (67). RSV is also an important pathogen in the elderly and adults with comorbidities such as chronic obstructive pulmonary disease and is estimated to cause 11,000-17,000 deaths annually in the USA (68–70). Historically the RSV peak season was from mid-October through April (66, 71, 72). However, the coronavirus disease 2019 (COVID-19) pandemic restrictions may have shifted the seasonality of the infection, with some studies reporting peak infection during the summer months of 2021 (73, 74). RSV causes acute lower respiratory infections in infants, and infants who develop severe RSV infections are more likely to develop asthma later in life (75, 76). The risk factors for severe RSV infection include age (0-5 months), low birth weight, premature birth, underlying cardiovascular and respiratory disorders specific to the perinatal period, congenital malformation of the heart or the great vessels, congenital defect originating in the perinatal period, neurological disorders, blood disease, and liver disease (77). Another risk factor for infants is the high surface area-to-volume ratio of the lungs. Human babies are born with nearly all their airways and alveoli (78), meaning the bronchiole lumen is narrower than in adults and more prone to airway obstruction (79).

RSV infection does not imbue long-term immunity, and reinfection throughout life is common (80, 81). RSV infection results in an innate and adaptive immune response that can be highly inflammatory but does not lead to long-term immunity. Innate immune cells such as

neutrophils, basophils, eosinophils, and mast cells have all been found to respond to initial infection with RSV, but the cell population primarily consists of neutrophils (82, 83). F protein has been found to bind TLR4 and induce NETosis, a phenomenon where neutrophils expel chromatin and granular contents into the extracellular space to trap pathogens, which has downstream proinflammatory effects (84). The binding of TLR4 also creates a feedback loop because it induces IL-8 upregulation, which recruits more neutrophils and may contribute to cell pathology (85). The adaptive immune response to RSV is often described as type 1 helper (Th1) cell or type 2 helper (Th2) cell responses. Th1 cells defend against intracellular pathogens, and Th2 cells defend against extracellular parasites. A Th1 response would be the ideal response by the immune system as RSV is an intracellular pathogen, but the response to natural infection is often the Th2 cell response. G protein has been shown to induce a Th2 immune cell response rather than a Th1 immune cell response (86, 87). The bias towards a Th2 response from RSV is also enhanced in the elderly population due to immunosenescence (88). Neutralizing IgG antibodies for F and G proteins have been documented in infants and increase between the acute and convalescent phases after initial infection with RSV (89). IgA antibodies have been associated with patients who developed bronchiolitis and later development of allergic sensitization (90). The immune responses to RSV create a challenge for generating effective treatments and vaccines for at-risk populations that vary by age and immune responses.

1.4 RSV Vaccines and Treatments

There are currently no vaccines for RSV or targeted treatments for active RSV infections. The first vaccine for RSV was attempted in the 1960s using formalin-inactivated RSV paired with an alum adjuvant and resulted in enhanced disease and two infant deaths upon natural infection by the virus (91–93). Severe eosinophilia was found in the lungs of the infants who died and eosinophils were found in the blood of the hospitalized vaccine recipients (92–94). Mouse studies found that the formalin-inactivated vaccine caused an inflammatory Th-2 immune response and eosinophilia (95, 96). Later studies found that the antibodies produced by the vaccine were non-neutralizing for the F protein and that it is most likely because formalin converts pre-fusion F protein to the post-fusion conformation (97, 98). Many vaccine strategies have been attempted in the following years targeting different populations. Currently, there are clinical trials for vaccines using F protein subunit, live attenuated virus,

RSV F nanoparticles, and vector-based approaches (99, 100). The target population for these vaccines are infants >6 months old and adults >60 years old, but a vaccine for herd immunity would also be beneficial. One approach to protect infants who cannot be vaccinated due to age is maternal vaccination because it takes advantage of transplacental antibody transfer and antibody transfer during breastfeeding (100). There are many promising vaccine candidates on the horizon, and the development of a vaccine for RSV would help mitigate a world health problem.

Children hospitalized with RSV infection are treated with supportive care such as high flow nasal cannula (HFNC) therapy with oxygen or Heliox (101–108). HFNC therapy is non-invasive, easy to administer, and well tolerated by infants. Heliox is a mixture of helium and oxygen that has been shown to facilitate gas flow in high-resistance airways (108). While mortality from RSV is relatively low in developed nations, it remains high in developing nations where access to health care may be limited (109, 110).

Small molecule drugs have been important in fighting other respiratory viruses such as influenza virus (111) and can potentially become a vital tool for the medical community to combat RSV infection. One small molecule drug used to treat RSV infection is ribavirin, a ribonucleic analog of guanosine that causes chain termination in RNA synthesis (112–116). However, ribavirin has been used with limited success since the 1980s and has mainly been discontinued for treatment except in specific critical patient populations (117). A new small molecule drug, rilematovir (JNJ-53718678), binds F protein and is currently in phase 2 clinical trials (118, 119). Other small molecule drugs are in development and clinical testing that target nucleoprotein (120, 121) and the viral RNA polymerase (122). The development of drugs specific for RSV infection is critical as there are currently no targeted treatments for active RSV infection.

Antibodies have been used to prevent RSV infection. The first antibody treatment for the prevention of RSV infection in premature infants and immunodeficient individuals was RespiGam (RSV-IVIG) (123, 124). RSV-IVIG was made by pooling the plasma of people with high circulating levels of neutralizing antibodies against RSV. RSV-IG was withdrawn from the market when the monoclonal antibody (mAb) palivizumab (MedImmune, USA) was approved (12). Palivizumab is given prophylactically to preterm and high-risk infants during RSV season. A new monoclonal antibody, MEDI8897 (nirsevimab), has been developed for

the prophylaxis of RSV and is currently in clinical trials (125, 126). Antibodies have been the best weapon in the fight against RSV since an effective vaccine has not been developed.

1.5 Monoclonal Antibodies

mAbs are a potent tool against viral pathogens because of the ability to target specific neutralizing epitopes. The use of mAbs for the prevention and treatment of viral infections has increased in the past few years. Palivizumab was the first mAb approved by the FDA to prevent a viral infection (127). Two additional mAb have received FDA approval since 2018, Trogarzo®, a mAb treatment for drug-resistant human immunodeficiency virus (HIV-1) infection (128), and Inmazeb™, a mAb treatment for Ebola virus (EBOV) infection (129). mAbs have also been critical in fighting severe acute respiratory syndrome coronavirus 2 (SARS-CoV-2) during the COVID-19 pandemic. The FDA has granted emergency use authorization for several mAb treatments for COVID-19 (130–132). The mAb, m102.4, previously used in compassionate cases for Hendra and Nipah virus infections, has completed phase 1 clinical trials in Australia (133). Additional mAbs are in development for other viral pathogens, including influenza and herpes simplex virus (134–136).

There are many ways to develop mAb that target proteins of interest. Rapid identification of neutralizing mAb has been critical in the COVID-19 pandemic, and one study used fluorescent activated cell sorting (FACS) to identify B cells from COVID-19 survivors that bound to a fluorescent spike protein, and the immunoglobulin G (IgG) gene was subcloned for expression of the mAbs of interest (137). FACS can also be used to find B cells of interest, and the B cells can be cloned or immortalized for mAb production (138). Another method for mAb identification is phage-displayed antibody libraries where mAb are isolated and cloned from immunized or infected animals or humans, displayed on filamentous phage, and the library is exposed to the antigen of interest (138). Phage that binds the antigen of interest are eluted and sequenced. mAbs have become an integral part of medicine to prevent and treat viral infections.

1.6 Palivizumab and Motavizumab

Palivizumab is a prophylactic mAb given to high-risk infants during peak cold and flu season to prevent RSV infection. As mentioned earlier, palivizumab is currently the only preventative treatment for RSV with FDA approval. Palivizumab targets the site II epitope of F protein (Figure 4) and prevents viral entry by inhibiting intermediary conformational changes

to the post-fusion conformation (139, 140). MEDI-493, which would become palivizumab, started as the murine mAb, MAb 1129. MAb 1129 was humanized by de novo assembly using polymerase chain reaction and mutagenesis of the variable light (VL) and variable heavy (VH) genes (63, 141). The VL and VH genes were subcloned into cDNA expressing human C-kappa and C-gamma-1 constant domains, respectively. Initial testing showed that the humanized mAb had similar neutralization capabilities as the murine mAb, had higher neutralization capabilities than RSV-IVIG, and prevented viral replication in cotton rats treated with the mAb (141). The guidance for palivizumab prophylaxis was last updated in 2014 by the American Academy of Pediatrics (AAP) and recommends administration in the first year of life to premature infants born at <29 weeks gestation, preterm infants with chronic lung disease, infants with hemodynamically significant heart disease, and in infants in the second
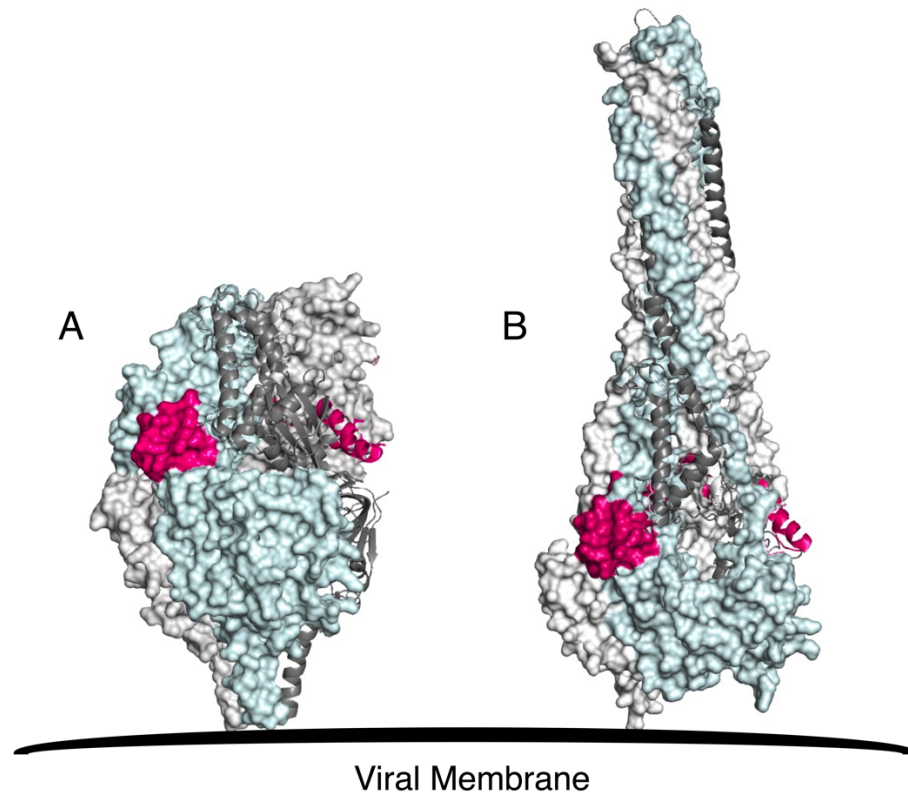
Figure 4. Site II epitope on F protein.
The site II epitope is highlighted in pink on (A) pre-fusion F protein (PDB ID: 4ZYP) and (B) post-fusion F protein (PDB ID:3RRT). The epitope is present in both conformations of the F protein and consists of residues 255-277.

year of life who required at least 28 days of supplemental oxygen and ongoing medical intervention (142). In addition, the AAP also recommended remaining on the administration schedule during cold and flu season despite the shift in seasonality of RSV cases in 2021 (143).

Attempts were made to improve palivizumab's affinity and neutralization. A correction to the light chain was the first alteration, reverting four amino acids to the murine MAb 1129 sequence because errors were introduced during the humanization process (144). Further humanization was attempted by amino acid substitutions in the light chain and heavy chain in the palivizumab derivative 493L1FR. These mutations were made to reduce the possibility of immunogenicity. Affinity maturation was performed using a library of every possible amino acid change at the six CDR regions, and 493L1FR Fab variants were screened by a filter-based capture lift method and semi-quantitative enzyme-linked immunosorbent assay (ELISA). A later study further developed 493L1FR into the mAb MEDI-524 (motavizumab) (145). In this study, the authors adapted 493L1FR with an S29R mutation, and it was found to be fourfold more potent than palivizumab. The resulting mAb, motavizumab, had thirteen mutations from palivizumab: six CDR changes and one framework change back to the murine CDR1 in the heavy chain, and the light chain contained five CDR changes and one framework change back to the murine CDR1. Motavizumab was found to have improved binding kinetics with a 70-fold greater binding avidity to RSV F protein, a six-fold faster on-rate, and an 11-fold slower off rate. It had a 20-fold more potent half-maximal inhibitory concentration (IC_{50}) and reduced viral lung titer in cotton rats compared to palivizumab. Motavizumab appeared to be a great candidate for the prophylaxis of RSV infection.

The structure of motavizumab and a peptide epitope was solved first and suggested that direct contact between hydrophobic residues of the F protein and motavizumab was responsible for the increased affinity (64). The next structure to be solved was the post-fusion conformation of F protein and motavizumab, which revealed that the binding epitope site II remained in the post-fusion F protein structure and that it was possible that motavizumab could neutralize late in the entry process (146). The structure of prefusion F protein and motavizumab and mAb AM14 was the next to be solved (Figure 5) (147). This study used a previously crystallized F protein, DS-Cav1, that was locked into prefusion conformation by a mutating S190F and V207L to fill a hydrophobic cavity and a disulfide bond introduced at residues S155C and S290C (148).
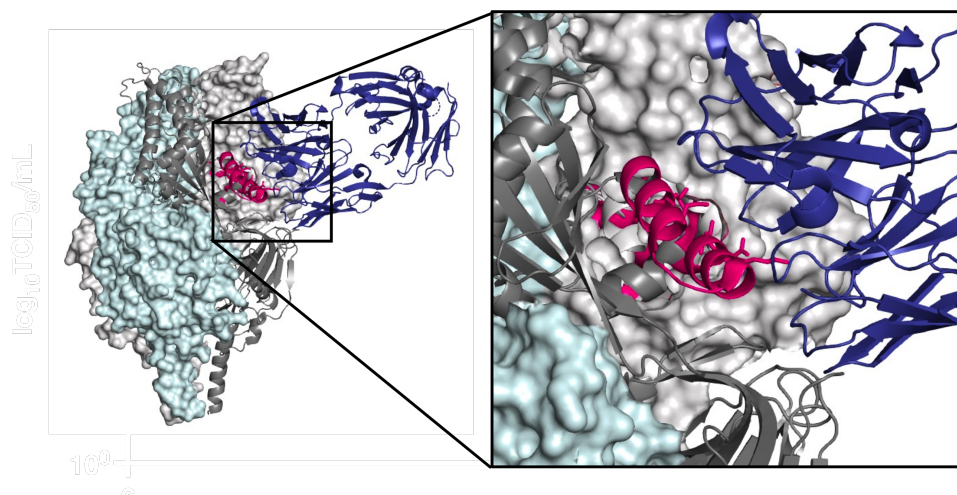
Figure 5. Interaction between F protein site II epitope (pink) and motavizumab (dark blue) (PDB ID: 4ZYP).

Motavizumab was subjected to clinical trials to test for safety and efficacy compared to palivizumab. In a randomized, double-blind, multinational, phase 3 trial, 6635 preterm infants that were less than six months or were less than 24 months with chronic lung disease of prematurity received either palivizumab or motavizumab once a month for five months (149). The motavizumab recipients had a 26% reduction in hospitalization compared to the palivizumab recipients. There was also a 50% reduction in medically attended respiratory tract infections in the infants who received motavizumab. Adverse events between motavizumab and palivizumab were not significant and mild. Another study was conducted in patients with congenital heart disease that were less than 24 months and received either motavizumab or palivizumab once a month for five months (150). Adverse events were reported in 93% of recipients, and 50% reported severe adverse events. Of the severe events reported, 19.3% of motavizumab and 16.2% of palivizumab recipients reported skin events. This study found that rates of hospitalization were similar between the two groups. A phase 3, randomized, double-blind placebo trial in healthy Native American infants demonstrated an 87% reduction in hospitalization for RSV infection in the group that received motavizumab compared to placebo. This study also found adverse reactions in the arm of the motavizumab recipients. The FDA ultimately rejected the license for motavizumab in August 2010, given concerns about the lack of greater efficacy of motavizumab in humans and increased adverse reactions in the above studies (142).

1.7 Antibody Escape

The caveat of using a mAb that targets a particular epitope is the tendency to select for antibody escape. Antibody escape is a phenomenon where viral proteins evolve to disrupt antibody binding. The COVID-19 pandemic has increased the concern over antibody escape given the loss of effectiveness of some of the mAb treatments with the emergence of the Delta and Omicron variants (151, 152). RNA viruses are prone to mutations with between 10^{-6} and 10^{-4} substitutions per nucleotide site per cell infection and a negative correlation between genome size and rates of mutations, where higher rates of mutations are observed in smaller genomes (153). Part of the high mutation rate among RNA viruses can be accounted for by the RNA-dependent RNA polymerase (RdRp) that lacks proofreading capability, except for viruses in the Nidovirales family that have larger genomes and require RdRp with proofreading capability (154). Antibody escape has been observed in several viruses, including EBOV, influenza virus, HIV-1, and measles virus (155–158).

Antibody escape has been studied extensively in RSV. The first study to look at monoclonal antibody resistant mutants (MARMs) used RSV A2 virus and mouse mAbs, including palivizumab precursor MAb 1129 (63). The study was conducted to map out and better understand the neutralizing epitopes of the F protein. Passage experiments with different mAbs were performed, and cross-neutralization studies were used to construct an operational map of the F protein epitopes. Subsequent studies used the same technique to identify additional antigenic sites and revealed a serine mutation at position 275 to phenylalanine (S275F)(Table 1)(159, 160). Additional studies have directly looked for palivizumab and motavizumab MARMs. One study used passage experiments where RSV A2 was propagated in HEp-2 cells in increasing concentrations of palivizumab (161). The MARM identified was a mutation from lysine to methionine at position 272 (K272M) (Table 1) and showed resistance to palivizumab prophylaxis in cotton rats. In follow-up studies by the same group, isolation of additional MARMs from passage experiments included lysine to glutamine at position 272 (K272Q) and asparagine to isoleucine at residue 268 (N268I)(Table 1)(162, 163). It was found that N268I was partially neutralized in microneutralization assays but was eliminated by palivizumab prophylaxis in cotton rats. It was also found that K272M had similar fitness to the wild type (WT) RSV A2 parent strain. Samples collected from an infant that received palivizumab prophylaxis and had breakthrough infection revealed a change from lysine to

glutamic acid at residue (K272E) and a different variant with a change from asparagine to tyrosine at residue 276 (N276Y)(Table 1)(164).

A 2011 study examined MARMs derived from passage experiments and patients receiving palivizumab or motavizumab (165). The passage studies confirmed K272M and K272Q as palivizumab MARM, and two new mutations were identified: lysine to threonine (K272T) and asparagine (K272N)(Table 1). The only escape variant identified in passage experiments for motavizumab was K272E. Analysis of patient samples found palivizumab MARMs including K272E, K272Q; MAb 1129 MARM S275F, and a novel palivizumab MARM at position 275 from serine to leucine (S275L)(Table 1). K272E and S275L were both found in the motavizumab-treated patients. However, S275L was found to be neutralized by motavizumab in neutralization assays. In another study examining patients that had breakthrough RSV infection after palivizumab prophylaxis found a MARM with a mutation from asparagine to aspartic acid (N262D)(Table 1)(166). A study examining the binding kinetics of MARM F proteins and palivizumab identified additional variants: asparagine to tyrosine at residue 262 (N262Y), asparagine to serine (N262S), and lysine to tyrosine at residue 272 (K272Y)(Table 1)(167). This study found that the binding on-rate was reduced for most mutants and appeared to be the escape mechanism. In surveys of infants hospitalized for RSV infection, N276S was the most common palivizumab MARM observed (Table 1)(168, 169). In addition, MARMs have been identified for nirsevimab through passage experiments, but none of the variants have been observed in circulating populations of RSV (170).

Multiple MARMs have been observed for palivizumab, while only one MARM has been observed for motavizumab. The current methodology for MARM discovery involves sequencing samples taken from patients or serially passaging virus with the antibody of interest to select for evolved mutations. One weakness of these methodologies is that it only identifies potential MARMs, and the variant would still require testing for neutralization *in vitro* and *in vivo*. This also presents a challenge because MARM discovery relies on detecting escape mutations already circulating in a population. Passage experiments are biased and can only detect mutations that can arise over a limited replication time in cell culture. The ability to predict escape variants and create a watch list of potential MARMs that could emerge would be a significant advancement.

Table 1. All MARMs identified for palivizumab and motavizumab.

MARM	Antibody	Source	Citation
S275F	MAb 1129, Palivizumab	Passage experiments, Patient samples	Beeler JA et al. 1989 López JA et al. 1998 Crowe JE et al. 1998 Zhu Q et al. 2011
K272M	Palivizumab	Passage experiments, Tested in rats	Zhao X et al. 2004 Zhao Q. et al. 2011
K272Q	Palivizumab	Passage experiments, Tested in rats	Zhao X et al. 2004 Zhao X et al. 2006 Zhao Q. et al. 2011
K272E	Palivizumab, Motavizumab	Patient samples, Passage experiments	Adams O et al. 2010 Zhu Q et al. 2011
N276Y	Palivizumab	Patient samples	Adams O et al. 2010
K272T	Palivizumab	Patient samples	Zhu Q et al. 2011
K272N	Palivizumab	Patient samples	Zhu Q et al. 2011
S275L*	Palivizumab	Patient samples	Zhu Q et al. 2011
N262D	Palivizumab	Patient samples	Zhu Q et al. 2012
N262Y	Palivizumab	Patient samples	Bates et al. 2014
N262S	Palivizumab	Patient samples	Bates et al. 2014
K272Y	Palivizumab	Patient samples	Bates et al. 2014
N276S	Palivizumab	Patient samples	Hashimoto et al. 2017 Chen et al. 2018

S275L was found in motavizumab treated patient samples but was neutralized by motavizumab in assays.

1.8 Molecular Modeling

Molecular modeling uses theoretical and computational methods to model the behavior of molecules. The advancement of computational methodologies and crystallography of 3D protein structures has allowed for the development of multiple molecular modeling methodologies. The RCSB Protein Data Bank (PDB) is a repository for 3D structures of macromolecules such as proteins and nucleic acids (171). The creation of this database has allowed for easy access to protein structures and is essential for modeling. Quantum mechanics (QM) methods study reactions in large molecular systems (172). QM is useful for modeling transition rates and reaction intermediates for systems like enzymes and substrates and comparing different spectroscopic data. Molecular docking is also a powerful tool in molecular modeling that is important in structure-based drug discovery. Multiple studies have used molecular docking to screen for compounds for SARS-CoV-2 and human targets to inhibit viral activity (173–175). Molecular dynamics (MD) is vital for understanding the structure and function of proteins and is used in molecular docking. One of the first studies to examine MD of a biological macromolecule explored bovine pancreatic trypsin inhibitor and solving the potential energy functions of the motion of atoms (176). This study helped elucidate the physiological function of the inhibitor.

Molecular modeling has been used to explain disruptions in antibody binding in influenza virus (177–179). Single-point amino acid changes were made using PyMol or Schrodinger and demonstrated the mAb and proteins clashing at the residues of interest. Several studies have used MD and molecular modeling to predict MARM for SARS-CoV-2 spike protein (180–182). These studies could predict mutations in the RBD that disrupted binding of neutralizing mAb, but empirical research was not performed to test the accuracy of the predictions. Previous studies have used MD and molecular modeling on four mAbs for the glycoprotein (G protein) of EBOV and created a watch list of potential MARMs (183, 184). Both studies performed MD on the EBOV G protein and mAbs and analyzed the simulations using FoldX software to calculate the change in free energy between the WT G protein and the potential mutants for the stability of folding and disruption of binding (185, 186). The group could accurately predict mutations previously seen in humans or were experimentally known to reduce mAb efficacy. The ability to predict antibody escape would expedite MARM

identification by eliminating the reliance on patient samples, surveillance studies, and passage experiments.

1.9 Reverse Genetics Infectious Clone System for RNA Viruses

Reverse genetics infectious clones are essential for studying RNA viruses in the laboratory setting. The system works by creating a virus (infectious clone) from a full-length viral genome from cDNA. A reverse genetics system allows for manipulation of the viral genome and has been used to study viral genes and attempt to attenuate viruses for vaccine use (187–190). The first reverse genetics system for a mammalian RNA virus was used to generate poliovirus from cDNA in 1981 (191). Positive-sense RNA viruses such as poliovirus were easier to generate since once the cDNA viral genome is transcribed to RNA, it is a messenger RNA that can immediately begin translation by host ribosomes. Negative sense RNA viruses, however, are not infectious as the negative-sense genome is complementary to messenger RNA (192). For a negative-sense RNA reverse genetics system to be infectious, it requires RdRp and the creation of ribonucleoprotein complexes to prevent host immune detection of double-stranded RNA (192). The first successful infectious negative-sense RNA virus cloned from cDNA was rabies virus in 1994 (193). This study utilized a plasmid containing the cDNA viral genome co-transfected with helper plasmids containing the viral genes necessary for creating the ribonucleoprotein complex (nucleoprotein and phosphoprotein) and RdRp polymerase. The plasmids were generated with a T7 RNA polymerase promoter, and the T7 polymerase was expressed by recombinant vaccinia virus. The T7 RNA polymerase was essential for generating RNA from the cDNA genome and helper plasmids. This study opened the gates for the generation of many reverse genetics systems for negative-sense RNA viruses, including RSV, Sendai virus, vesicular stomatitis virus, measles virus, human parainfluenza virus, bovine RSV, Newcastle disease virus, canine distemper virus, and EBOV (187, 194–201).

RSV reverse genetics systems require the proteins to create the ribonucleic protein complex, RdRp, and transcription elongation factor M2-1 protein for effective generation of the virus (187, 202). One of the first systems used also require coinfection with the recombinant vaccinia virus containing the T7 polymerase (187). A cell line containing a gentamicin-resistant plasmid with the T7 polymerase was later established and eliminated the need for the recombinant vaccinia virus (198). Hotard et al. established a stabilized RSV reverse genetics system that could be altered by recombination-mediated mutagenesis (203). The genome and

the helper plasmids were human codon-optimized which helped with the expression of the virus. This study used the A2 strain and F gene from line 19 for the viral genome, and it was cloned as three segments into the bacterial artificial chromosome (BAC) pKBS2 to generate the plasmid pSynkRSV-line19F. The low-copy BAC plasmid was used to help stabilize the cDNA genome. In addition, to create a reporter virus, the far-red fluorescent protein monomeric Katusha 2 (mKate2) was added in the first gene position of the genome (204). The authors also created a variant with a luciferase reporter gene. The mKate2 and luciferase reporter gene variants replicated without growth restriction *in vitro* and *in vivo.* In a follow-up paper from Meng et al., the authors created pSynk-A2 (205). pSynk-A2 was created by removing the line 19 F gene flanked by Sac-II and Sal-I restriction sites in the BAC and subcloning a synthetic F gene from the A2 strain. The A2 F gene was added because the authors were attenuating RSV for potential live vaccine use. The 19F gene had been associated with enhanced viral loads, mucus, and airway dysfunction in mice (206). The authors also created strains with codon deoptimized immune suppressive proteins, NS1 and NS2, to attenuate the virus (205).

Other reverse genetics systems exist for RSV, including a green fluorescent protein reporter virus based on a B strain of RSV isolated from a patient (207) and a strain based on the RSV Long strain (208). A study from 2021 created a reverse genetics system from contemporary isolates of RSV A and B strains (209). Their system also used the BAC backbone for genome stability, and they created reporter viruses with dTomato red fluorescent protein and green fluorescent protein. In our studies, we utilized pSynk-A2 as it was amenable to site-directed mutagenesis for the F gene, the A2 F gene was used to generate the crystal structure of motavizumab and F protein and contained the reporter gene for mKate2 to track infection and use in assays.

1.10 RNA Virus Evolution and Population Genetics

RNA viruses are inherently genetically diverse. Furthermore, many characteristics contribute to the high genetic variability: (a) Large population sizes. Populations can be as large as 10^{12} in an infected organism, and an infectious particle can generate 100,000 copies on average (210) (b) High replication rates. The average eclipse phase for RNA viruses is 2-5 hours (211) (c) Small genomes. The average genome size for RNA viruses is 3-20 kb (210) (d) High mutation rate. Most RNA viruses have a high mutation rate due to the RNA-dependent

RNA polymerase lacking proofreading capability (212). RNA viruses have the highest mutation rate among organisms, with approximately one mutation per genome per replication cycle (213, 214). Genome size and mutation are related because a high mutation rate is expected to limit genome size (215). A mutation rate that exceeds the maximum mutation rate tolerable for a given genome size, the error threshold, would lead to too many errors in the genome, and the virus would go extinct. RNA viruses with a high mutation rate close to the error threshold could also produce mutations that could benefit the viral population and its ability to adapt.

Quasispecies has been used to describe the distribution of mutants in the viral population. Eigen and Schuster initially coined the term to describe simple replicons at the population level (216). Quasispecies are a steady-state mutant distribution dominated by a master sequence with the highest replication rate among the variants of the population spectrum. The viral quasispecies theory is defined as a population of closely related viral genomes that are continually evolving, competing with variants within the population, and has a distribution of the fittest variants in a given environment (217). The inherent diversity of viral quasispecies could permit rapid adaptation to new environments and the evolution of resistance to anti-viral drugs (218–220).

While genetic diversity is vital for the adaptation of RNA viruses, population size is equally important. Population size influences evolution in that the survival or elimination of a variant in a population is proportional to the population size (221–223). Rotem et al. found that viral diversity in an evolution study with murine norovirus was proportional to the size of the viral population (224). If the population evolved in a bottlenecked population size of about 100 virions, the fitness of the population was low. However, the fitness increased if the population evolved at about 10^8 virions. Similarly, studies using vesicular stomatitis virus found that the transmission population size needed to maintain the fitness of the virus was dependent on its initial fitness (225, 226). A virus with low fitness required a smaller transfer population to maintain the same fitness as opposed to a virus with high fitness that required a larger transfer population to remain as fit. Genetic bottlenecks are probably a common occurrence for RNA viruses in the transmission between hosts and new species and the invasion of new tissues (218). If viral population sizes decrease, the relative fitness of the quasispecies also decreases, and the outcome of the frequency and the fate of the mutations will rely on genetic drift (215,

227). Population size impacts the heterogeneity of a population and can impact the evolutionary outcome.

Clonal interference is a common phenomenon in asexual populations where beneficial mutations will compete until fixation (228). Gerrish and Lenski modeled the trajectory of beneficial mutations with clonal interference as a contributing factor (228). The authors found that (a) the likelihood of a beneficial mutation becoming fixed in a population decreases both with population size and mutation rate. (b) As the rate of mutation or population size increases, so do adaptive mutations that result in a gain of fitness. (c) The rate of adaptation is an increasing but slowing function of both population size and mutation rate. (d) There is an abundance of beneficial mutations that do not achieve fixation because of the abundance of beneficial mutations. (e) There is a "leap-frog" effect in that the most common genotype may be less closely related to the preceding genotype than an earlier one. Clonal interference occurs in RNA virus populations. Miralles et al. used mAb-resistant and non-resistant vesicular stomatitis viruses and a mAb as the selective environment to examine clonal interference in viral evolution (229). The authors found that as population size increases, there was a shorter waiting time for the appearance of multiple beneficial mutations. In addition, they found that there was a limit to the rate of adaptations to become fixed in a viral population imposed by clonal interference. Other studies have shown that clonal interference can prevent a more fit mutant from becoming fixed in a population and that a more fit variant must overcome a population threshold to be competitive (230). Clonal interference is an important factor to consider when examining viral evolution and populations.

CHAPTER 2

Materials and Methods

2.1 In silico predictions of MARMs using MDS+FoldX approach

To predict RSV F protein escape mutations against motavizumab mAb, we applied our approach from previous studies that combines classical molecular dynamics simulations (MDS) and FoldX software (MDS+FoldX) (183, 184). To designate a mutation as an escape mutation it requires: 1) disrupt binding to a mAb, and 2) leave the F protein monomer stable thus allowing it to fold and assemble. It is thus necessary to determine how amino acid mutations alter stabilities ($\Delta\Delta G$ values) for F protein monomer folding ($\Delta\Delta G_{Fold}$) and binding to motavizumab ($\Delta\Delta G_{Bind}$). Therefore, we used our MDS+FoldX approach to estimate the folding stability of F protein monomer and F protein trimer/motavizumab complex binding affinities due to all possible single mutations.

2.2 Structure preparation

The X-ray crystal structure of RSV F glycoprotein bound to motavizumab was downloaded from Protein Data Bank (PDB ID:4ZYP). The 3D coordinates file was first modified to remove all but F protein trimer and three copies of heavy and light chains of motavizumab bound to each F protein monomer (147). The MODELLER software was then used to alter engineered residues and build the missing residues in all the chains (231). Missing amino acid residues 96 to 137 in F protein monomer represent liberated glycopeptide because of proteolysis by furin like proteases. These residues were ignored in our simulations.

2.3 Molecular dynamics simulations

F protein monomer and F protein trimer/motavizumab complex structures were used as starting structures for MDS. Similar MDS protocol was applied as reported in our previous studies for both the structures (183, 184). Briefly, the AMBER99SB*-ILDNP forcefield and the GROMACS 5.1.2 software package were used for generating topology files and performing simulation (232, 233). The final production simulation was run for 50 ns and snapshots were saved every 1 ns resulting in 50 snapshots for the F protein monomer and F protein trimer/motavizumab complex.

2.4 FoldX

FoldX software was used to analyze MDS snapshots of F protein monomer to estimate $\Delta\Delta G_{Fold}$ and F protein trimer/motavizumab snapshots were used to estimate $\Delta\Delta G_{Bind}$ for all possible mutations at each site in F protein. Our FoldX analysis protocol involved processing each snapshot six times in succession using RepairPDB command to energy minimize the snapshot, BuildModel command to generate all possible 19 single mutations at each site in F protein, and then the folding (ΔG_{Fold}) and binding affinity (ΔG_{Bind}) were estimated using Stability and AnalyseComplex commands, respectively. Both folding and binding $\Delta\Delta G$ values for each mutation was calculated by taking a difference between mutated and WT ΔG_{Fold} and ΔG_{Bind} values. For each mutation, we then averaged $\Delta\Delta G_{Fold}$ and $\Delta\Delta G_{Bind}$ values across all individual snapshot estimates. To estimate $\Delta\Delta G_{Bind}$ values for all possible 19 mutations at each amino acid site of F protein, we performed 1,276,800 FoldX calculations (448 F protein residues × 19 possible mutations at each site × 50 MD snapshots × 3 copies of F protein/motavizumab). Similarly, to estimate $\Delta\Delta G_{Fold}$ values for all possible 19 mutations at each amino acid site of F protein monomer we performed 425,600 FoldX calculations (448 F protein residues × 19 possible mutations at each site × 50 MD snapshots). Averaging estimates across all individual snapshots ultimately resulted in 8493 $\Delta\Delta G_{Fold}$ and $\Delta\Delta G_{Bind}$ values for all possible mutations of F protein (see Supplementary Material).

2.5 Cell Lines

HEp-2 cells (ATCC CCL 23) were maintained in minimal essential media (MEM) with Earle's salts, 10% fetal bovine serum (FBS), 1% MEM non-essential amino acids, 1% penicillin-streptomycin-amphotericin (PSF), and 5 mM L-glutamine. BHK-21 BSR-T7/5 (198) were supplied by Dr. Ursula Buchholz (NIH) and maintained in Glasgow's MEM supplemented with 10% FBS, 2% MEM amino acids, 2 mM L-glutamine, and 1% PSF. BSR-T7/5 were passaged every other passage with 1 mg/mL geneticin to maintain the T7 polymerase-expressing plasmid. HEK 293 A cells were supplied by Dr. Elizabeth Fortunato (University of Idaho) and were maintained in Dulbecco's Modified Eagle's media with 10% FBS, 1% penicillin and streptomycin, and 2 mM L-glutamine. All cells were incubated at 37°C and 5% CO_2. FreeStyle™ CHO-S™ Cells (Invitrogen) were maintained in FreeStyle™ CHO™ Expression Medium with 8 mM L-glutamine and incubated shaking at 37°C and 8% CO_2.

2.6 Plasmid Preparation and Viral Propagation

Bacterial artificial chromosome (BAC) containing the antigenomic cDNA of RSV-A2 mKate2 and four RSV helper plasmids (human codon bias optimized N,P,L, M2-1) were provided by Dr. Martin Moore (Emory University). RSV BAC and helper plasmids (WT) were transfected into BSRT7 BHK-21 cells (234). Media and cells were harvested, flash frozen in liquid nitrogen, rapid thawed in 37°C water bath, sonicated in an ice water bath 3 times at 30%, and centrifuged at 800xg for 5 minutes at 4°C. Supernatant media was harvested, flash frozen and stored at -80°C. A working stock of the WT virus was generated by infecting HEp-2 cells for 1-hour rocking at 37°C and 5% CO_2, adding complete media, monitoring cells for fluorescence and cytopathic effect (CPE), and was harvested as described above when fluorescence was detected throughout the flask.

The F gene was subcloned from RSV BAC into pBluescript SK + using SacII and SalI restrictions sites. Site-directed mutagenesis to generate the variants of interest was performed by Bioinnovatise Inc. Variant F genes were cloned back into genomic RSV BAC and transfected into BSRT7 BHK-21 cells as described above. The K272M and N262K variants were created by site-directed mutagenesis in pBluescript SK + using primers designed in NEBaseChanger™ (Table 2). Briefly, the pBluescript + F gene underwent PCR using Phusion Master Mix (New England BioLabs Inc.(NEB)) followed by DpnI treatment overnight at 37°C. The PCR product was then treated with polynucleotide kinase at 37°C for 30 minutes and deactivated at 65°C for 10 minutes. PCR cleanup was performed using PureLink™ PCR Purification Kit (Invitrogen) and ligation was performed overnight with T4 ligase at 4°C. Top10 *E. coli* cells were transformed with 2 µL of ligation product. F gene sequence was confirmed using Elim T7 Forward, Elim T3, and FwtA2seqR1(K272M) or Mota Amp Seq1 R (N262K) (Table 2). The F gene was subcloned using SacII and Sal I restriction sites back into pSynk and transformed into 10-beta *E. coli* (NEB). Colonies were picked and F gene was sequence confirmed using RSV F 5', RSV F 3', and FwtA2seqR1(K272M) or Mota Amp Seq1 R (N262K) (Table 2).

The pSynk mutant plasmids were purified using NucleoBond ® BAC 100 (Macherey-Nagel). Virus stocks were generated as described above. Each mutant was plaque purified from HEp-2 cells (235) and confirmed with Sanger sequencing. Working stocks of the mutant F

gene viruses were propagated as described above. All viruses were titrated by 50% tissue culture infectious dose ($TCID_{50}$) on HEp-2 cells.

2.7 Tissue Culture Infectious Dose ($TCID_{50}$)

HEp-2 cells were seeded at $1x10^4$ cells/well in a 96-well flat bottom plate the day prior to the assay. Cells were washed in warm Earle's MEM prior to infection. 135 μL (full log) or 130 μL (half log) of Earle's MEM to was added to all wells of a 96-well U-bottom plate. For a full log dilution, 15 μL of virus was added to 3 wells per replicate and for a half log dilution, 60 μL of virus was added to 3 wells per replicate. A negative control well and 2 positive control wells were included per plate. The virus was mixed and transferred down the plate by 15 μL (full log) or 60 μL (half log). The wash MEM was aspirated from the cells and 100 μL of diluted virus was transferred. The virus was rocked and incubated for 1 hour at 37°C and 5% CO_2. Following the incubation, 100 μL of MEM was added to plate and fluorescent cells and cytopathic effect was monitored by fluorescent microscopy over five days. $TCID_{50}$ was calculated using the Reed and Muench method (236) in a Microsoft Excel calculator created by Dr. Brett D. Lindenbach (Yale University).

2.8 Antibodies

Motavizumab and 101F antibodies and plasmids to produce these antibodies were provided by Dr. Jason McLellan (University of Texas, Austin) (64, 237). Plasmids expressing the heavy and light chains were co-transfected into FreeStyle™ CHO-S™ cells (Invitrogen) in serum free FreeStyle™ CHO™ Expression medium. Cell medium was harvested 6-8 days post-transfection and concentrated using a Vivaflow 200. The concentrated medium was purified using a HiTrap protein A column (GE Healthcare) as previously described (64, 237) and dialyzed into PBS. Antibodies were stored at -20°C.

2.9 Growth Curves

HEp-2 cells were infected at a multiplicity of infection (MOI) of 0.1 in MEM. Cells were rocked for 1 hour at 37°C and 5% CO_2. Cells were washed twice with PBS and the second wash was saved as the zero-hour time point. Complete media was added after aspiration of the PBS. Cell media was sampled at 6, 9, 12, 15, 18, 24, 36, and 48 hours. Viral titers were performed by $TCID_{50}$ assay on HEp-2 cells.

2.10 Microneutralization Assay

Assay was performed as previously described (238). Motavizumab was serially diluted two-fold starting at 10000 ng/mL and ending at 156.5 ng/mL in a 96-well U bottom plate. Variants were incubated with antibody for 1 hour prior to infecting HEp-2 cells at an MOI of 1. Cells were incubated at 37°C and 5% CO_2 and harvested 18 hours post infection. Cells were washed in PBS for 10 minutes rocking 37°C and 5% CO2, PBS was aspirated and trypsin was applied to lift cells. HEp-2 CMEM was added and cells were mixed gently to break up clumps. Cells were spun down at 200xg for 2 minutes 4°C. The media was aspirated, and the cells were resuspended 1% formaldehyde in PBS and incubated at 4°C for 20 minutes in the dark. Cells were spun down again as previously described and washed in FACS buffer (1% BSA and 0.1% sodium azide in PBS) and spun down again. Cells were resuspended in FACS buffer and counted via flow cytometry using a Beckman Coulter Cytoflex-S. mKate2 expression was monitored in the ECD channel. The gain settings for forward scatter (FSC) and side scatter (SSC) were 350, and ECD was 110. The threshold was set to 1000000 for height. The initial cell population was gated from FSC vs SSC. Data was analyzed using CytExpert software 2.4.0.28. Inhibition curves and IC_{50} values were calculated using GraphPad Prism v.9.

2.11 F gene and Sequencing

RNA was isolated from virus stocks using Quick-RNA Viral Kit (Zymo Research). Viral cDNA was generated using SuperScript™ IV VILO™ Master Mix (Thermo Fisher Scientific). The F gene was PCR amplified using F 5' and 3' Primers (Table 2) and Phusion Master Mix (NEB). Sanger sequencing was performed by Elim Biosciences.

2.12 F Gene Library and Expression Vector

The F gene variant library was generated by Twist Bioscience, based on the codon-optimized F expressing plasmid, pHRSVFoptA2, provided by Dr. Mark Peeples (The Ohio State University)(187, 239). Each amino acid change at 17 residues within 5 angstroms of the motavizumab binding site, based on the co-crystal structure (237), were incorporated into the variant library and designed to be flanked by recombination sites, attB1 and attB2, which are compatible with the Gateway Cloning™ system (240). The pooled F gene segments (25 ng) were cloned into pDONR-221 (150 ng) using a BP Clonase II enzyme reaction (2 μL of enzyme, 4.5 μL TE buffer) overnight at room temperature. Following overnight incubation, the reaction was treated with proteinase K (1 μL) for 10 minutes at 37°C. pDONR-221 + F

gene pools were transformed into 10-beta *E. coli* and plasmids were purified using DNA mini-prep kit (Zymo). The pDONR-221 + F gene variants (200 ng) were then cloned into mammalian expression vector pcDNA3.1-GW (200 ng) by LR Clonase II enzyme reaction (0.5 µL enzyme, 1 µL TE buffer) at room temperature overnight followed by proteinase K treatment as described above. pcDNA3.1-GW + F gene plasmids were transformed into 10-beta E. coli. Bacterial stocks were plated on LB-ampicillin plates and colonies were picked and Sanger sequence confirmed for each variant. Plasmids for transfection were generated using PureLink™ HiPure Plasmid Midiprep Kit (Invitrogen).

2.13 Flow cytometry

HEK 293A cells were transiently transfected with pcDNA3.1-F plasmid variants or pcDNA3.1 as an empty vector control using Lipofectamine 3000™ reagents (Invitrogen). For the transient transfection, HEK 293A cells were seeded at 6.5×10^5 cells/well in a 96-well plate one day prior to transfection. 190 ng of plasmid/well and 0.4 µL/well of P3000 were diluted in a final volume of 5 µL/well of Opti-MEM™ in an Eppendorf tube. In a separate Eppendorf tube, 0.3 µL/well of Lipofectamine 3000 was diluted in a final volume of 5 µL/well of Opti-MEM™. The tubes were combined and mixed by flicking the tube and allowed to incubate for 15 minutes. The media was aspirated from the cells and 10 µL of transfection mixture was added to the well and an additional 15 µL of Opti-MEM™ was added to help cover the cells. After 6 hours cell media was added to variants L258E, L258K, L258V, K272E, K272G, and K272R to increase protein expression. After 24 hours cells were lifted using Accutase (Innovative Cell Technologies, Inc.) and washed in PBS. Motavizumab and 101F were conjugated using Alexa Fluor 488 and 594 Antibody Labeling Kits (Invitrogen). Cells were stained with 1 µg/mL of Alexa Fluor 488 conjugated motavizumab and 0.7 µg/mL of Alexa Fluor 594 conjugated 101F antibody. Flow cytometry was performed using a Beckman Coulter Cytoflex-S. Alexa Fluor 488 was monitored in the FITC channel and Alexa Fluor 594 was monitored in the ECD channel. The gain settings for forward scatter (FSC) and side scatter (SSC) were 350, ECD was 110, and FITC was 2. The threshold was set to 1000000 for height. The initial cell population was gated from FSC vs SSC. Data was analyzed using CytExpert software 2.4.0.28.

2.14 Viral Purification

WT, L258K, K272E, and S275H clonal virus stocks were used to infect HEp-2 cells. Uninfected HEp-2 cells were included as a control. Cells and supernatant media were harvested when mKate2 fluorescence was observed throughout cell culture flasks with fluorescence microscopy. Harvested cells and media were flash frozen in liquid nitrogen and rapidly thawed in 37°C water bath. The cells and media were then sonicated in ice water bath at 30% for 30 seconds three times. Cell debris was pelleted at 800xg supernatant medium was removed and centrifuged again. The supernatant medium was loaded into Ultra-Clear 1 x 3.5 in. ultracentrifuge tubes (Beckman Coulter) with a 15% sucrose cushion in 10 mM Tris–HCl, pH 7.5, 100 mM $MgSO_4$ and 0.25 M sucrose. Samples were spun at 20000xg for 2 hours at 4°C and pellets were resuspended in PBS. F protein concentration was determined using RSV-F ELISA Kit (SinoBiological).

2.15 Surface Plasmon Resonance

All SPR experiments were performed on a Nicoya OpenSPR™ Rev 3 one channel and Protein A Sensors Kit (Nicoya) was used to attach 30 μg/mL of motavizumab in PBS to the chip. Purified virions at concentrations 40 nM, 20 nM, 10 nM, and 5 nM were allowed to associate for 5 minutes at 20 μL/minute and disassociate for 5 minutes at 20 μL/minute. Chips were regenerated between runs with 10 mM glycine pH 3 and motavizumab was reattached. All kinetics analysis was performed in TraceDrawer 1.9.

2.16 PyMol Modeling

The X-ray crystal structure of RSV F glycoprotein bound to motavizumab was downloaded from Protein Data Bank (PDB ID:4ZYP). The structure was loaded into PyMol (version 2.1.1). Residues within 4 Å of residues of interest were identified using the around function. Mutations were made using the mutagenesis function. Measurements between residues were calculated using the measurement function.

2.17 Passage Experiments

HEp-2 cells were infected at a MOI of 0.03 with WT virus and transferred to fresh HEp-2 cells once mKate2 fluorescence was observed by fluorescence microscopy throughout the flask for a total of five times to make control passage 5 virus (Cp5). 1mL of Cp5 was allowed to infect HEp-2 cells at a MOI of 0.03 before 4 mL of media containing 0.625μg/mL of motavizumab was added, bringing the concentration to 0.5 μg/mL of motavizumab. Cells

were monitored for fluorescence and CPE. Once mKate2 fluorescence was observed throughout the flask, virus was harvested and passaged by adding 1 mL of passaged virus to fresh HEp-2 cells, rocking for 1 hour, and then adding 4 mL of media containing 0.625 µg/mL of motavizumab for a total of five times. The F gene was amplified as described above and next-generation sequencing was performed on an Illumina MiSeq by University of Idaho Institute for Interdisciplinary Data Sciences Genomics and Bioinformatics Resources Core.

2.18 Bioinformatics Analysis

The reads were first mapped against the F gene sequence from pSynk-A2 using bowtie2 v 2.3.4.1 with "-local" parameter (241). The BAM file was further analyzed using SAMtools v1.5 to confirm the depth of the mapping across the F gene (242). Variants were called using BCFtools (243).

2.19 Selection Coefficient Calculation

Selection coefficients were calculated by adapting the enrichment score calculation by dividing by the units of time between two sample. The enrichment score is the log ratio of the variant frequency relative to wild type frequency in the same time point (244).

$$L_{\frac{v,t}{t}} = \frac{log_2\left(\frac{c_{v,t}}{c_{wt,t}}\right) - log_2\left(\frac{c_{v,0}}{c_{wt,0}}\right)}{T_e}$$

$c_{v,t}$ is the count of the variant in the population at the final time point and $c_{wt,t}$ is the count of the WT population at the final time point. $c_{v,0}$ is the count of the variant at the initial time point point and $c_{wt,0}$ is the count of WT in the population at the initial time point. Base-2 was used to represent doublings per hour. T_e represents total elapsed hours between passages.

2.20 Relative Fitness Assay

HEp-2 cells were seeded at 7.5×10^5 cells/well in a 6-well dish the day before the assay. Cells were counted and an equal MOI (0.05) of variant virus and WT virus were incubated with 0.25 µg/mL of motavizumab 30 minutes prior to infection of HEp-2 cells. Virus was removed and cells were washed twice with PBS before adding new media with or without a final concentration of 0.25 µg/mL motavizumab and incubated at 37°C and 5% CO_2. Supernatant media was harvested at 48 hours, diluted 1:10 and allowed to infect new cells with or without motavizumab for a total of three passages. Viral RNA was extracted from the media and the F gene was amplified as previously described. A sequencing library was created for

each replicate. The motavizumab binding epitope of the F gene was PCR amplified using Phusion Master Mix (NEB) with Mota Amp Seq1 F and R primers (Table 2). A second round of PCR was used to attach CS-Tags (Table 2) to the amplified motavizumab binding epitope PCR products. A third round of PCR was performed to add on unique barcode adaptors to each sample for identification during analysis. The University of Idaho Institute for Interdisciplinary Data Sciences Genomics and Bioinformatics Resources Core performed next-generation sequencing on an Illumina MiSeq and sequence analysis. The reads were mapped back to the F gene and the number variants at each amino acid residue were identified for the F gene section that was surveyed.

2.21 Motavizumab Fitness Assay

Virus variants (MOI=0.1) were incubated with 0.25 µg/mL of motavizumab prior to infection HEp-2 cells. Virus was allowed to infect for one hour before removal and cells were washed twice with PBS and media with motavizumab at a final concentration of 0.25 µg/mL was added. A control without antibody was also performed. Supernatant media was harvested at 48 hours and titrated using $TCID_{50}$.

Table 2. Primers for sequencing, site-directed mutagenesis, and creation of F gene next-generation sequencing library.

Primer Name	Sequence (5'-3')
K272M F	TGATCAGAAAatgTTAATGTCCAAC
K272M R	TTTGTTATAGGCATATCATTG
N262K F	GTCATTAATCaaaGATATGCCTATAAC
N262K R	AATAATTCACTATTAGTTAACATGTAAG
RSV F 5'	GCAAGGATTCCTTCGTGAC
RSV F 3'	CACACCACGCCAGTAG
Elim T7 F	AATACGACTCACTATAGGG
Elim T3	AATTAACCCTCACTAAAGGG
FwtA2seqR1	GTGGTAATTGTACTACATATGC
Mota Amp Seq1 F	GAGATCACCAGGGAATTTAGTG
Mota Amp Seq1 R	CTTTACATGTTTCAGCTTGTGG
Forward Name	**Forward Sequence with CS-Tag in Red (5'-3')**
CS1-Mota_Primer1-for	ACACTGACGACATGGTTCTACAGAGATCACCAGGGAATTTAGTG
CS1-Mota_Primer2-for	ACACTGACGACATGGTTCTACACGAGATCACCAGGGAATTTAGTG
CS1-Mota_Primer2-for	ACACTGACGACATGGTTCTACATCGAGATCACCAGGGAATTTAGTG
CS1-Mota_Primer4-for	ACACTGACGACATGGTTCTACAATCGAGATCACCAGGGAATTTAGTG
CS1-Mota_Primer5-for	ACACTGACGACATGGTTCTACAGATCGAGATCACCAGGGAATTTAGTG
CS1-Mota_Primer6-for	ACACTGACGACATGGTTCTACACGATCGAGATCACCAGGGAATTTAGTG
CS1-Mota_Primer7-for	ACACTGACGACATGGTTCTACATCGATCGAGATCACCAGGGAATTTAGTG
Reverse Name	**Reverse Sequence with CS-Tag in Red (5'-3')**
CS2-Mota_Primer1-rev	TACGGTAGCAGAGACTTGGTCTCTTTACATGTTTCAGCTTGTGG
CS2-Mota_Primer2-rev	TACGGTAGCAGAGACTTGGTCTTCTTTACATGTTTCAGCTTGTGG
CS2-Mota_Primer3-rev	TACGGTAGCAGAGACTTGGTCTATCTTTACATGTTTCAGCTTGTGG
CS2-Mota_Primer4-rev	TACGGTAGCAGAGACTTGGTCTGATCTTTACATGTTTCAGCTTGTGG
CS2-Mota_Primer5-rev	TACGGTAGCAGAGACTTGGTCTCGATCTTTACATGTTTCAGCTTGTGG
CS2-Mota_Primer6-rev	TACGGTAGCAGAGACTTGGTCTTCGATCTTTACATGTTTCAGCTTGTGG
CS2-Mota_Primer7-rev	TACGGTAGCAGAGACTTGGTCTATCGATCTTTACATGTTTCAGCTTGTGG

Lower case letters indicate codon mutation different from A2 F gene sequence

CHAPTER 3

Molecular Modeling Identifies Novel Escape Variants in Respiratory Syncytial Virus Fusion Glycoprotein

3.1 Overview

Monoclonal antibodies (mAbs) are increasingly used to prevent and treat viral infections in humans. The first mAb approved for the prophylaxis of viral infection was palivizumab in 1998 (127). Since then, additional mAbs have been approved for the treatment of drug-resistant human immunodeficiency virus 1 (HIV-1) and the treatment of Ebola virus (EBOV) infection (128, 129). There have also been several mAb treatments granted FDA emergency use authorization for severe acute respiratory syndrome coronavirus 2 (SARS-CoV-2) during the coronavirus disease 2019 (COVID-19) pandemic (130–132). mAbs are a very powerful tool because of the ability to target specific neutralizing epitopes on viral pathogens.

The downside of using a targeted therapy such as mAbs is the increased selective pressure on viral pathogens. RNA viruses and retroviruses are prone to mutations given the high error rate of the RNA-dependent RNA polymerase and reverse transcriptase, respectively (153). The combination of a high error rate and selective pressure will likely result in a phenomenon known as antibody escape, where mutations occur in the binding epitope on the viral protein that allows the virus to evade neutralization by mAb. Monoclonal antibody resistant mutants (MARMs) can be identified by sequencing patient samples or by serially passaging the virus in the presence of mAb in cell culture or animal models. The downside of sequencing patient samples is that the MARM identified are already circulating in the population. Passage experiments are biased given the limitation of replication cycles in cell culture. The ability to predict amino acid changes that disrupt the binding of mAb to viral proteins would be beneficial to predict what variants might be seen circulating in the population and potentially adapt current therapies if the MARMs become dominant in the population.

Previous studies have used protein biophysical modeling to predict disruptions between the EBOV envelope glycoprotein (GP) and mAb KZ52 using the available co-crystal structure (183). A follow-up study by the same group included additional mAbs Antibody 100, Antibody

114, and 13F6-1-2 (184). The studies used molecular dynamic simulations and FoldX (MDS+FoldX) to estimate the folding stability of GP and the binding disruption of the four mAbs. This approach identified 127 mutations that predicted GP to fold correctly and disrupt binding. Three potential MARMs that MDS+FoldX identified have been seen in experiments and surveillance studies (245, 246). While some of the predicted MARM were confirmed by other studies, the predictions could not be tested empirically to assess the accuracy.

RSV causes severe lower respiratory infections in infants, the elderly, and immune-compromised people (12). There is no vaccine for RSV and the only targeted treatment approved by the FDA is the prophylactic mAb, palivizumab, which targets the fusion glycoprotein (F protein). F protein has been the target of treatments and vaccines because it facilitates entry of the virus into the host cell, it is highly antigenic, and there is conservation of multiple antigenic sites across RSV strains (3, 47, 62, 63, 65, 148). MARMs for palivizumab have been identified from cell culture, animal models, and clinical samples (Table 3) (159–167, 247–249). No co-crystal structure exists for palivizumab and F protein, but there is a crystal structure between a derivative of palivizumab, motavizumab, and F protein (147). Motavizumab binds the same epitope as palivizumab and differs by only 13 amino acids from palivizumab: three residues were changed to hydrophobic residues that cause direct interaction between the mAb and F protein (64). While motavizumab is not used in clinical settings, it is still of interest given that it binds the same site as palivizumab and does have a known MARM, K272E (Table 3) (165).

Table 3. Known RSV MARM for palivizumab and motavizumab.

Monoclonal Antibody	Known MARM
Palivizumab	S275F, K272M$^\Diamond$, K272Q$^\Diamond$, K272E, N276Y, K272T$^\Diamond$, K272N$^\Diamond$, S275L$^\Diamond$, N262Y, N262S, K272Y, N276S
Motavizumab	K272E

$^\Diamond$*Indicates palivizumab MARM neutralized by motavizumab, other variants were not tested*

In this study, we examined if MDS+FoldX could predict single amino acid changes that disrupt the binding of motavizumab but do not disrupt the folding of F protein. We generated predicted MARM in an infectious recombinant clonal virus and tested the variants for fitness, neutralization by motavizumab, and mAb binding of eight predicted MARM variants. This approach confirmed that MDS+FoldX could accurately predict K272E as a MARM and identified five novel variants.

3.3 Results

3.3.1 MDS+FoldX predicted amino acid residues of interest in the F protein monomer and motavizumab interaction.

MDS+FoldX was used to predict single amino acid residue changes that would cause disruption of binding of motavizumab and still allow for the correct folding of the monomer. All 19 amino acid changes were performed for all 448 amino acids for F protein monomer folding ($\Delta\Delta G_{Fold}$) and its binding to motavizumab ($\Delta\Delta G_{Bind}$) (Figure 6). Based on the previous EBOV studies, mutations for $\Delta\Delta G_{Fold}$ values less than 2 kcal/mol are not predicted to affect F protein stability and are likely to arise under selective pressure (183, 184). Of the 8493 modeled residues, 5716 mutations were predicted to fold correctly (Figure 6A). Since the EBOV GP and mAb were unable to be empirically tested, it was never determined if there was any significance to an increase in $\Delta\Delta G_{Bind}$ value. Therefore, we selected eight mutations along the $\Delta\Delta G_{Bind}$ x-axis at approximately 0.5 kcal/mol that also encompassed the residues of interest while not overlapping with already known palivizumab MARMs (Figure 6B, Table 4). Interestingly, only 81 mutations met the criteria of a $\Delta\Delta G_{Fold}$ <2 kcal/mol and a $\Delta\Delta G_{Bind}$ >0.5 kcal/mol (Figure 6A). K272E was included in the selection as a positive control as the known MARM (165).

3.3.2 The eight variants replicated and exhibited reduced growth kinetics.

To assess if the $\Delta\Delta G_{Fold}$ values less than 2 kcal/mol did not disrupt F protein function, we tested the growth kinetics of the eight selected variants. The variants were generated using site-directed mutagenesis and subcloned into a mKate2 recombinant RSV infectious clone (234). HEp-2 cells were infected at a multiplicity of infection (MOI) of 0.1, and supernatant media was collected over 48 hours and titrated by $TCID_{50}$ assay. All eight mutations propagated new virus (Figure 7). There was a delay of growth for both L258K and
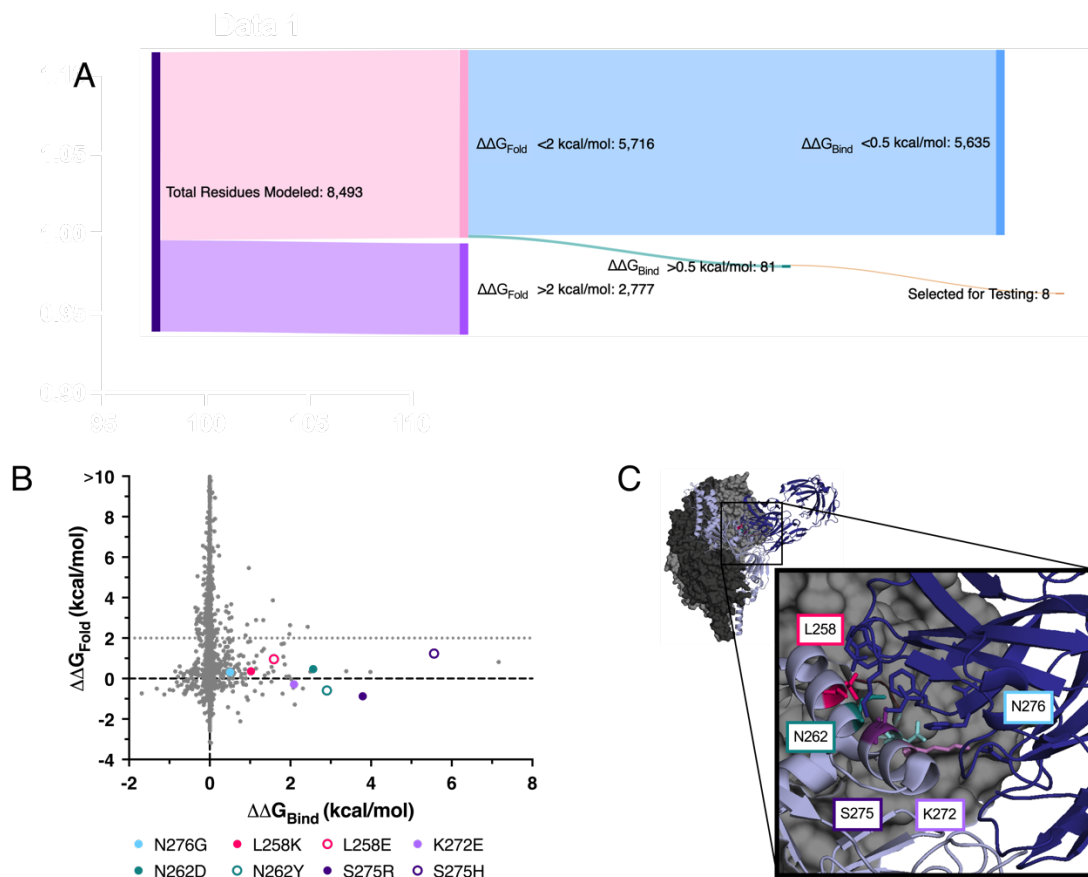
Figure 6. Molecular modeling of F protein and motavizumab interaction.
(A) Sankey diagram of MDS+FoldX modeling predictions filtering. Of the 8493 total residues modeled, only 81 F protein variants were predicted to fold correctly ($\Delta\Delta G_{Fold}$ <2 kcal/mol) and potentially disrupt binding ($\Delta\Delta G_{Bind}$>0.5 kcal/mol). We selected 8 variants to test. (B) Plot of MD+FoldX predictions of $\Delta\Delta G_{Fold}$ and $\Delta\Delta G_{Bind}$ of all possible mutations in F with eight selected variants. (C) F protein trimer (dark gray) monomer (light blue ribbon) with motavizumab (dark blue ribbon) structure with interacting residues of interest: L258 (pink), N262 (teal), K272 (lavender), S275 (purple), and N276 (blue).

Table 4. $\Delta\Delta G_{Fold}$ and $\Delta\Delta G_{Bind}$ values and standard deviations of eight selected variants.

Mutation	$\Delta\Delta G_{Bind}$	SD of Bind	$\Delta\Delta G_{Fold}$	SD of Fold
N276G	0.50	0.59	0.32	0.43
L258K	1.02	0.52	0.37	0.53
L258E	1.59	0.48	0.96	0.29
K272E	2.09	0.98	-0.28	0.59
N262D	2.56	1.11	0.48	0.67
N262Y	2.90	3.61	-0.58	0.73
S275R	3.79	2.76	-0.87	0.90
S275H	5.56	3.82	1.24	1.45
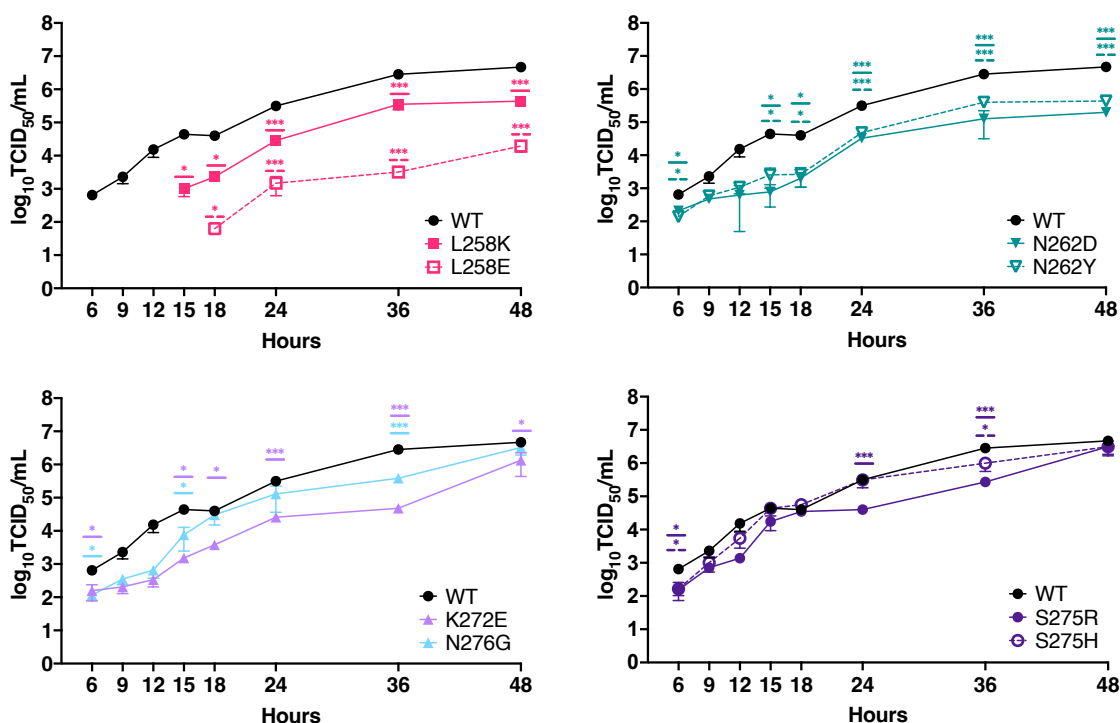
Figure 7. All eight variants demonstrated ability to replicate and propagate new virus.
HEp-2 cells were infected with 0.1 MOI of variant or WT virus and supernatant media were collected over time. Virus was titrated by $TCID_{50}$ assay on HEp-2 cells. Three independent experiments were performed and error bars indicate SEM. *p <0.05; **p<0.005; ***p<0.001.

L258E, with virus remaining undetectable until 15 and 18 hours, respectively. L258K, L258E, N262D, and N262Y had significantly reduced viral titers in an unpaired t-test compared to the wild type (WT) virus over the 48 hours. S275H and S275R had similar growth to WT, with significant reductions in titers at 6, 24, and 36-hour time points. K272E had reduced viral titers at all time points, and N276G had a growth pattern similar to WT with a significant reduction in viral titers at 6, 15, and 36-hour time points. The eight variants could replicate and support that the $\Delta\Delta G_{Fold}$ value less than 2 kcal/mol was an appropriate limit for selecting mutants. All eight variants had some deficit in growth when compared to WT.

3.3.3 Decreased neutralization by motavizumab was observed in six variants.

All eight variants were able to replicate, so the next step was to test the neutralization of the variants by motavizumab. Microneutralization assays were used to test for neutralization. Briefly, virus variants at an MOI of 1 were incubated in a 2-fold serial dilution of motavizumab for one hour before infection of HEp-2 cells, and mKate2-expressing cells
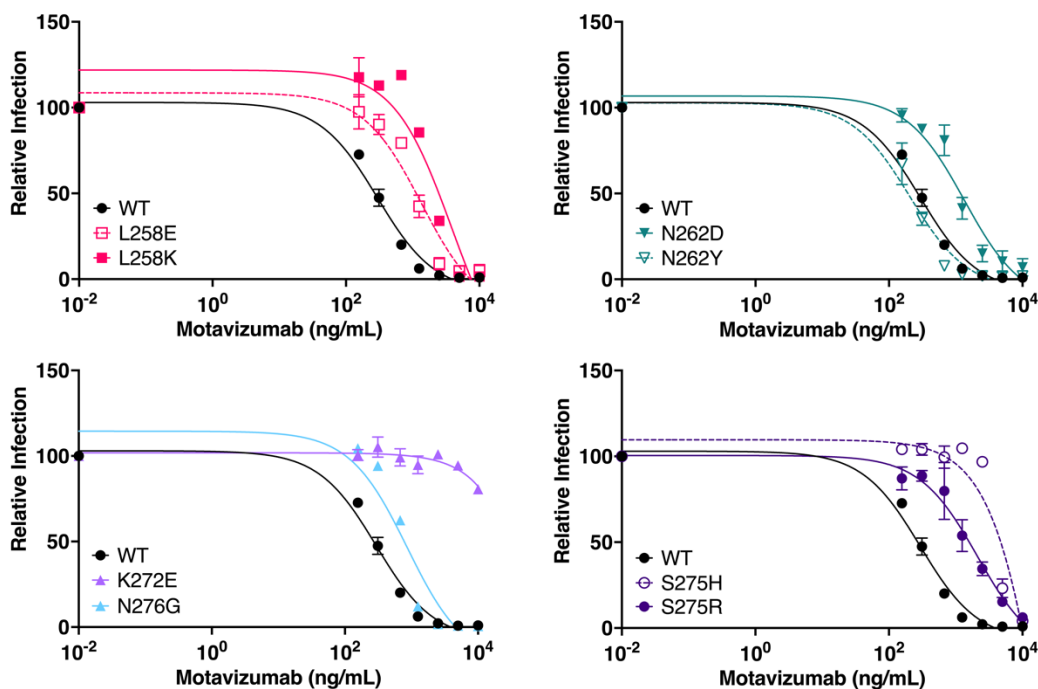
Figure 8. Microneutralization assay revealed reduced neutralization by motavizumab for six of the eight variants.
Motavizumab was serially diluted two-fold (10000 ng/mL-156 ng/mL) and incubated with variants prior to infection of HEp-2 cells at an MOI of 1. mKate2-positive cells were counted by flow cytometry at 18 hours post infection. Error bars indicate SEM of three independent experiments.

Table 5. Motavizumab IC$_{50}$ values for selected variants and fold change compared to WT.

Variant	WT	L258E	L258K	N262D	N262Y	K272E	S275H	S275R	N276G
IC$_{50}$ (ng/mL)	290.4	1101	1890	1081	223.5	>10000	3966	1633	756.4
Fold change	-	3.8	6.5	3.7	0.8	-	13.7	5.6	2.6

were counted by flow cytometry after 18 hours. Six of the variants displayed a reduction in neutralization by motavizumab (Figure 8). The known MARM, K272E, was not completely neutralized at the highest concentration of mAb used (10 µg/mL). Zhu et al. determined that the IC$_{50}$ for K272E was 30.04 ± 611.35 µg/mL (165). N262Y and N276G were similar in neutralization compared to WT (Figure 8). Variants L258E and N262D were greater than 3-fold in IC$_{50}$ compared to WT (Figure 8, Table 5). S275H, S275R, K272E, and L258K all had a greater than 5-fold increase in IC$_{50}$ (Figure 8, Table 5). We confirmed that MDS-FoldX

predicted K272E as a MARM and identified five novel MARM that have not been previously identified.

3.3.4 Flow cytometry confirmed reduced binding of motavizumab to identified MARMs.

The binding of motavizumab to F protein was assessed using flow cytometry. This assay used a plasmid that expressed F protein that was transiently transfected in HEK 293A cells (Figure 9). We tested the six variants that demonstrated reduced neutralization (L258E, L258K, K272E, S275H, S275R, and N276G) and some additional variants based on the modeling (L258V, K272G, K272R, and S275A). The additional variants had $\Delta\Delta G_{Bind}$ values close to 0 kcal/mol except for K272G (1.86 kcal/mol), which has a value close to K272E (2.09 kcal/mol). The values closer to 0 kcal/mol were expected to have similar binding to WT. We used the mAb 101F that binds a unique antigenic epitope from motavizumab to measure F protein expression (Figure 9) (237). 101F was conjugated with Alexa Fluor 594 (101F-594), and motavizumab was conjugated with Alexa Fluor 488 (motavizumab-488) (Figure 9). Cells were gated on 101F-594 positive cells, and the median fluorescent intensity of Alexa Fluor 488 of the 101F-594 positive cells was used to indicate motavizumab binding. A reduction in motavizumab-488 fluorescence intensity in relation to 101-594 fluorescent intensity was observed in the peak shifts for L258E, L258K, K272E, K272G, S275H, and S275R (Figure 10A). Cells that expressed F protein were gated based on the 101F-594 positive population,
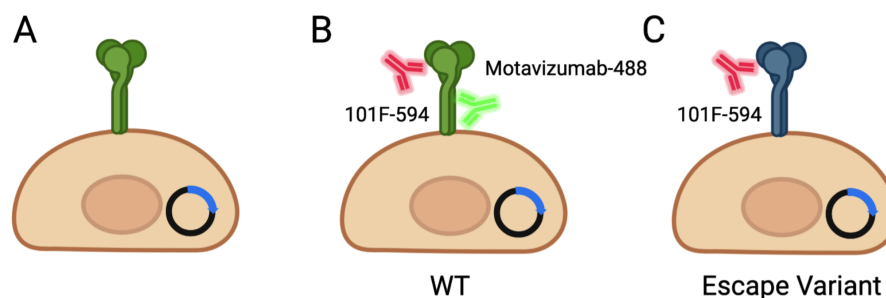
Figure 9. Cartoon diagram of F protein detection using flow cytometry.
(A) HEK 293A cells were transiently transfected with an expression vector with F protein (green). (B) F protein (green) was detected with two fluorescent antibodies. 101F-594 is a monoclonal antibody that binds a unique epitope from motavizumab and was used to measure F protein expression on the cell surface. The WT F protein is expected to bind both 101F-594 and motavizumab-488 as there is no disruption of binding in the site II epitope. (B) Escape variant F proteins (blue) should have reduced or absence of motavizumab-488 binding and will have reduced median fluorescent intensity compared to WT. Diagram created using Biorender.

and the percentage of motavizumab-488 (Figure 10B) was analyzed for median fluorescent intensity (MFI). There was a significant reduction in MFI for L258E, L258K, K272E, S275H, and S275R compared to WT (Figure 10C), which suggests a reduction in binding of motavizumab. Some reduction of MFI was observed in L258V, N276G, and K272G but were not statistically significant when compared to WT. Variants K272R and S275A had MFI values similar to WT, which was expected given that the $\Delta\Delta G_{Bind}$ values were close to 0 kcal/mol. The variants with decreased neutralization (Figure 8) also demonstrated reduced binding of motavizumab (Figure 10C). The coefficient of correlation (R=0.7) demonstrated a correlation between $\Delta\Delta G_{Bind}$ values and motavizumab binding (MFI), and the slope was significant (p=0.025). The coefficient of determination ($R^2 = 0.49$) indicated a moderate fit of the data line to the data points (Figure 10D). We calculated the p-value for the coefficient of determination by randomizing the data set one hundred times and calculating the coefficient of determination of each data set. The resulting p-value (p=0.05) indicated that the coefficient of determination was significant. As a control, $\Delta\Delta G_{Fold}$ was compared to MFI of motavizumab-488 as no correlation between the values was expected, and none was observed (R=0.06, $R^2 = 0.002$) (Figure 10E). The p-value for the coefficient of determination was calculated as above for $\Delta\Delta G_{Fold}$ and MFI-488 and was not significant (p=0.90).

3.3.5 Reduced on-rate of motavizumab is the mechanism of escape.

Binding kinetics of motavizumab and purified virion were measured using surface plasmon resonance (SPR). We evaluated the binding kinetics of motavizumab for K272E, L258K, and S275H based on the increase of IC_{50} compared to WT. There was a significant reduction of on-rate (k_a) for all three variants (Figure 11A, Table 6). No significant difference between the variants and WT was observed for off-rate (k_d) (Figure 11B, Table 6). A reduction in equilibrium disassociation constant (KD) for K272E and S275H indicated lower affinity between those variants and motavizumab compared to WT (Figure 11C, Table 6). Because of the limited data points, a simple linear regression was used to fit lines for $\Delta\Delta G_{Bind}$ and binding kinetics values. We observed an inverse correlation between $\Delta\Delta G_{Bind}$ and on-rate (R=0.92, R^2 =0.84, slope p=0.0005); as $\Delta\Delta G_{Bind}$ increased, the on-rate decreased (Figure 11E). No correlation was observed between $\Delta\Delta G_{Bind}$ and off-rate (R=0.37, $R^2 = 0.14$, slope p=0.32) (Figure 11F). There was a linear correlation between KD and $\Delta\Delta G_{Bind}$ (R=0.87, $R^2 = 0.76$, slope p=0.002); as $\Delta\Delta G_{Bind}$ increased, KD also increased (Figure 11G). Reduced association
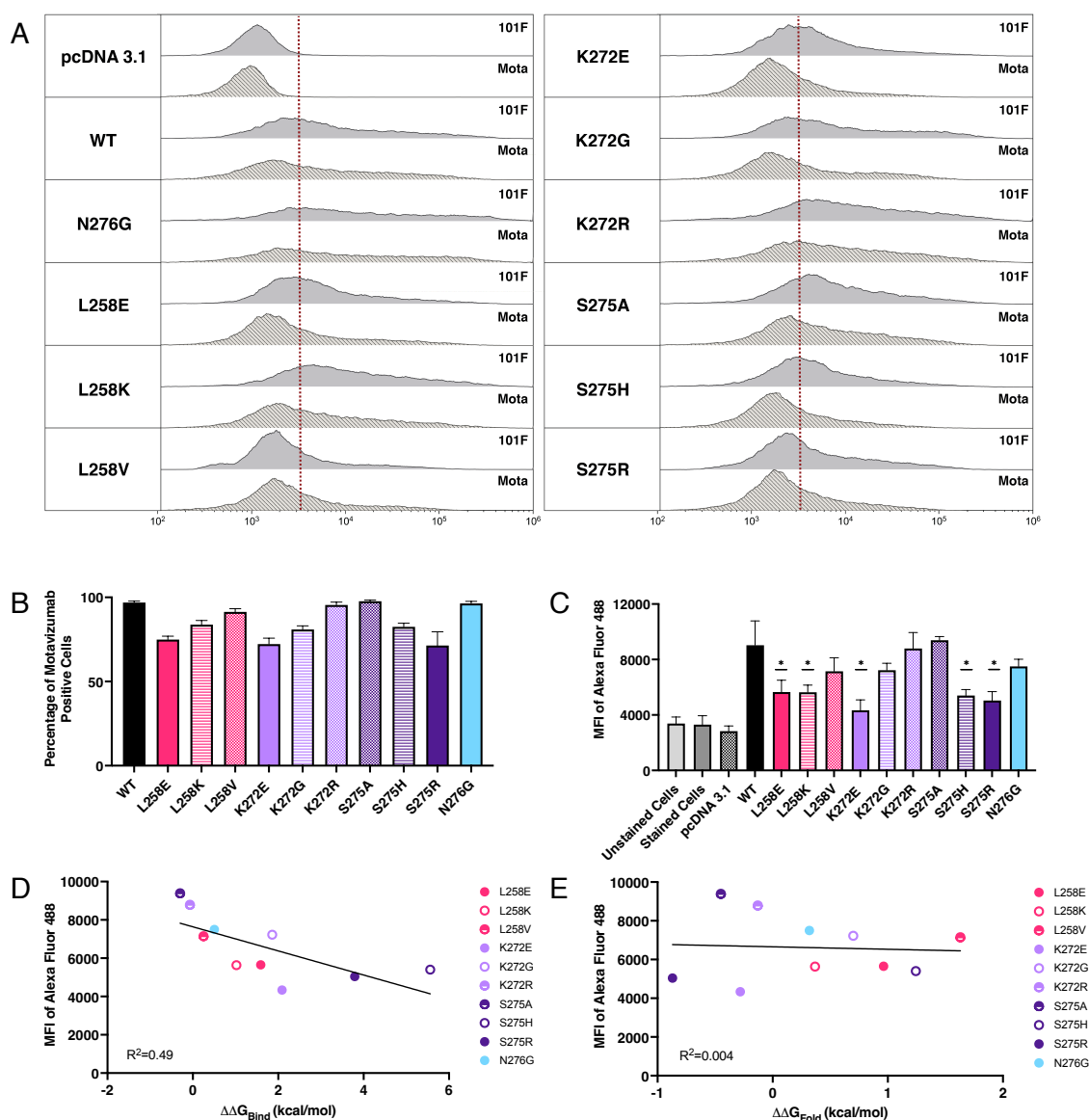
Figure 10. Flow cytometry revealed reduced binding of motavizumab for some variants.
HEK 293A cells were transiently transfected with variant F protein-expressing plasmids or an empty vector control (pcDNA3.1) and dual stained with motavizumab-488 and 101F-594. (A) Representative histograms of 101F-594 and motavizumab-488 positive cells. Cells right of red line are positive. The cells were gated on 101-594 positive cells and the median fluorescent intensity (MFI) of the (B) motavizumab-488 positive cells was measured. (C) MFI of motavizumab-488 positive cells on 101F-594-gated cell population. Error bars indicate SEM of three replicate experiments. (D) Graph of ΔΔG_{Bind} vs. MFI of motavizumab-488 demonstrated linear inverse correlation between MFI and ΔΔG_{Bind}. (E) Graph of ΔΔG_{Fold} vs. MFI of motavizumab-488 demonstrated no correlation between the values. Error bars indicate SEM of 3 independent experiments, *p <0.05.
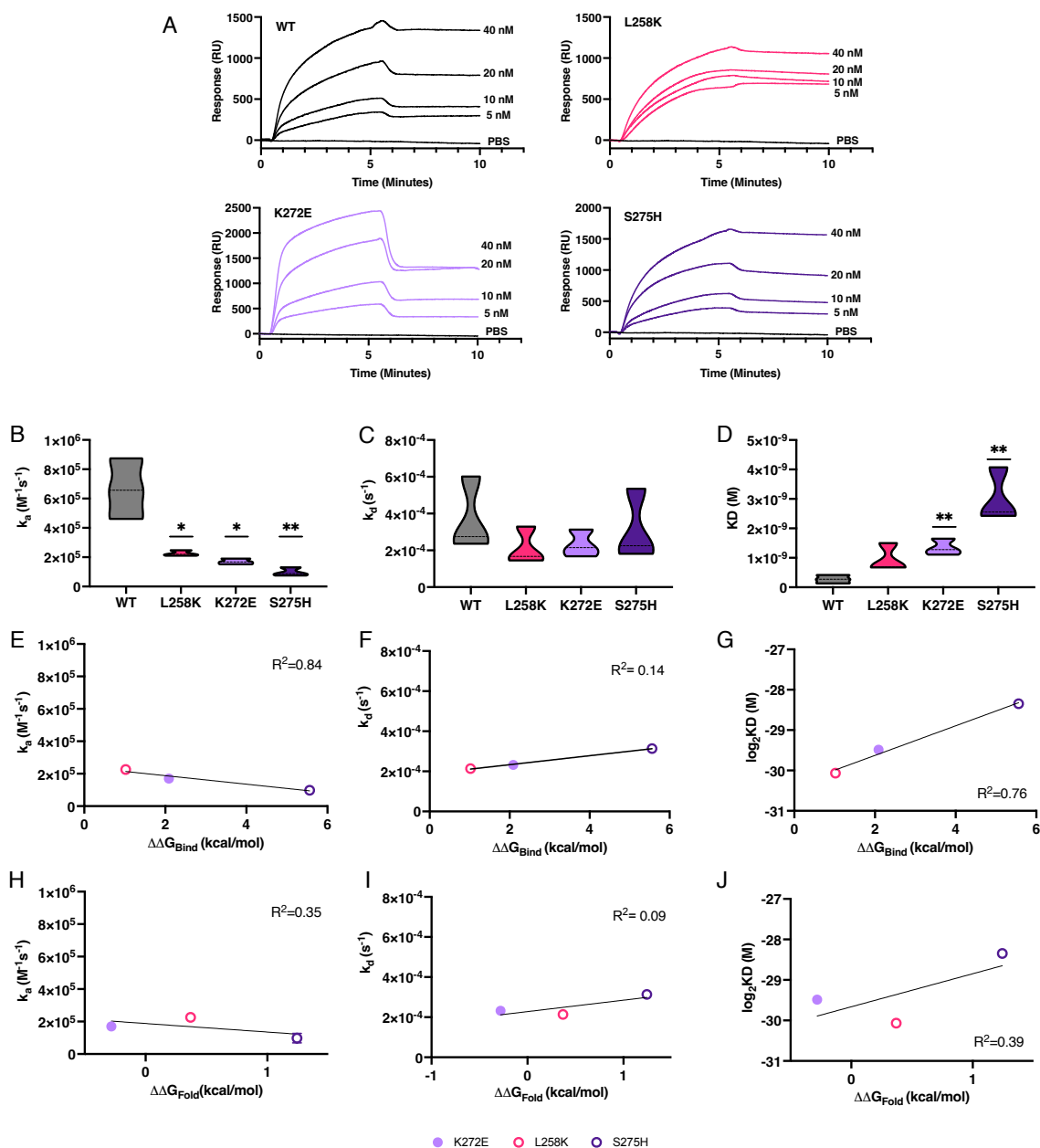
Figure 11. SPR revealed reduced on-rate as escape mechanism for variants*.*
(A) Representative SPR curves of the MARMs and motavizumab. Purified virions were flowed over motavizumab at 40 nM, 20 nM, 10 nM, and 5 nM and (B) on-rate, (C) off-rate, and (D) affinity measurements were calculated. Three independent experiments were carried out for each variant, *p <0.05; **p<0.005. Graphs of (E) on-rate, (F) off-rate, and (G) affinity and ΔΔG$_{Bind}$. Graphs of (H) on-rate, (I) off-rate, and (J) affinity and ΔΔG$_{Fold.}$

Table 6. Binding kinetics of selected variants to motavizumab.

Variant	k_a (M^{-1}s^{-1}) (x 10^4)	Fold change[#]	k_d (s^{-1}) (x 10^{-4})	Fold change[#]	KD (M) (x 10^{-10})	Fold change[#]
WT	60.1	-	4.64	-	9.2	-
L258K	22.6	-2.7	2.14	-2.2	9.56	+1.0
K272E	17.0	-3.5	2.32	-2.0	13.5	+1.5
S275H	9.8	-6.1	3.14	-1.5	30.1	+3.3

[#]Fold change values were calculated by dividing the WT value by the variant value for fold decreases (−) and dividing the value of the variant by the WT for fold increases (+).

with motavizumab is the mechanism of escape for all three variants, and S275H and K272E demonstrated a lower affinity for motavizumab. We also compared $\Delta\Delta G_{Fold}$ to the kinetics values as a negative control as we do not expect to see a correlation between the values. There was no correlation between on-rate (R=0.59, R^2 = 0.35, slope p=.09) (Figure 11H), off-rate (R=0.30, R^2 = 0.09, slope p=0.43) (Figure 11I), and KD (R=0.62, R^2 = 0.39, slope p=0.07) (Figure 11J).

3.4 Discussion

We used MDS+FoldX to predict the disruption of the binding of motavizumab to F protein. All eight of our selected variants could replicate and propagate new virus. Reduced neutralization was observed in six of the selected variants, and the six variants also demonstrated reduced binding of motavizumab via flow cytometry. Binding kinetics suggested that a reduced on-rate was the escape mechanism for the variants tested. K272E and S275H demonstrated a significant increase in KD compared to WT, which indicates a reduction of affinity for motavizumab. We empirically tested and validated the accuracy of MDS+FoldX and found that six of the eight selected variants demonstrated reduced neutralization and binding by motavizumab.

Multiple MARMs have been identified for palivizumab, and K272E was previously the only known escape variant for motavizumab (159–167, 247–249). This study utilized the co-crystal structure of F protein and motavizumab to predict novel MARM. The escape mechanism of K272E has been studied previously using purified F protein and palivizumab and found that the binding on-rate was significantly reduced (167). We replicated the previous

study's findings and determined that the reduced on-rate was also the mechanism of escape for the variants tested. In previous studies, antibody association rates have also been correlated with viral neutralization (144).

We examined the known escape MARMs for palivizumab (159–167, 247–249) and the modeling values for motavizumab (Table 7). The palivizumab MARMs had a $\Delta\Delta G_{Fold}$ below 2 kcal/mol and are expected to fold correctly. K272M, S275L, and N276Y had $\Delta\Delta G_{Bind}$ values below 0.5 kcal/mol. Previous studies have demonstrated that S275L and K272M are palivizumab MARMs, but not motavizumab MARMs (165). MDS+FoldX accurately predicted palivizumab mutants that could fold correctly. The difference in $\Delta\Delta G_{Bind}$ values was expected because there are differences in the antigen binding site of motavizumab and palivizumab. A future study may want to confirm if the palivizumab MARMs that were not tested for motavizumab neutralization are MARMs for motavizumab and test the accuracy of our modeling.

Table 7. Motavizumab and F protein $\Delta\Delta G_{Fold}$ and $\Delta\Delta G_{Bind}$ values and standard deviations for known palivizumab MARMs

Mutation	$\Delta\Delta G_{Bind}$	SD of Bind	$\Delta\Delta G_{Fold}$	SD of Fold
N262Y	2.90	3.61	-0.58	0.73
N262S	0.89	0.95	0.01	0.51
K272E	2.09	0.98	-0.28	0.59
K272M[◊]	-0.29	0.76	-0.41	0.54
K272N[◊]	1.58	0.98	0.36	0.55
K272Q[◊]	0.77	0.81	0.06	0.57
K272T[◊]	1.15	0.92	0.50	0.65
K272Y	0.67	1.49	-0.19	0.57
S275F	3.38	2.60	0.36	1.62
S275L[◊]	0.45	1.38	-1.41	0.89
N276S	0.59	0.63	0.21	0.31
N276Y	0.05	0.73	-0.09	0.44

[◊]Indicates palivizumab MARM neutralized by motavizumab, other variants were not tested
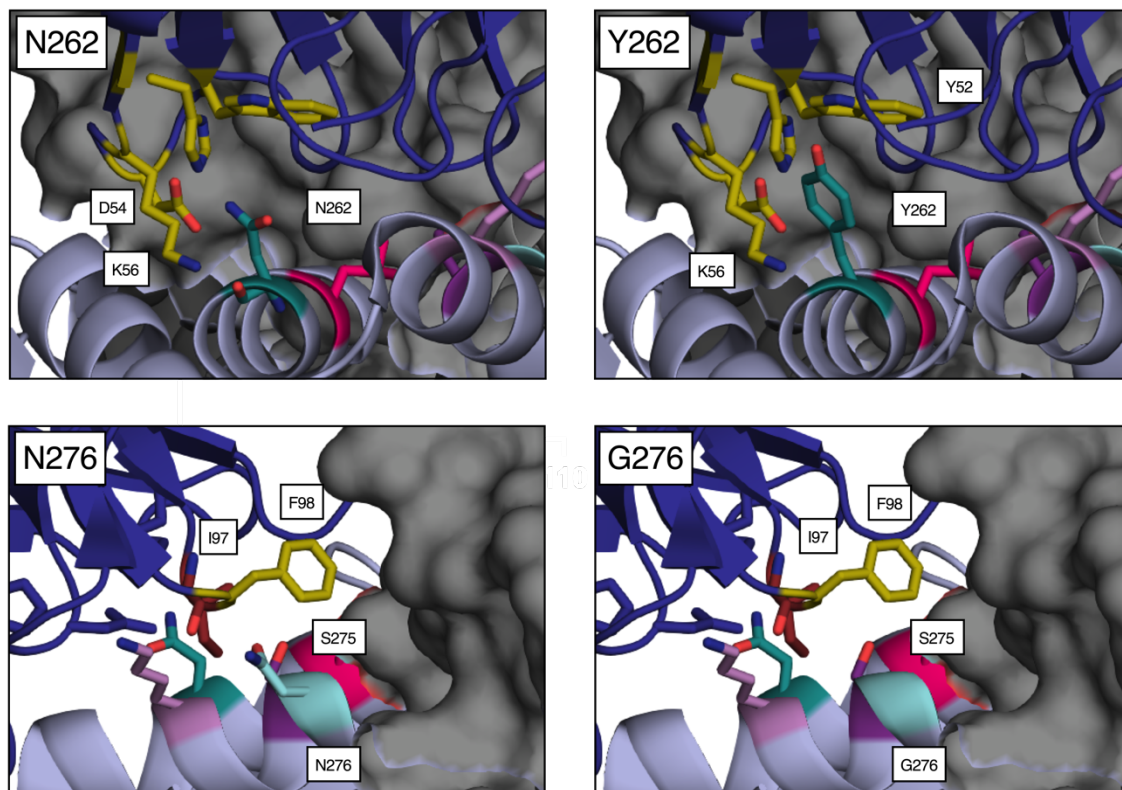
Figure 12. Interaction between motavizumab and WT or non-MARM F protein variants.
In PyMol, residues (yellow) on motavizumab (dark blue) within 4 Å of residues of interest (262: teal, 276: cyan) on F protein (light blue) were identified. N262 forms hydrogen bonds with D54 and K56 on motavizumab. Y262 could have hydrophobic interaction with Y52 on motavizumab or there could be a cation-π interaction between the Y262 and K56. N276 does not interact with motavizumab, but S275(purple) forms a hydrogen bond with the carbonyl oxygen on I97 (red). G276 would allow for more flexibility in the protein and may cause S275(purple) to interact with F98.

N262Y did not demonstrate resistance to motavizumab. The structure of N262 and Y262 may explain the increased neutralization of N262Y (Figure 12). N262 forms a hydrogen bond with D54 and K56 on motavizumab (64). Y262 could have a hydrophobic interaction with Y52 on motavizumab or form a cation-π interaction with K56. Both interactions could explain a higher affinity and the lower neutralization concentration of motavizumab that we observed. When we look at the modeling values for N262Y (2.90 kcal/mol), we expect to see a disruption of binding since the other six variants that had reduced neutralization had $\Delta\Delta G_{Bind.}$ values >1.0 kcal/mol. However, the standard deviation (3.61) indicates that the variation around the mean is large. Interestingly, the other aromatic residues modeled at 262 also have $\Delta\Delta G_{Bind}$ values >1.0 kcal/mol and large standard deviations (N262F: $\Delta\Delta G_{Bind}$: 1.12 SD: 2.93,

N262W: 2.07 SD: 3.61). Future studies could examine if the other aromatic residues are MARMs and if the modeling needs to be adjusted for aromatic residues. N276G did have some reduced neutralization compared to WT, with a 2.8-fold change in IC_{50}. N276 does not interact with motavizumab, and S275 forms a hydrogen bond with the carbonyl oxygen on I97 on motavizumab (64). The change of N276 to glycine would allow for more flexibility in the protein and may permit the interaction between S275 and F98. The S275 OH may weakly repel the hydrophobic F98 and cause a reduction in binding. The $\Delta\Delta G_{Bind}$ value for N276G was 0.5 kcal/mol, and it could be that ≤0.5 kcal/mol will not disrupt binding. A future study could investigate more variants with a $\Delta\Delta G_{Bind}$ value above, at, or below 0.5 kcal/mol to define the exact threshold value for disruption of binding.

The correlation between MFI and $\Delta\Delta G_{Bind}$ demonstrated a linear relationship. The p-value for the coefficient of determination (p=0.05) was significant. However, only ten variants were tested, and future studies should test more mutations to examine the accuracy of this correlation. As mentioned above, there could be a threshold for $\Delta\Delta G_{Bind}$ and that beyond a certain value of kcal/mol, there is disruption of binding, but it is not directly correlated to the kcal/mol value. We also examined the correlation between the binding kinetics values and $\Delta\Delta G_{Bind}$. A correlation between on-rate and $\Delta\Delta G_{Bind}$ was observed, and no correlation was observed between off-rate and $\Delta\Delta G_{Bind}$. There was a correlation between KD and $\Delta\Delta G_{Bind}$. While there was a correlation between on-rate and KD, only three variants were tested, and more would need to be tested to confirm the accuracy. We also compared the $\Delta\Delta G_{Fold}$ values as a negative control and found no correlation with on-rate, off-rate, and KD. The binding kinetics experiments highlight the difficulty of testing protein-protein interactions empirically in a high throughput methodology and the further need to validate the modeling predictions empirically.

Previously, the only known escape variant for motavizumab from clinical trials and passage experiments was K272E. Our study found five variants that had reduced neutralization to motavizumab and some with better growth kinetics than K272E. A future study could examine the emergence of K272E as the dominant mutation despite having poor replication compared to other MARMs found in this study. This study would also help determine the relevance of the predicted mutants and their likelihood of arising. Testing more variants at each predicted site would also help refine the modeling, and testing mutations outside of the direct

binding site may also reveal escape variants, as seen in other viral fusion proteins (180). In addition, testing other mAbs such as nirsevimab and other viral pathogens that use mAbs such as SARS-CoV-2 would help refine the modeling and test the accuracy of the predictions.

MDS+FoldX predicted MARMs in RSV F protein and could expedite the identification of MARMs in other viruses. Biophysical modeling has the potential for other applications, such as designing and optimizing the development of mAb. The ability to identify MARMs before the emergence of the variant in human population could allow for the development of treatments for novel variants.

3.4.1 Limitations of This Study

MDS+FoldX predicted MARMs, but a drawback of this methodology is that it requires a crystal structure of the proteins of interest. We used the motavizumab-F protein structure for our study as there is no structure for palivizumab and F protein. Cryo-EM has expedited the process of solving structures, and many of the mAbs in development for medical use have crystal structures available (148, 250). Another limitation of co-crystal structures is that the viral proteins used in laboratory settings often may not reflect the current viral population. The current circulating strain of RSV is ON1, and the prototypic lab strain is based on the A2 strain (9, 10). The F protein used in the co-crystal structure is DS-Cav1, based on the A2 strain, and has additional mutations to keep it locked in pre-fusion conformation (237). Future studies should examine current circulating strains to test the clinical relevance of the predictions, and contemporary isolates of RSV have been created using the same reverse genetics systems used in these experiments (209). MDS+FoldX is also limited because it can only calculate single-point mutations. While all identified mutations for palivizumab and motavizumab have been single-point mutations, some MARMs identified for nirsevimab have two mutations that allow the virus to escape neutralization (170). Future studies may be able to predict double mutations as advancements are made in biophysical modeling.

This experiment was limited by our inferences about the $\Delta\Delta G_{Bind}$ and $\Delta\Delta G_{Fold}$ values. We biased our experiment by assuming that proteins >2 kcal/mol $\Delta\Delta G_{Fold}$ would not fold correctly. Variants with a $\Delta\Delta G_{Fold}$ >2 kcal/mol should have been included as controls in our experiment to confirm that the threshold was accurate. The flow cytometry assay was the only assay to include variants with $\Delta\Delta G_{Bind}$ values <0.5 kcal/mol. While the data supported that a $\Delta\Delta G_{Bind}$ near 0 would behave like WT in an ideal experiment, we should have tested more

variants to confirm our assumptions. Developing a high-throughput methodology for assessing binding and folding would have been beneficial. An expression vector containing the F gene with mutations to lock the protein in pre-fusion conformation would have been useful for assessing the binding of motavizumab. Cells could be transiently transfected and assessed for F protein expression and binding through an enzyme-linked immunosorbent assay (ELISA) or flow cytometry. While we did perform a similar assay with the flow cytometry experiment, the F protein was able to transition from pre-fusion to post-fusion conformation, and motavizumab binds both conformations. It would have been more accurate to the modeling to assess binding to the pre-fusion conformation only. We only assessed viral titers over time as a measure of F protein function. A cell fusion assay using an expression plasmid with F protein and tracking the rate of syncytia formation and the size of syncytia would have been useful to assess $\Delta\Delta G_{Fold}$ as a function of F protein function. Another limitation of this study was that we focused exclusively on the F protein and how it related to the modeling. We did not consider epistasis in the viral genome that could be affecting viral fitness. Whole genome sequencing would have highlighted changes in other viral genes that may also affect viral fitness.

CHAPTER 4

Respiratory Syncytial Virus Fusion Glycoprotein Evolution is Constrained by Codons and Loss of Fitness Mutations

4.1 Overview

Monoclonal antibodies (mAbs) are important for preventing and treating viral diseases. The emergence of severe acute respiratory syndrome coronavirus 2 (SARS-CoV-2) and the coronavirus disease 2019 (COVID-19) pandemic has resulted in FDA emergency authorization use for multiple mAb therapies (131, 132, 251, 252). The FDA has approved mAbs for Ebola virus (EBOV) (129) and drug-resistant human immunodeficiency virus 1 (HIV-1) (128), and there are ongoing clinical trials for mAbs against EBOV and HIV-1 (253–256). Additional mAb treatments are in development for other viral pathogens, including herpes simplex virus 1 and 2 (135, 136, 257) and a mAb cocktail for rabies virus prophylaxis (258, 259). In 1998, the first mAb approved by the FDA for the prophylaxis of viral infection was palivizumab, which targets respiratory syncytial virus (RSV) fusion glycoprotein (F protein) (260).

RSV A2 was first discovered in children in 1961 (10) and is a prototypic strain still used in research labs. The dominant circulating strain of RSV is ON1, which was first discovered in Ontario, Canada, in 2012 (9). While there is variation between strains, many of the antigenic sites targeted by antibodies on the F protein remain conserved (3, 47, 62, 63, 65, 148). The murine mAb that would be engineered to become palivizumab was created by exposing mice to the RSV A2 strain, and hybridoma cells were produced to make mAbs (63). Further engineering of palivizumab resulted in the mAb motavizumab that targeted the same epitope as palivizumab and had a higher affinity for F protein (145). The advantage of a mAb is that it can target a particular neutralizing epitope. However, it is also a downfall in that the continuous targeting of a specific epitope places selective pressure on the virus to evolve into monoclonal antibody resistant mutants (MARMs). Resistance to palivizumab has been observed in clinical studies, empirical experiments, and surveillance studies (161–169, 247, 249, 261, 262). Many factors drive the evolution of RNA viruses. A high natural error rate per genome due to the RNA-dependent RNA polymerase is common in RNA viruses, including RSV (34, 35, 263). Selective pressure by host antibodies will also guide the evolution of viruses and has been observed in the antigenic changes of influenza A virus (IAV) over two

flu seasons (155, 264). While laboratory strains of viruses are valuable and essential tools for research labs, there are limitations in applying discoveries to the possible evolution outcomes in circulating viral populations.

Studies described in Chapter 3 found that molecular modeling could accurately predict the disruption of motavizumab binding to RSV F protein in empirical experiments. We used FoldX software combined with molecular dynamics simulations (MDS+FoldX) to estimate F protein's folding stabilities and the F protein-motavizumab interaction. Multiple MARMs exist for the motavizumab precursor, palivizumab, and nirsevimab, a mAb for RSV currently in clinical studies (151–159, 189, 191, 204, 205). Previous experiments have found one MARM for motavizumab: lysine to glutamic acid at residue 272 (K272E) (165). We confirmed that our modeling accurately predicted K272E as a MARM and found that six of the eight selected variants we tested demonstrated at least some resistance to neutralization by motavizumab (Chapter 3). In addition, we examined the fitness of the variants over time in the absence of motavizumab. We found that all eight variants had at least some deficiency in replication when compared to the wild type virus (Chapter 3). While growth curves can measure viral titers at fixed points in time, the assay is limited in that it is not sensitive enough to identify minor differences in viral titer, viral entry, and release of the virus, which could impact the success of the virus in the presence of other variants (265). Relative fitness assays have been used to examine vesicular stomatitis virus variants in populations and discern the fitness of MARMs in the presence of an antibody (266). This assay examines the relative fitness of variants by infecting a variant and a standard competitor wild type virus simultaneously in the presence or absence of mAb. Since no other MARMs have been identified for motavizumab from passage studies, we explored if the relative fitness of the variants and the genetic background of the virus would affect the likelihood of the appearance of predicted MARMs.

In this study, we passaged recombinant RSV A2 (WT) with motavizumab to select for MARMs. We examined the relative fitness of K272E and two of our previously identified MARMs with the highest fold-change in half-maximal inhibitory concentration (IC_{50}), L258K and S275H, to WT virus in the presence of motavizumab. Finally, we tested if the evolution pathway of the F protein under motavizumab selection could be altered by changing the codon of K272 to methionine to prevent the mutation to lysine. We found that the altered codon

changed the evolutionary direction of the virus and that codons are a likely predictor of whether a mutation will occur in relation to molecular modeling predictions.

4.3 Results

4.3.1 K272E was the only motavizumab MARM that arose during selective passage experiments.

We first examined if any other MARM for motavizumab would arise in passage experiments since a previous study had only found K272E (165). We started by passaging 0.03 multiplicity of infection WT with a subinhibitory concentration of motavizumab (0.25 µg/mL) for passage 1. In subsequent passages, supernatant media from the previous passage was diluted 1:10 and allowed to infect new cells in the presence of motavizumab. At passage five, Sanger sequencing of the F gene revealed only K272E (AAG→GAG). We hypothesized that other mutations could be present before K272E dominated the population at earlier passages. Next-generation sequencing (NGS) was used to sequence the F gene from passages 1 and 2 and passage 5 from a control virus passaged without motavizumab. We chose to sequence the F gene and not the entire genome because we were only interested in F protein variants as it related to our modeling.

Passage 1 had 352,197 reads that could be mapped back to the F gene, and passage 2 had 341,374 reads. The control passage had 347,268 reads mapped back to the F gene. Control passage 5 was used to establish the background mutation rate, and there were no single nucleotide polymorphisms (SNP) above 1% difference from the WT F gene (Figure 13). No SNP above 1% was present in passage 1 with motavizumab (Figure 13). Passage two had a synonymous mutation at L273 and K272E emerged as the only non-synonymous SNP (Figure 13, Table 8). K272E went from a very low frequency in passage 1 (0.1%) to detectable in passage 2 (6.6%). The selection coefficient for K272E was 0.128 between passage 1 and passage 2, which implies that the K272E mutation was beneficial under selective conditions.

4.3.2 Relative fitness of MARMs varied in the presence and absence of motavizumab.

Our previous study identified MARMs for motavizumab utilizing molecular modeling and empirical experiments. Since no other MARM besides K272E has been identified from passage experiments, we tested two of our identified MARMs with the highest fold-change in IC_{50} (L258K and S275H) and K272E against WT to test the relative fitness of the variants with
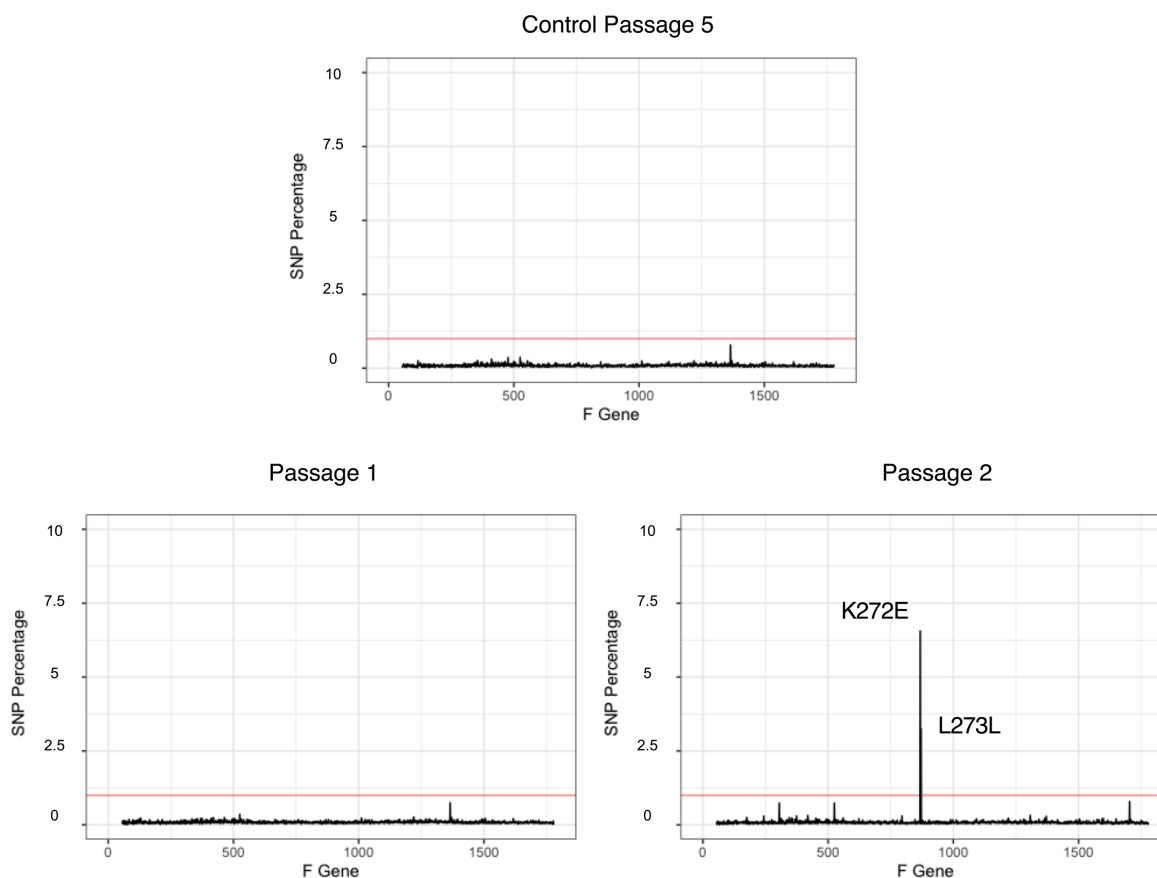
Figure 13. Next-generation sequencing revealed K272E as an emerging variant in early passages of WT virus with motavizumab.
Passage experiments were performed with motavizumab (0.25 mg/mL), and a control virus was passaged five times in the absence of mAb. Next-generation sequencing was performed on the F gene, and SNP frequency was calculated at each nucleotide. No SNP above 1% (denoted by the red line) for control passage 5 or passage 1, and K272E and L273L arose in passage 2.

Table 8. Mutations present in passage 2 of WT passaged with motavizumab.

Residue	Nucleotide Change	Amino Acid Change	Mutation	Percent of population
K272	AAG→GAG	E	Nonsynonymous	6.6
L273	TTA→CTA	L	Synonymous	3.2

and without motavizumab. WT and MARM viruses were incubated at an equal concentration with 0.25 μg/mL motavizumab prior to infection, and the virus was allowed to infect HEp-2 cells for one hour. The concentration of motavizumab was selected because it is the IC_{50} of WT, and anything higher may have been too inhibitory for WT virus. Media containing motavizumab was added following washing of the cells. Passages were performed every 48 hours for three passages for three independent replicates. A control experiment was run concurrently with no mAb. NGS was performed on the part of the F gene that encompassed the site II epitope because we were interested in tracking the mutants of interest in the site II epitope.

WT became dominant in the untreated replicates (Figure 14A, C, and E). Interestingly, in K272E+WT replicate passage 1, a MARM we identified in a previous study, L258E, emerged from the WT background but disappeared by the second passage (Figure 14A). K272E remained in the population for all three replicates of WT+K272E without motavizumab but did not maintain a dominant presence and the population size by read count was consistent through the passages (Figure 14A, Table 9). There were also minor variants present (Table 10). The selection coefficients for all three replicates were negative for K272E by the third passage and indicated that the variant is selected against in the absence of motavizumab (Table 11). In the K272E+WT+mAb replicates, K272E became the dominant variant by passage three for all three replicates, and there were also minor variants present (Figure 14B, Table 10). In replicate 2, there was a decrease of K272E, but the population became predominantly K272E by the third passage. The drop in K272E also correlated with a drop in read counts in replicate 2 passage 2 and a drop in selection coefficient for K272E (Tables 9 and 11). The selection coefficients for K272E in the K272E+WT+mAb experiments were greater than zero except for replicate 2 passage 2 implying that K272E was beneficial under motavizumab selection (Table 11). K272E was the dominant mutation and has increased fitness in the presence of motavizumab compared to WT.

L258K maintained a minor presence in the WT+L258K untreated passages for all three replicates and was selected against in the absence of motavizumab (Figure 14C, Table 12). Replicate 2 passage 3 was the only non-motavizumab passage with other variants (Figure 14C, Table 10). The selection coefficients were negative except for replicate 1 passage 3, which implied that L258K was selected against in the absence of motavizumab. In the L258K+WT+

Figure 14. Viral populations revealed a loss of dominance in non-selective conditions for all MARMs and variable persistence in the population in motavizumab conditions.
Equal proportions of WT and a MARM were incubated in the presence and absence of motavizumab prior to infection. The virus was allowed to infect for one hour before rinsing twice with PBS and replacing media with or without motavizumab. The virus was passaged every 48 hours for three passages. K272E and WT (A and B), L258K and WT (B and C), and S275 and WT (E and F) were tested, and a segment of the F gene containing the site II epitope was sequenced using next-generation sequencing.

Table 9. Number of next-generation sequence reads from relative fitness assays.

Replicate	Passage 1	Passage 2	Passage 3
K272E + WT 1	31671	16845	24622
K272E + WT 2	21172	10789	16134
K272E + WT 3	17018	24432	22093
K272E + WT + mAb 1	18579	18653	27020
K272E + WT + mAb 2	32242	1014	3714
K272E + WT + mAb 3	33648	15182	18208
L258K + WT 1	16504	13067	8922
L258K + WT 2	19553	6043	8323
L258K + WT 3	18920	31870	15827
L258K + WT + mAb 1	7403	1684	9325
L258K + WT + mAb 2	4513	2109	2374
L258K + WT + mAb 3	15323	4	3563
S275H + WT 1	12191	14009	6297
S275H + WT 2	10846	6266	2512
S275H + WT 3	15389	8865	15026
S275H + WT + mAb 1	19384	3336	2455
S275H + WT + mAb 2	12033	4414	717
S275H + WT + mAb 3	18409	2360	4411

Table 10. Minor variants <3% of the population present in the relative fitness assays

Viruses	Replicate	Passage	Variants
WT + K272E	1	1	**N276G**, **N262Y**, **L258K**/Q279K, **L258K**/R336I
WT + K272E	1	3	N268K/**K272E**, N268H, T335A
WT + K272E	2	1	D269N
WT + K272E	2	2	E294K, L316P
WT + K272E	3	3	E328V, S285N, **K272Q**, T335I, G329R, C313S
WT + K272E + Motavizumab	1	1	**K272E**/C333R, **K272E**/C343G, **K272E**/Y342H,
WT + K272E + Motavizumab	1	2	T244V/**K272E**
WT + K272E + Motavizumab	1	2	**K272E**/D344N,
WT + K272E + Motavizumab	2	1	**K272E**/D338N, **K272E**/D263Y
WT + K272E + Motavizumab	2	2	D310Y, G307C
WT + K272E + Motavizumab	3	2	**K272E**/N325D
WT + K272E + Motavizumab	3	3	**K272E**/E294K
WT + L258K + Motavizumab	2	3	S248R
WT + L258K + Motavizumab	1	1	**L258K**/V281A
WT + L258K + Motavizumab	1	3	**K272E**/D338N, Y250H/**L258K**, V243A, **K272E**/Q279R
WT + L258K + Motavizumab	3	1	V296F, E256STOP, **L258K**/S319F
WT + L258K + Motavizumab	3	3	G347R, V278A, M289L
WT + S275H	1	1	G242C, L260F/**S275H**
WT + S275H	1	2	**T253T/N262S**, **S275H**/C333R
WT + S275H	2	1	A298V
WT + S275H	3	1	G329W, **S275H**/I280K
WT + S275H	3	3	**S275H**/C343F, K272R, **K272E**, P304L, Y286C
WT + S275H + Motavizumab	1	1	Y299S
WT + S275H + Motavizumab	1	3	**K272E**/C333R
WT + S275H + Motavizumab	3	1	**S275H**/V247I, K272R/**S275H**, Q270K
WT + S275H + Motavizumab	3	2	A241V/**K272E**, T323A
WT + S275H + Motavizumab	3	3	**L258K**/Q270R

Bolded residue changes indicate a $\Delta\Delta G_{Bind} > 0.5$ kcal/mo

Table 11. Selection coefficients for K272E in relative fitness assays treated with and without motavizumab.

Replicate	Passage	K272E
K272E + WT 1	1	-0.082
K272E + WT 1	2	0.051
K272E + WT 1	3	-0.027
K272E + WT 2	1	-0.004
K272E + WT 2	2	0.003
K272E + WT 2	3	-0.071
K272E + WT 3	1	-0.014
K272E + WT 3	2	-0.024
K272E + WT 3	3	-0.034
K272E + WT + mAb 1	1	0.063
K272E + WT + mAb 1	2	0.058
K272E + WT + mAb 1	3	0.007
K272E + WT + mAb 2	1	0.061
K272E + WT + mAb 2	2	-0.149
K272E + WT + mAb 2	3	0.582
K272E + WT + mAb 3	1	0.072
K272E + WT + mAb 3	2	0.046
K272E + WT + mAb 3	3	0.072

mAb passages, L258K was a major variant for the first passage for replicates 1 and 3, was undetected in passage 2, and returned as a minor variant in passage 3 (Figure 14D). The loss of L258K in replicates 1 and 3 passage 2 also correlated to a decrease in reads (Figure 14, Table 9). Replicate 2 lost L258K by passage 2, and WT became dominant (Figure 14D). K272E emerged by passage 3 for replicates 1 and 3, and other minor variants were present in the L258K replicate 1 and replicate 3 motavizumab treated passages (Figure 14D, Table 10). The selection coefficients for L258K under motavizumab in passage 1 for all three replicates were greater than zero, which implied that the mutation was beneficial (Table 12). However, in subsequent passages for replicates 1 and 2 the selection coefficients were negative suggesting that the mutation is deleterious in the presence of motavizumab. The selection coefficient for replicate 3 passage 3 was positive, but this also correlated to a reduction in reads in passage 2 to an increase in reads in passage 3 (Tables 9 and 12). The selection coefficients for K272E in the L258K+WT+mAb were positive, indicating it was a beneficial mutation under motavizumab selection (Table 12). L258K was less fit than WT in the presence of motavizumab.

S275H remained in two of the three S275H+WT replicates, but WT remained dominant (Figure 14E). Replicate 2 passage 3 only had WT present, but there was a reduction in reads (Figure 14E, Table 9). Other variants were present in all three replicates of the untreated S275H (Figure 14E, Table 10). S275H was selected against in passage 1 for all three S275H+WT replicates (Table 13). It was selected against in passage 2 for replicates 1 and 3, but selected for in replicate 2 which correlated with a drop in reads (Tables 9 and 13). The selection coefficients S275H were positive for replicate 1 and 3 passage 3 and negative for replicate 2 passage 3 (Table 13). S275H does not appear to be a beneficial mutation in the absence of motavizumab. All three S275H+WT+mAb passages had the emergence of K272E by the third passage and a double mutant, A271V/K272E, in replicate 3 passage 2 (Figure 14F). S275H was the MARM selected for two passages in replicates 1 and 3, but K272E became the selected variant in replicate 1 and WT in replicate 3 by passage 3 (Figure 14E). S275P became the dominant variant in replicate 2 passage 2 but was undetectable by passage 3 (Figure 14F). The loss of S275P also correlated with a reduction in the number of reads (Figure 14F, Table 9). Remarkably, S275P was not a predicted MARM identified in the modeling parameters of Chapter 3 since it was not predicted to fold correctly and was not predicted to disrupt binding

Table 12. Selection coefficients for L258K and K272E in relative fitness assays treated with and without motavizumab.

Replicate	Passage	L258K	K272E
L258K + WT 1	1	-0.029	0
L258K + WT 1	2	-0.006	0
L258K + WT 1	3	0.003	0
L258K + WT 2	1	-0.025	0
L258K + WT 2	2	-0.010	0
L258K + WT 2	3	-0.031	0
L258K + WT 3	1	-0.024	0
L258K + WT 3	2	-0.001	0
L258K + WT 3	3	-0.003	0
L258K + WT + mAb 1	1	0.015	0.428
L258K + WT + mAb 1	2	-0.462	0.108
L258K + WT + mAb 1	3	0.356	0
L258K + WT + mAb 2	1	-0.028	0
L258K + WT + mAb 2	2	-0.432	0
L258K + WT + mAb 2	3	-0.007	0
L258K + WT + mAb 3	1	0.004	0
L258K + WT + mAb 3	2	-0.087	0
L258K + WT + mAb 3	3	0.031	0.036

Table 13. Selection coefficients for S275H, K272E, and S275P in relative fitness assays treated with and without motavizumab.

| Replicate	Passage	S275H	K272E	S275P
S275H + WT 1	1	-1.420	0.000	0.000
S275H + WT 1	2	-0.001	0.000	0.000
S275H + WT 1	3	0.001	0.000	0.000
S275H + WT 2	1	-0.755	0.000	0.000
S275H + WT 2	2	0.001	0.000	0.000
S275H + WT 2	3	-0.456	0.000	0.000
S275H + WT 3	1	-1.193	0.000	0.000
S275H + WT 3	2	-0.018	0.000	0.000
S275H + WT 3	3	0.015	0.000	0.000
S275H + WT + mAb 1	1	0.977	0.000	0.000
S275H + WT + mAb 1	2	-0.012	0.000	0.000
S275H + WT + mAb 1	3	-0.285	0.494	0.000
S275H + WT + mAb 2	1	2.038	0.000	0.000
S275H + WT + mAb 2	2	-0.319	0.000	1.069
S275H + WT + mAb 2	3	0.000	0.494	-0.900
S275H + WT + mAb 3	1	0.864	0.000	0.000
S275H + WT + mAb 3	2	-0.015	0.000	0.000
S275H + WT + mAb 3	3	-0.279	0.393	0.000
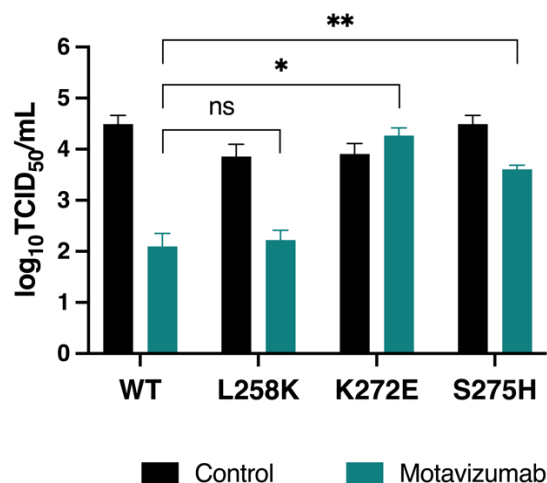
Figure 15. Viral titers at 48 hours in the presence and absence of motavizumab.
WT or variant RSV was incubated with 0.25 μg/mL of motavizumab for 30 minutes prior to infecting HEp-2 cells. The virus was allowed to infect for one hour, removed, washed twice with PBS, and media with or without motavizumab was added. Supernatant media was harvested at 48 hours and titrated by $TCID_{50}$ assay. Three independent experiments were carried out. *p <0.05; **p<0.005.

of motavizumab. Other variants were present in all three motavizumab treated replicates (Table 10). S275H was initially a beneficial mutation in the first passage for all three S275H+WT+mAB replicates (Table 13). By passage 2, the selection coefficient was negative for all three replicates, which also correlated with a drop in read count (Tables 9 and 13). S275P emerged in replicate 2 of S275H+WT+mAb passage 2 and was a beneficial mutation but was a deleterious mutation in passage 3, which also correlated with a decrease in reads (Tables 9 and 13). The selection coefficient for K272E in passage 3 for all three replicates was positive, indicating the mutation was beneficial under selection (Table 13). S275H was not a beneficial mutation in the presence of motavizumab by passage 3 (Table 13). S275H was selected for initially, but K272E was the more beneficial mutation in the presence of motavizumab.

We examined the number of transversions and transitions for the segment of the F gene we surveyed for all the replicates and passages and found that there were 44 transitions, 32 transversions, and 1 transition/transversion.

L258K did not sustain a dominant presence in the motavizumab passages, and K272E emerged in two of the three replicates. K272E is a more fit MARM than L258K in the presence of motavizumab because it has a larger IC_{50} and greater loss of binding in kinetics studies (165, 167, Chapter 3). L258K also has delayed detection of virus when compared to WT and K272E and reduced viral titers over time compared to WT in the absence of motavizumab (Chapter

3). To assess fitness under selective pressure, we compared viral titers at 48 hours between the variants and WT in the presence and absence of motavizumab. The virus was incubated with or without motavizumab for one hour before infection, and viral titers were measured 48 hours post infection. There was no significant difference in viral titers between WT and L258K in the presence of mAb, but there was a significant difference between WT and S275H and WT and K272E (Figure 15). The lack of difference in viral titers between WT and L258K and the selection coefficients of L258K in the motavizumab relative fitness assays indicate it is unlikely to arise during motavizumab selection.

4.3.3 Substitution of lysine with methionine at residue 272 allowed a novel MARM to emerge.

K272E was the dominant mutation in passage experiments and emerged in the relative fitness assays under selective pressure by motavizumab. We hypothesized that codons were biasing the evolution of K272 to glutamic acid (Figure 16). The lysine codon at K272 is AAG in the WT recombinant virus and only requires one nucleotide change to mutate to glutamic acid (GAG). In contrast, L258K, L258E, S275H, and S275R require at least two nucleotide changes to get to the resistant mutation (Figure 16A). N262D only requires one nucleotide change like K272E (Figure 16A). Our next hypothesis was that changing the codon to another amino acid would change the evolution pathway and allow other MARMs to emerge. A synonymous mutation at K272 would not remedy the bias as both codons for lysine (AAA/AAG) are one step mutations to either of the glutamic acid codons (GAA/GAG). We needed to identify a mutation with a similar growth fitness to WT and was also neutralized by motavizumab, which would require two mutations to change to glutamic acid. A previous study identified palivizumab MARMs with a similar growth pattern to the parental strain but were not motavizumab MARMs (165). We selected K272M (AAG→ATG) as the mutant to test because it would require two nucleotide changes to evolve to E272 and may remove the bias towards K272E and allow for other MARMs to emerge (Figure 16A).

We analyzed fitness and neutralization by motavizumab after engineering K272M into rRSV (Figure 16B and C). There were no significant differences between the growth of K272M and WT viruses. There was a difference in IC_{50} values between WT and K272M, where K272M was neutralized at a lower concentration of motavizumab (Figure 16C). After confirming that K272M had a similar fitness in growth as WT, we passaged the virus five times
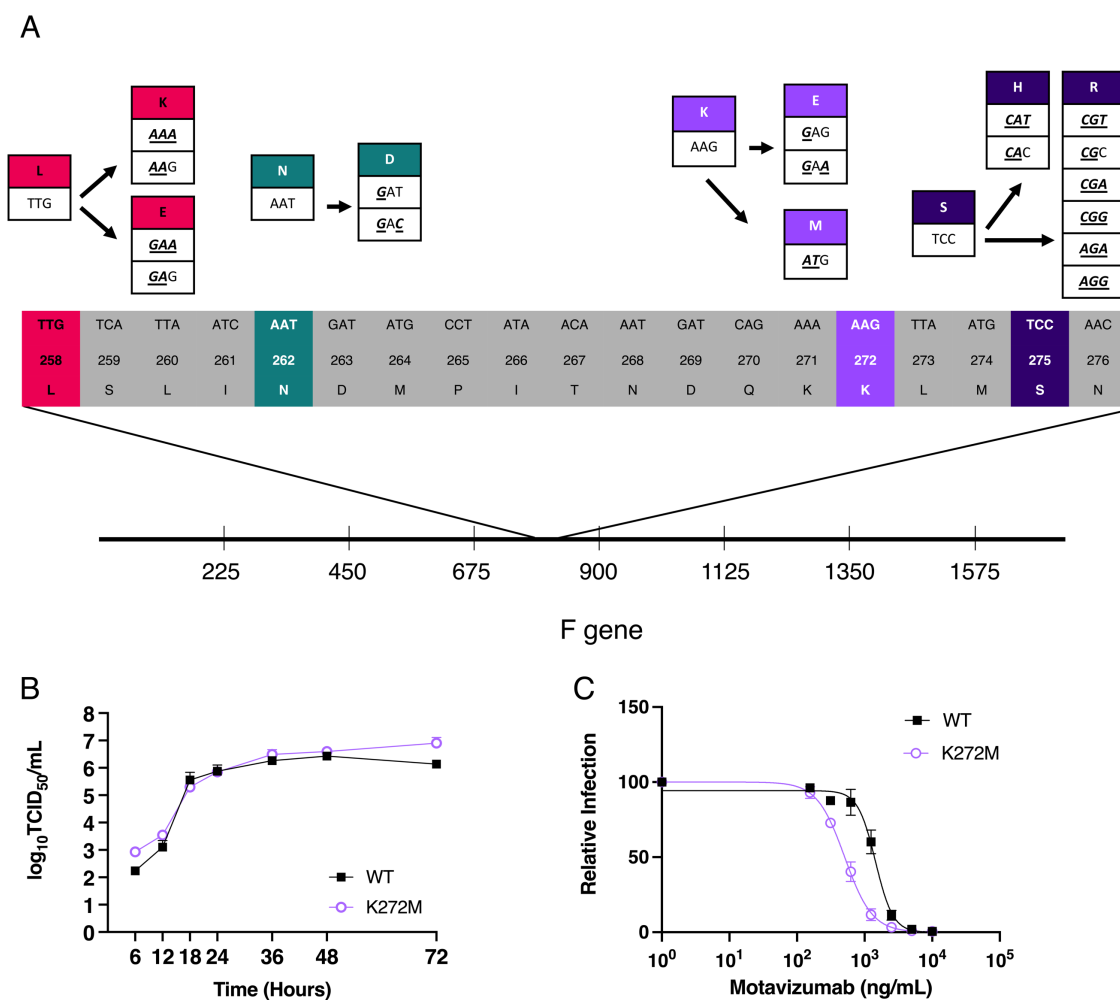
Figure 16. Replication of K272M was similar to WT and was neutralized by motavizumab.
(A) Diagram of F gene and codons at the sites of interest. Arrows indicate mutations from the current codon to variant codon for identified MARMs. (B) Growth curve of WT and K272M. No significant difference was observed between the viral titers of WT and K272M. (C) Neutralization curve for WT and K272M. K272M and WT were fully neutralized by motavizumab (10μg/mL). All experiments represent three independent replicates.
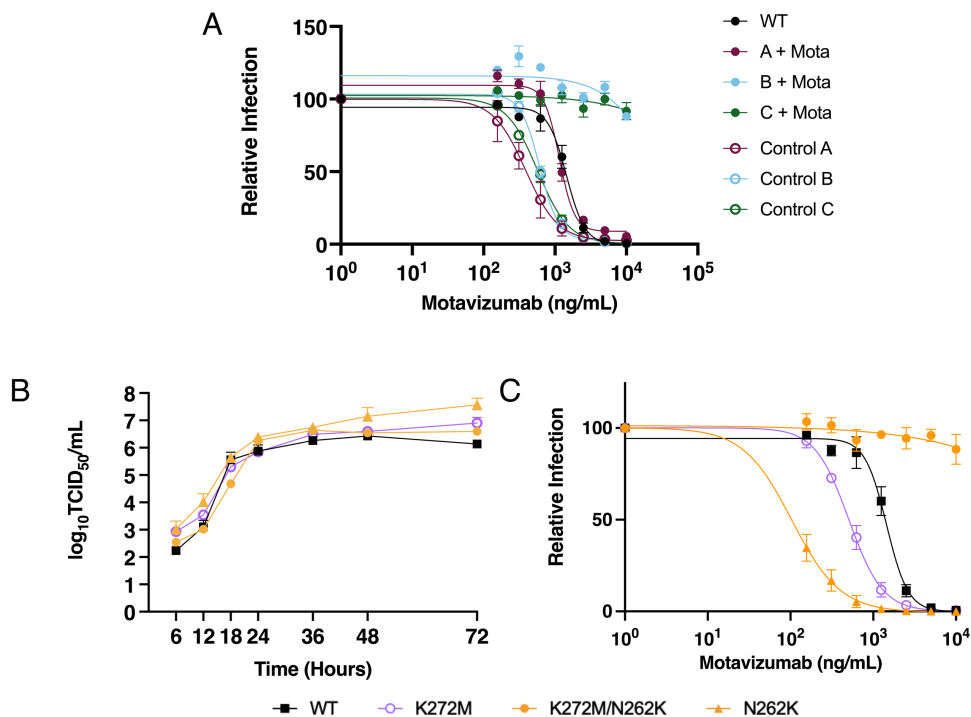
Figure 17. Passage experiments revealed novel MARM with growth similar to WT.
(A) Passage 5 for all lines was tested for neutralization by motavizumab by incubating the virus with a 2-fold serial dilution of motavizumab one hour prior to infection, and cells were counted by flow cytometry at 18 hours post infection. Replicates B + Motavizumab (Mota) and C + Mota were not neutralized at the maximum concentration of motavizumab (10μg/mL). A + Mota was neutralized similar to WT. (B) Growth curves of viral variants. The isolated K272M/N262K variant had similar viral titers over time compared to WT. (C) Neutralization assays were performed as described above for all variants. K272M/N262K was not neutralized at the highest concentration of motavizumab used (10μg/mL) and N262K was inhibited at a lower concentration of motavizumab than WT. Three independent replicates were carried out for all experiments except the growth curve for N262K, which had two replicate experiments.

Table 14. Mutations present in K272M passage experiments with and without motavizumab.

Virus Line	Mutation
A	M272K
B	N262K
C	N262K
Control A	No change
Control B	No change
Control C	No change

in the presence of 0.25 µg/mL of motavizumab in triplicate. Passage 5 for all three replicates (A, B, and C) was tested for neutralization and sequenced using the Sanger method (Figure 17, Table 14). Replicate A had a neutralization pattern similar to WT and replicates B and C could not be neutralized at the highest concentration of motavizumab (10 µg/mL) (Figure 17A). A novel escape variant, K272M/N262K, was identified in replicates B and C. Replicate A had a reversion of M272K back to the WT codon. When K272M was passaged five times without motavizumab (Controls A, B, and C), no mutations occurred, and the virus retained neutralization by motavizumab (Figure 17A, Table 14).

We isolated the virus from B passage 3 by plaque purification and sequenced by Sanger method to confirm K272M/N262K as the only mutations in the F gene and then tested for growth and neutralization by motavizumab. K272M/N262K had no significant changes in growth when compared to WT or K272M (Figure 17B and C). The IC$_{50}$ for K272M/N262K could not be determined as it was not neutralized by the highest concentration of motavizumab (10 µg/mL), similar to K272E (Chapter 3). Next, we created the single mutant, N262K, in rRSV using site-directed mutagenesis and tested the growth of the variant and neutralization by motavizumab. N262K had a growth pattern similar to WT (Figure 17B) and was more neutralized by motavizumab than WT and thus is not a MARM unless it is in combination with K272M (Figure 17C).

4.4 Discussion

K272E was the only MARM found in the passage experiments and was a beneficial mutation in the presence of mAb. In addition, K272E evolved multiple times in the relative fitness assay for the other variants. We determined that a codon can impact the evolutionary pathway of the F protein for RSV. Changing K272 to methionine altered the trajectory of the evolution of rRSV under motavizumab selection, which resulted in a novel MARM, K272M/N262K. K272M/N262K had similar growth to WT and was not neutralized at the highest concentration of antibody used. Codons and order of mutations are likely to impact whether MARMs predicted by molecular modeling will appear under selective conditions.

K272E swept the population in the presence of motavizumab in the relative fitness assay and evolved in the L258K and S275H motavizumab treated replicates. None of the three variants maintained a significant presence in the population in the absence of motavizumab.

Studies have found similar results that in the absence of mAb selective pressure MARMs were unable to maintain a significant presence but became the dominant variant in the presence of the antibody (165, 170, 224). Our previous experiments revealed a significant reduction in viral titers over time by L258K compared to WT and an increase in IC_{50} compared to WT (Chapter 3). In the relative fitness assay, L258K was not a more fit variant in the presence of motavizumab, and K272E emerged in two replicates. A reasonable conclusion is that despite L258K having an increase in IC_{50}, it is not enough to overcome the deficiency in viral replication and cannot maintain a presence in a population under selective pressure. S275H was selected for in the relative fitness assay in the presence of motavizumab before the emergence of K272E. A study found that RNA virus quasispecies populations can suppress MARM variants that may be more fit unless the virus is seeded at a certain threshold to surpass the rest of the population (230). This may explain why we do not see the emergence of S275H in passage studies and loss of the variant in the relative fitness assays. A future study could examine the relative fitness between S275H and K272E to elucidate the exact differences between the fitness of the mutants.

The emergence of L258E in K272E+WT replicate 1 passage 1 was unexpected. Contamination was ruled out as a cause for L258E as the same viral preparations were used for all three experiments, and preparations for PCR were performed in a laboratory that does not use RSV. It is possible that mutations could arise from PCR amplification of the F gene; however, given the frequency versus the mutational rate of polymerase, it seemed unlikely. We also only measured a small region of the F gene, so it is possible that other mutations could have been occurring within the F gene or viral genome that allowed this mutation to appear.

The relative fitness assays only used one concentration of virus and motavizumab. The study used a subinhibitory concentration of motavizumab for WT that allowed for WT to remain in the population. If a higher concentration of motavizumab was used it might have allowed S275H and L258K to outcompete WT. Future studies could address different concentrations of motavizumab and the fitness outcomes for the variants and WT. In addition, the concentration of virus and ratio of the viral population at the start of the experiment have been shown to affect the outcome of the populations (265). Viral population size influences viral evolution in that the survival or elimination of a variant in a population is proportional to the population size (221). When population sizes are kept small, the fitness landscape remains

flat, and when the population is large, there is an increase in the fitness landscape (224). This was seen in the relative fitness assays, where when there was a drop in the number of reads, there was also a loss of MARM variants (Figure 14B and D, Table 9). Future studies should examine different concentrations and ratios of variants to examine how that affects the fitness of the MARM variants. There was also the emergence of more variants in the relative fitness assays than in the first passage experiment with just WT. One possible explanation is that the genetic background was closer to being a quasispecies rather than a clonal background. A study found that switching the low fidelity, viral RNA-dependent RNA polymerase (RdRp) for a high fidelity polymerase in poliovirus allowed the virus to replicate like wild type poliovirus, but it was unable to adapt to adverse conditions (267). The lack of genetic diversity resulting from the typical errors of viral RdRp reduced the genetic diversity and was a detriment to the viral population in the poliovirus study. An increase in genetic diversity in the viral population could explain why we saw more variants in the relative fitness assays than in the passage experiments. It has been hypothesized that viral quasispecies have many potentially beneficial mutations at the population level that allow for a greater probability of adaptation (218–220). We only surveyed the F gene and a section of the F gene for the passage experiments and relative fitness assays. While our study focused on the modeling of the F protein and the interaction with motavizumab, there is always the possibility of epistatic changes elsewhere in the RSV genome that could affect viral fitness. Synergistic epistasis between different genes has been observed in other viruses (268–271) and could account for fitness.

Evolution can be constrained by epistasis and specific mutations can rely on previous mutations to be tolerated (272, 273). John Maynard Smith used a word model for understanding protein evolution by converting WORD to GENE with only using valid words in between: WORD→WORE→GORE→GONE→ GENE. The D must be changed to an E before the W is changed to a G since GORD is not a valid word (274). The same applies to protein evolution in that mutations must happen in a specific order for the protein to remain functional. In the research by Gong et al., they determined that mutations in the nucleoprotein of IAV must follow a particular trajectory to compensate for deleterious mutations (272). Similarly, Harms and Thornton recreated the evolution of the specificity of glucocorticoid receptor (273). The study focused on historical contingency of protein evolution and the order of mutations. The authors found that permissive mutations were required before change of

function mutations. Permissive mutations are mutations that allow for subsequent mutations to be tolerated. The change of function mutations were contingent on the permissive mutations and the authors found that permissive mutations were a rare occurrence. The emergence of N262K only happened with the initial mutation of K272M. One possible explanation is that the K272M was required as an epistatic change before the N262K mutation. This is further reinforced by the evidence that N262K as a single mutation was not a MARM and was neutralized at a lower concentration of motavizumab than WT.

The structure of the protein after the mutations also supports the requirement of epistatic mutations. The WT and variant residues were modeled in PyMol and the interaction with residues within 4 Å were identified (Figure 18). In WT, K272 and an asparagine on the antibody interact and H bonds form between N262 and the antibody (Figure 18B)(64). Non-polar M272 interacts with aromatic rings on the antibody, which probably results in a more stable interaction between the antibody and protein than lysine and the aromatic rings (Figure 18C). This interaction could account for the lower IC_{50} for M272 because the antibody has a higher affinity due to the interaction of the hydrophobic residues. N262K could interact with tryptophan and form a cation-π interaction, which could account for a higher affinity and the lower neutralization concentration of motavizumab (Figure 18D). An additional reason that there is a lower neutralization concentration for N262K is that there are three lysines (K262, K271, and K272) located in close proximity that could be interacting and the repulsion of the positive charges could open the protein exposing hydrophobic residues on F protein allowing for interaction with the hydrophobic residues on motavizumab (Figure 18D). K262/M272 can come within 3.3 Å of each other and the positive lysine could be attracted the methionine (Figure 18E). This interaction could stabilize K262by keeping it from interacting with K271 and the positive charge of the K262 could repulse the aromatic rings on motavizumab (Figure 18E).

The evolution of K272 to glutamic acid has a gain of fitness in the presence of motavizumab, and K272M has a loss of fitness (Figure 19). The pathway to get to K272M/N262K first requires a loss of fitness but ultimately results in a gain of fitness over K272E as K272M/N262K has no reduction in growth compared to WT and is not neutralized by the highest concentration of motavizumab (Figures 17B and C). However, the likelihood of the mutation of K272M as a permissive mutation is low given that it results in a loss of fitness
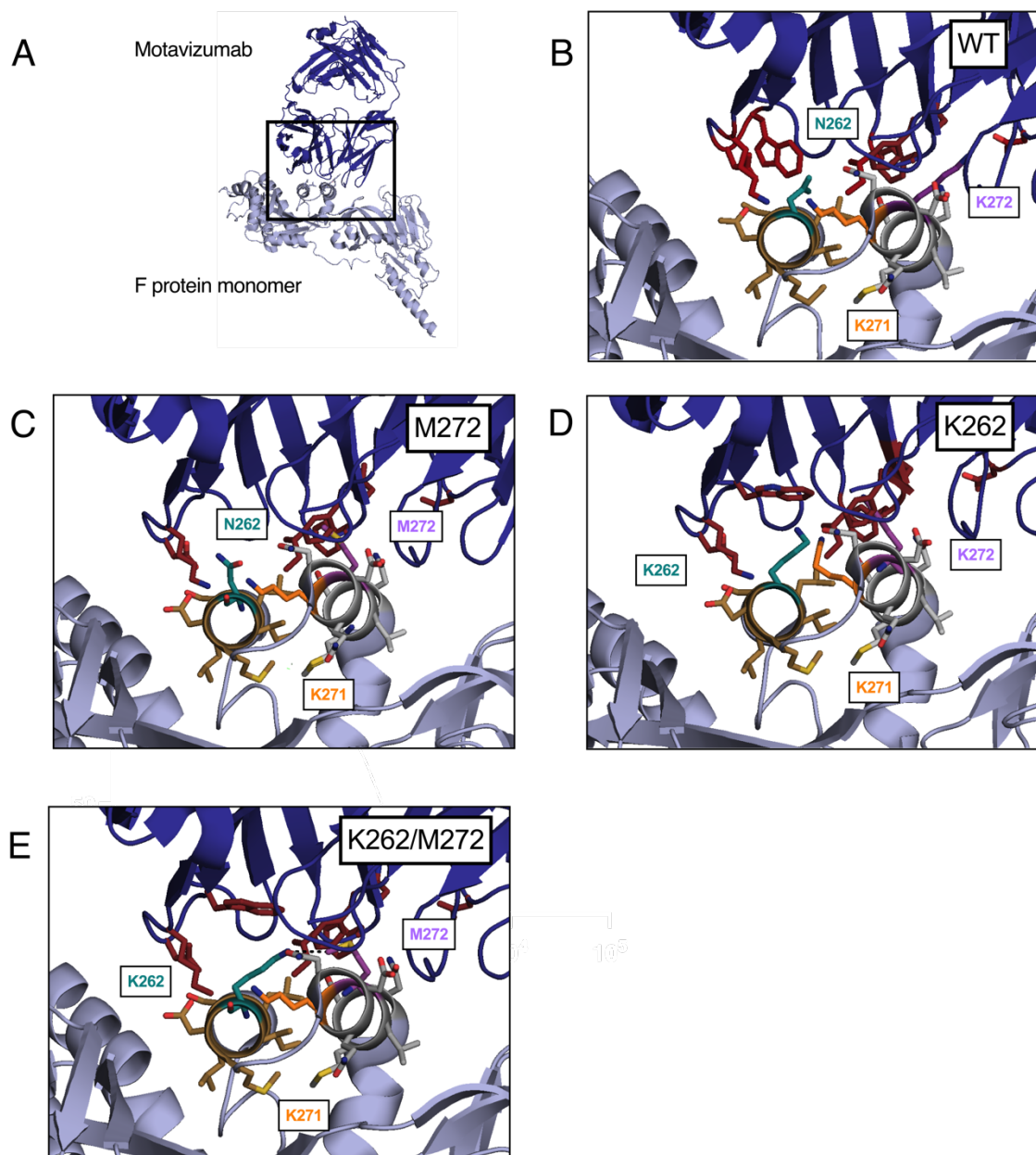
Figure 18. Motavizumab interaction with F protein variants.
(A) F protein monomer (light blue) and motavizumab (dark blue) (PDB: 4ZYP). Residues within 4 Å of 262 (gold side chains) and 272 (grey side chains) were identified in PyMol. K271 (orange) is within 4 Å of 262 and 272 and residues on motavizumab within 4 Å of 271 and 272 are colored red. Mutations were made using the mutagenesis function. (B) WT F protein monomer and motavizumab. (C) M272 F protein monomer and motavizumab. (D) K262 F protein monomer and motavizumab. (E) K262/M272 F protein monomer and motavizumab. The black dotted line indicates 3.3 Å between K262 and M272.

in the presence of motavizumab and therefore makes the emergence of K272M/N262K unlikely to occur. N262K is also not likely to arise under the selective pressure of motavizumab as it also has a loss of fitness since it was more neutralized than WT (Figure 17C and Figure 19).

Our passage studies of WT resulted in the emergence of K272E as the only variant. The M272 variant allowed for the emergence of N262K since it required two nucleotide changes to mutate from lysine to glutamic acid. When we examine isolated strains from surveillance studies in the past seven years (35, 209, 261, 275–282) and look at the codons at our sites of interest for our previously identified MARMs from Chapter 3, it only requires one nucleotide change for the K272E, K272M, N262D, and N262K mutations and two nucleotide changes for S275H, S275R, L258E, and L258K (Table 15). When we examine the rate of transitions versus transversions in the relative fitness assay mutations in the F gene section we surveyed, there are more transitions than transversions. This is consistent with previous data that found more transitions in the RSV genomes of virus grown in HEp-2 cell culture (283). Since transitions are more likely than transversions, it will also bias the evolution of the virus and limit the possible codons. Direct mutations to the MARM codons would require at least

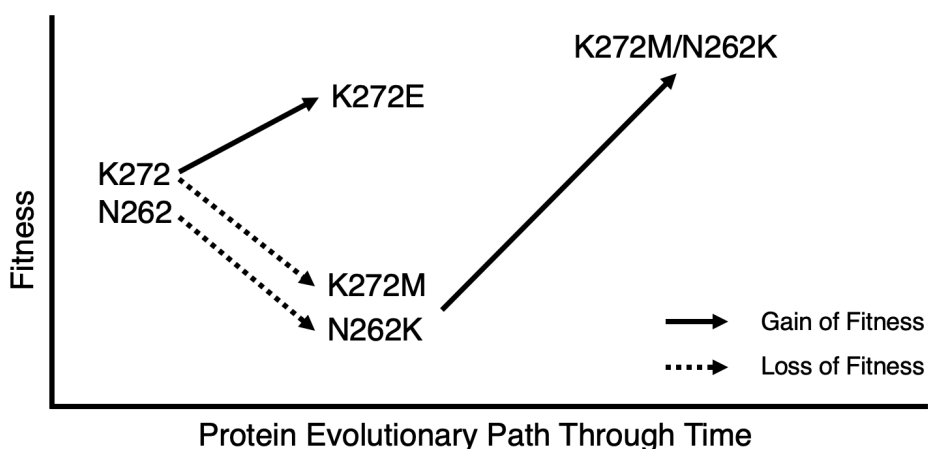**Figure 19. Fitness diagram of K272 and N262 evolution.**
K272E has a gain of fitness in the presence of motavizumab. N262K and K272M as single mutations have a loss of fitness in the presence of motavizumab. The double mutant, K272M/N262K, had a gain of fitness in the presence of motavizumab but required the loss of fitness of the K272M mutation first, which will be unlikely to arise under selective pressure.

Table 15. Codons of the variants found in surveillance studies and all possible codons for motavizumab resistant variants identified in Chapter 3 and K272M passage study (MARM Codons).

	L258	N262	K272	S275
Circulating Strain Codons	TTG	AAT	AAG	TCC
	TTA		AAA	TCA
	CTA			
MARM Codons	**E258**	**D262**	**E272**	**H275**
	GAG (2)	GAT (1)	GAG (1)	CAC (2)
	GAA (2)	GAC (2)	GAA (1)	CAT (3)
	K258	**K262**	**M272**	**R275**
	AAG (2)	AAG (1)	ATG (1)	CGC (2)
	AAA (2)	AAA (1)		CGA (2)
				AGA (2)
				CGG (3)
				CGT (3)
				AGG (3)

Numbers in parentheses indicate the number of nucleotide changes from the circulating strain codon to the MARM codon.

Table 16. $\Delta\Delta G_{Bind}$ and $\Delta\Delta G_{Fold}$ values of potential intermediate mutations for L258E, L258K, S275H, and S275R.

Mutation	Codon Change	$\Delta\Delta G_{Bind}$	$\Delta\Delta G_{Bind}$ Standard Deviation	$\Delta\Delta G_{Fold}$	$\Delta\Delta G_{Fold}$ Standard Deviation
L258M	TTG→ATG	0.06	0.69	0.04	0.31
L258I	CTA→ATA	0.20	0.52	0.68	0.36
L258Q	CTA→CAA	1.16	0.50	1.13	0.48
L258V	TTG→GTG TTA→GTA	0.25	0.56	1.63	0.47
S275P	TCC→CCC TCA→CCA	0.42	0.63	3.57	1.77
S275Y	TCC→TAC	3.98	3.11	0.33	1.33
S275T	TCA→ACA	-0.41	0.96	0.49	0.73
S275C	TCC→TGC	0.06	0.82	-0.20	0.61

one transversion mutation for all L258 and S275 mutants. The codons limit the possibility of these mutations; out of all six possible codons for serine, all require at least two nucleotide changes to evolve to histidine, and the same is true for leucine to lysine. The likelihood of these mutations naturally occurring is low and would probably require intermediate mutations to other amino acids before this mutation could occur. Several mutations could be intermediate mutations between the WT codon and the MARM codons for L258 and S275 (Table 16). All the intermediates except S275P have a protein folding stability value ($\Delta\Delta G_{Fold}$) below the 2 kcal/mol cutoff for protein folding and would likely be viable but may not be as fit as WT. However, S275P is a viable mutant since it arose during the relative fitness assay and one possible explanation is that the standard deviation for $\Delta\Delta G_{Fold}$ (SD = 1.77) is high and there was a large variance between the averages of the $\Delta\Delta G_{Fold}$ values at this site. The disruption of binding values ($\Delta\Delta G_{Bind}$) for the intermediate mutations may also be MARMs since L258Q and S275Y are greater than 1 kcal/mol (Table 16). Future studies should examine changing codons to ones that may set up other variants to be advantageous to evolve. We are limited in the tradeoff between residue changes and the replication efficiency of the virus, so some codon changes may not be possible. A study that uses the currently circulating strains of RSV would also be advantageous as it would be a closer reflection of the possible MARM that could arise, and reverse genetics systems of contemporary isolates are available (273).

In our previous study, we estimated the effect of each possible mutation of RSV F protein for all amino acid sites and 19 possible substitutions at each site for both F protein monomer folding ($\Delta\Delta G_{Fold}$) and its binding with motavizumab ($\Delta\Delta G_{Bind}$)(Chapter 3). We determined that there was some correlation between $\Delta\Delta G_{Bind}$ and loss of binding, where an increase in $\Delta\Delta G_{Bind}$ correlated with an increase in loss of binding. The $\Delta\Delta G_{Bind}$ values for K272E, L258K, and S275H are 2.09, 1.02, and 5.56 kcal/mol, respectively. However, we did not have N262K as a possible MARM as our minimal cutoff for $\Delta\Delta G_{Bind}$ was 0.5 kcal/mol. As a single mutation, the $\Delta\Delta G_{Bind}$ for N262K is 0.35 kcal/mol, and the neutralization assay revealed that it is more susceptible to motavizumab than WT. As noted above, the epistatic order of mutations may also imbue stability changes to the protein that allows for the emergence of N262K, and interactions between the M272 and K262 may be required for escape.

The genetic landscape of an organism will direct evolution and determine the phenotypic characteristics that allow for evolutionary success. The likelihood and relevance of molecular modeling predictions will rely on the codons and number of nucleotide changes required to achieve the mutation and epistatic mutations that may need to proceed with the MARM mutation. The genetic background and epistatic mutations influence the evolution of RSV F protein and impacts the emergence of MARMs.

CHAPTER 5

Summary and Conclusions

Monoclonal antibody resistant mutants (MARMs) previously relied on testing patient samples, surveillance studies, or passage experiments. The potential MARMs identified in patient studies and surveillance studies would also have to be tested for neutralization to confirm if it is an escape variant. Passage experiments present a challenge as they are biased toward mutations that can occur in a limited number of replication cycles. We confirmed that biophysical modeling of proteins is an accurate methodology for identifying MARMs. This study tested molecular modeling predictions of single-point mutations in the F protein that allowed the escape from motavizumab. Molecular modeling accurately predicted mutations in F protein that resulted in reduced neutralization and binding of motavizumab. We generated eight mutations in a recombinant virus that were able to propagate new virus, albeit with some deficiencies. Six of the eight mutations, including the known MARM K272E, demonstrated reduced neutralization in microneutralization assays and flow cytometry. L258K, K272E, and S275H all demonstrated a reduced on-rate in the SPR studies. Correlations were observed in MFI and $\Delta\Delta G_{Bind}$ and in the binding kinetics studies between on-rate, affinity and $\Delta\Delta G_{Bind}$. However, more variants will have to be tested to confirm the accuracy and threshold of $\Delta\Delta G_{Bind}$, but overall, $\Delta\Delta G_{Bind}$ appears to be an accurate indicator of reduced binding.

While we used MDS+FoldX to accurately predict mutations that escape motavizumab, no other variant has been found as a MARM for motavizumab besides K272E. We wanted to understand how to interpret our modeling results and the likelihood of our predicted variants arising in viral populations. First, we examined if any other mutations were possible by passaging our recombinant clonal virus in the presence of motavizumab. The only variant that was present was K272E, even in early passages. Next, we examined the relative fitness between wild type (WT) and our variants (K272E, L258K, S275H) to understand if the mutants could establish themselves in a population. All three variants maintained a minor presence in the absence of mAb. However, in the presence of mAb, K272E was the only virus to sweep the population and arose in both the L258K and S275H motavizumab trials. L258K was the least fit of the three variants and lost dominance in the presence of motavizumab. The replication of L258K in the absence of motavizumab had a delay in the detection and reduced

viral titers over time. In the presence of motavizumab, the viral titers of L258K were not significantly different from that of WT. This suggests that the replication deficiency of L258K cannot be overcome even when WT is disadvantaged in the presence of motavizumab. S275H was initially selected for in the presence of motavizumab but could not compete with K272E in later passages.

We altered the trajectory of the evolution of F protein by changing K272 to methionine and found a novel MARM, K272M/N262K. Changing lysine (AAG) to methionine (ATG) made it so it would take two nucleotide changes to evolve to glutamic acid (GAG). This put all three variants at equal nucleotide changes to get to a mutant codon, S275H (TCC→CAT/CAC) and L258K (TTG→AAA/AAG). The resulting mutation for two of our replicates was N262K (AAT→AAA) while retaining the K272M mutation, which notably only required one nucleotide change. It is possible that this mutation was the result of epistatic control in that it could only happen because K272 was mutated to methionine first. This was further supported by the single mutant N262K having increased neutralization by motavizumab compared to WT, which indicates that the two mutations are required for antibody escape. We have shown in the passage studies and the relative fitness assays that K272E is the most beneficial first step mutation. K272M had a loss of fitness in the presence of motavizumab, making it more unlikely that N262K will arise if the previous mutation is required. The codon usage at our sites of interest appeared to impact the likelihood of our predicted mutations occurring. While it would be interesting to examine if changing the codons at S275 and L258, all possible codons for those amino acids would require at least two nucleotide changes to get to that mutation. An intermediary mutation would likely have to precede the evolution of L258K or S275H for those variants to take hold in a population. Future modeling work should address currently circulating strains and the codons at the sites of interest to determine the likelihood of the mutations.

MDS+FoldX can identify MARMs, but it is a limited system. While all eight selected variants were able to propagate new virus, all had at least some deficiency in growth when compared to WT. The $\Delta\Delta G_{Fold}$ value may not be the most accurate way to predict protein function similar to WT. S275P had a $\Delta\Delta G_{Fold}$ value >2 kcal/mol, yet it emerged during the relative fitness experiments. More variants would have to be tested to confirm whether $\Delta\Delta G_{Fold}$ is an accurate measurement of protein function and if <2 kcal/mol is an accurate threshold for

protein folding. A future study could examine all variants with predicted $\Delta\Delta G_{Fold}$ <4 kcal/mol for F protein function to better understand $\Delta\Delta G_{Fold}$ as an indicator of protein function. An additional limitation of MDS+FoldX is that it can only model single mutations. While only single mutation MARMs have been isolated from patients for palivizumab and motavizumab, double mutant escape variants have been observed for nirsevimab in passage experiments. Furthermore, Chapter 4 found that a permissive mutation was required for the emergence of a novel MARM. MDS+FoldX cannot recreate a complex phenomenon like contingent evolution, and further advancement in fast protein-protein modeling would be required to predict the effects of more than one mutation. Our study demonstrated that MDS+FoldX could predict escape variants and identified the limitations that need to be addressed to improve future modeling predictions.

This project has demonstrated that molecular modeling is a powerful tool for examining the interaction between biomolecules and predicting escape variants. The increased use of mAbs for viral prophylaxis and infections will heighten the need for rapid identification of potential escape variants, particularly in the case of SARS-CoV-2, HIV-1, and influenza virus that have all demonstrated escape from targeted anti-viral drugs. Future studies should examine other viral pathogens and mAbs to help further refine the MDS+FoldX approach and understand the significance of our modeling predictions.

Literature Cited

1. Papadopoulos NG, Gourgiotis D, Javadyan A, Bossios A, Kallergi K, Psarras S, Tsolia MN, Kafetzis D. 2004. Does respiratory syncytial virus subtype influences the severity of acute bronchiolitis in hospitalized infants? Respir Med 98:879–882.

2. Jafri HS, Wu X, Makari D, Henrickson KJ. 2013. Distribution of respiratory syncytial virus subtypes A and B among infants presenting to the emergency department with lower respiratory tract infection or apnea. Pediatr Infect Dis J 32:335–340.

3. Melero JA, Moore ML. 2013. Influence of Respiratory Syncytial Virus Strain Differences on Pathogenesis and Immunity. Curr Top Microbiol Immunol 372:59–82.

4. Walsh EE, Hall CB. 2015. Respiratory Syncytial Virus (RSV). Mand Douglas Bennetts Princ Pract Infect Dis 1948-1960.e3.

5. Laham FR, Mansbach JM, Piedra PA, Hasegawa K, Sullivan AF, Espinola JA, Camargo CA. 2017. Clinical Profiles of Respiratory Syncytial Virus Subtypes A and B among Children Hospitalized with Bronchiolitis. Pediatr Infect Dis J 36:808–810.

6. Yassine HM, Sohail MU, Younes N, Nasrallah GK. 2020. Systematic Review of the Respiratory Syncytial Virus (RSV) Prevalence, Genotype Distribution, and Seasonality in Children from the Middle East and North Africa (MENA) Region. Microorganisms 8:713.

7. Blount RE, Morris JA, Savage RE. 1956. Recovery of cytopathogenic agent from chimpanzees with coryza. Proc Soc Exp Biol Med Soc Exp Biol Med 92:544–549.

8. Chanock RM. 1957. Recovery of a new type of myxovirus from infants with croup. Ann N Y Acad Sci 67:287–295.

9. Eshaghi A, Duvvuri VR, Lai R, Nadarajah JT, Li A, Patel SN, Low DE, Gubbay JB. 2012. Genetic Variability of Human Respiratory Syncytial Virus A Strains Circulating in Ontario: A Novel Genotype with a 72 Nucleotide G Gene Duplication. PLoS ONE 7:e32807.

10. Lewis FA, Rae ML, Lehmann NI, Ferris AA. 1961. A Syncytial Virus Associated with Epidemic Disease of the Lower Respiratory Tract in Infants and Young Children. Med J Aust 2:932–933.

11. Ke Z, Dillard RS, Chirkova T, Leon F, Stobart CC, Hampton CM, Strauss JD, Rajan D, Rostad CA, Taylor JV, Yi H, Shah R, Jin M, Hartert TV, Peebles RS, Graham BS, Moore ML, Anderson LJ, Wright ER. 2018. The Morphology and Assembly of Respiratory Syncytial Virus Revealed by Cryo-Electron Tomography. Viruses 10:446.

12. Griffiths C, Drews SJ, Marchant DJ. 2017. Respiratory Syncytial Virus: Infection, Detection, and New Options for Prevention and Treatment. Clin Microbiol Rev 30:277–319.

13. Zhang L, Peeples ME, Boucher RC, Collins PL, Pickles RJ. 2002. Respiratory Syncytial Virus Infection of Human Airway Epithelial Cells Is Polarized, Specific to Ciliated Cells, and without Obvious Cytopathology. J Virol 76:5654–5666.

14. Johnson SM, McNally BA, Ioannidis I, Flano E, Teng MN, Oomens AG, Walsh EE, Peeples ME. 2015. Respiratory Syncytial Virus Uses CX3CR1 as a Receptor on Primary Human Airway Epithelial Cultures. PLoS Pathog 11:e1005318.

15. Jeong K-I, Piepenhagen PA, Kishko M, DiNapoli JM, Groppo RP, Zhang L, Almond J, Kleanthous H, Delagrave S, Parrington M. 2015. CX3CR1 Is Expressed in Differentiated Human Ciliated Airway Cells and Co-Localizes with Respiratory Syncytial Virus on Cilia in a G Protein-Dependent Manner. PLoS ONE 10:e0130517.

16. Krusat T, Streckert HJ. 1997. Heparin-dependent attachment of respiratory syncytial virus (RSV) to host cells. Arch Virol 142:1247–1254.

17. Hallak LK, Kwilas SA, Peeples ME. 2007. Interaction between respiratory syncytial virus and glycosaminoglycans, including heparan sulfate. Methods Mol Biol Clifton NJ 379:15–34.

18. Yuan X, Hu T, He H, Qiu H, Wu X, Chen J, Wang M, Chen C, Huang S. 2018. Respiratory syncytial virus prolifically infects N2a neuronal cells, leading to TLR4 and nucleolin protein modulations and RSV F protein co-localization with TLR4 and nucleolin. J Biomed Sci 25:13.

19. Mastrangelo P, Chin AA, Tan S, Jeon AH, Ackerley CA, Siu KK, Lee JE, Hegele RG. 2021. Identification of RSV Fusion Protein Interaction Domains on the Virus Receptor, Nucleolin. Viruses 13:261.

20. Anderson CS, Chirkova T, Slaunwhite CG, Qiu X, Walsh EE, Anderson LJ, Mariani TJ. 2021. CX3CR1 Engagement by Respiratory Syncytial Virus Leads to Induction of Nucleolin and Dysregulation of Cilia-related Genes. J Virol 95:JVI.00095-21.

21. Marr N, Turvey SE. 2012. Role of human TLR4 in respiratory syncytial virus-induced NF-κB activation, viral entry and replication. Innate Immun 18:856–865.

22. Kurt-Jones EA, Popova L, Kwinn L, Haynes LM, Jones LP, Tripp RA, Walsh EE, Freeman MW, Golenbock DT, Anderson LJ, Finberg RW. 2000. Pattern recognition receptors TLR4 and CD14 mediate response to respiratory syncytial virus. Nat Immunol 1:398–401.

23. Currier MG, Lee S, Stobart CC, Hotard AL, Villenave R, Meng J, Pretto CD, Shields MD, Nguyen MT, Todd SO, Chi MH, Hammonds J, Krumm SA, Spearman P, Plemper RK, Sakamoto K, Peebles RS, Power UF, Moore ML. 2016. EGFR Interacts with the Fusion Protein of Respiratory Syncytial Virus Strain 2-20 and Mediates Infection and Mucin Expression. PLoS Pathog 12:e1005622.

24. Behera AK, Matsuse H, Kumar M, Kong X, Lockey RF, Mohapatra SS. 2001. Blocking Intercellular Adhesion Molecule-1 on Human Epithelial Cells Decreases Respiratory Syncytial Virus Infection. Biochem Biophys Res Commun 280:188–195.

25. Griffiths CD, Bilawchuk LM, McDonough JE, Jamieson KC, Elawar F, Cen Y, Duan W, Lin C, Song H, Casanova J-L, Ogg S, Jensen LD, Thienpont B, Kumar A, Hobman TC, Proud D, Moraes TJ, Marchant DJ. 2020. IGF1R is an entry receptor for respiratory syncytial virus. Nature 583:615–619.

26. Ghildyal R, Hartley C, Varrasso A, Meanger J, Voelker DR, Anders EM, Mills J. 1999. Surfactant Protein A Binds to the Fusion Glycoprotein of Respiratory Syncytial Virus and Neutralizes Virion Infectivity. J Infect Dis 180:2009–2013.

27. Feldman SA, Audet S, Beeler JA. 2000. The Fusion Glycoprotein of Human Respiratory Syncytial Virus Facilitates Virus Attachment and Infectivity via an Interaction with Cellular Heparan Sulfate. J Virol 74:6442–6447.

28. Karron RA, Buonagurio DA, Georgiu AF, Whitehead SS, Adamus JE, Clements-Mann ML, Harris DO, Randolph VB, Udem SA, Murphy BR, Sidhu MS. 1997. Respiratory syncytial virus (RSV) SH and G proteins are not essential for viral replication in vitro: Clinical evaluation and molecular characterization of a cold-passaged, attenuated RSV subgroup B mutant. Proc Natl Acad Sci 94:13961–13966.

29. Techaarpornkul S, Barretto N, Peeples ME. 2001. Functional Analysis of Recombinant Respiratory Syncytial Virus Deletion Mutants Lacking the Small Hydrophobic and/or Attachment Glycoprotein Gene. J Virol 75:6825–6834.

30. King T, Mejias A, Ramilo O, Peeples ME. 2021. The larger attachment glycoprotein of respiratory syncytial virus produced in primary human bronchial epithelial cultures reduces infectivity for cell lines. PLoS Pathog 17:e1009469.

31. Noton SL, Fearns R. 2015. IInitiation and regulation of paramyxovirus transcription and replication. Virology:545–554.

32. García J, García-Barreno B, Vivo A, Melero JA. 1993. Cytoplasmic inclusions of respiratory syncytial virus-infected cells: formation of inclusion bodies in transfected cells that coexpress the nucleoprotein, the phosphoprotein, and the 22K protein. Virology 195:243–247.

33. García-Barreno B, Delgado T, Melero JA. 1996. Identification of protein regions involved in the interaction of human respiratory syncytial virus phosphoprotein and nucleoprotein: significance for nucleocapsid assembly and formation of cytoplasmic inclusions. J Virol 70:801–808.

34. van Niekerk S, Venter M. 2011. Replacement of Previously Circulating Respiratory Syncytial Virus Subtype B Strains with the BA Genotype in South Africa. J Virol 85:8789–8797.

35. Agoti CN, Otieno JR, Gitahi CW, Cane PA, Nokes DJ. 2014. Rapid Spread and Diversification of Respiratory Syncytial Virus Genotype ON1, Kenya. Emerg Infect Dis 20:950–959.

36. Braun MR, Noton SL, Blanchard EL, Shareef A, Santangelo PJ, Johnson WE, Fearns R. 2021. Respiratory syncytial virus M2-1 protein associates non-specifically with viral messenger RNA and with specific cellular messenger RNA transcripts. PLoS Pathog 17:e1009589.

37. Tran T-L, Castagné N, Dubosclard V, Noinville S, Koch E, Moudjou M, Henry C, Bernard J, Yeo RP, Eléouët J-F. 2009. The Respiratory Syncytial Virus M2-1 Protein Forms Tetramers and Interacts with RNA and P in a Competitive Manner. J Virol 83: 6363-6374.

38. Bermingham A, Collins PL. 1999. The M2–2 protein of human respiratory syncytial virus is a regulatory factor involved in the balance between RNA replication and transcription. Proc Natl Acad Sci 96:11259–11264.

39. Gower TL, Pastey MK, Peeples ME, Collins PL, McCurdy LH, Hart TK, Guth A, Johnson TR, Graham BS. 2005. RhoA signaling is required for respiratory syncytial virus-induced syncytium formation and filamentous virion morphology. J Virol 79:5326–5336.

40. Liljeroos L, Krzyzaniak MA, Helenius A, Butcher SJ. 2013. Architecture of respiratory syncytial virus revealed by electron cryotomography. Proc Natl Acad Sci 110:11133–11138.

41. Chang T-H, Segovia J, Sabbah A, Mgbemena V, Bose S. 2012. Cholesterol-rich lipid rafts are required for release of infectious human respiratory syncytial virus particles. Virology 422:205–213.

42. Marty A, Meanger J, Mills J, Shields B, Ghildyal R. 2003. Association of matrix protein of respiratory syncytial virus with the host cell membrane of infected cells. Arch Virol 149:199–210.

43. Mehedi M, McCarty T, Martin SE, Le Nouën C, Buehler E, Chen Y-C, Smelkinson M, Ganesan S, Fischer ER, Brock LG, Liang B, Munir S, Collins PL, Buchholz UJ. 2016. Actin-Related Protein 2 (ARP2) and Virus-Induced Filopodia Facilitate Human Respiratory Syncytial Virus Spread. PLoS Pathog 12:e1006062.

44. Rey FA, Lok S-M. 2018. Common Features of Enveloped Viruses and Implications for Immunogen Design for Next-Generation Vaccines. Cell 172:1319–1334.

45. Earp LJ, Delos SE, Park HE, White JM. 2004. The Many Mechanisms of Viral Membrane Fusion Proteins, p. 25–66. *In* Marsh, M (ed.), Membrane Trafficking in Viral Replication. Springer Berlin Heidelberg, Berlin, Heidelberg.

46.   Allison SL, Schalich J, Stiasny K, Mandl CW, Kunz C, Heinz FX. 1995. Oligomeric rearrangement of tick-borne encephalitis virus envelope proteins induced by an acidic pH. J Virol 69:695–700.

47.   McLellan JS, Ray WC, Peeples ME. 2013. Structure and Function of RSV Surface Glycoproteins. Curr Top Microbiol Immunol 372:83–104.

48.   Collins PL, Huang YT, Wertz GW. 1984. Nucleotide sequence of the gene encoding the fusion (F) glycoprotein of human respiratory syncytial virus. Proc Natl Acad Sci 81:7683–7687.

49.   Arumugham RG, Seid RC, Doyle S, Hildreth SW, Paradiso PR. 1989. Fatty Acid Acylation of the Fusion Glycoprotein of Human Respiratory Syncytial Virus. J Biol Chem 264:10339–10342.

50.   Bolt G, Pedersen LO, Birkeslund HH. 2000. Cleavage of the respiratory syncytial virus fusion protein is required for its surface expression: role of furin. Virus Res 68:25–33.

51.   Collins PL, Mottet G 1991. Post-translational Processing and Oligomerization of the Fusion Glycoprotein of Human Respiratory Syncytial Virus. J Gen Virol 72:3095–3101.

52.   Gruber C, Levine SY 1983. Respiratory Syncytial Virus Polypeptides. III. The Envelope-associated Proteins. J Gen Virol 64:825–832.

53.   Day ND, Branigan PJ, Liu C, Gutshall LL, Luo J, Melero JA, Sarisky RT, Del Vecchio AM. 2006. Contribution of cysteine residues in the extracellular domain of the F protein of human respiratory syncytial virus to its function. Virol J 3:34.

54.   Begoña Ruiz-Argüello M, González-Reyes L, Calder LJ, Palomo C, Martín D, Saíz MJ, García-Barreno B, Skehel JJ, Melero JA. 2002. Effect of Proteolytic Processing at Two Distinct Sites on Shape and Aggregation of an Anchorless Fusion Protein of Human Respiratory Syncytial Virus and Fate of the Intervening Segment. Virology 298:317–326.

55.   Zimmer G, Trotz I, Herrler G. 2001. N-Glycans of F Protein Differentially Affect Fusion Activity of Human Respiratory Syncytial Virus. J Virol 75:4744–4751.

56.   Srinivasakumar N, Ogra PL, Flanagan TD. 1991. Characteristics of fusion of respiratory syncytial virus with HEp-2 cells as measured by R18 fluorescence dequenching assay. J Virol 65:4063–4069.

57.   Kahn JS, Schnell MJ, Buonocore L, Rose JK. 1999. Recombinant Vesicular Stomatitis Virus Expressing Respiratory Syncytial Virus (RSV) Glycoproteins: RSV Fusion Protein Can Mediate Infection and Cell Fusion. Virology 254:81–91.

58.   Bose S, Jardetzky TS, Lamb RA. 2015. Timing is everything: Fine-tuned molecular machines orchestrate paramyxovirus entry. Virology 479:518–531.

59.   Krzyzaniak MA, Zumstein MT, Gerez JA, Picotti P, Helenius A. 2013. Host Cell Entry of Respiratory Syncytial Virus Involves Macropinocytosis Followed by Proteolytic Activation of the F Protein. PLoS Pathog 9:e1003309.

60.   Battles MB, McLellan JS. 2019. Respiratory syncytial virus entry and how to block it. Nat Rev Microbiol 17:233–245.

61.   Zhao X, Singh M, Malashkevich VN, Kim PS. 2000. Structural characterization of the human respiratory syncytial virus fusion protein core. Proc Natl Acad Sci 97:14172–14177.

62.   McLellan JS. 2015. Neutralizing Epitopes on the Respiratory Syncytial Virus Fusion Glycoprotein. Curr Opin Virol 11:70–75.

63.   Beeler JA, van Wyke Coelingh K. 1989. Neutralization epitopes of the F glycoprotein of respiratory syncytial virus: effect of mutation upon fusion function. J Virol 63:2941–2950.

64.   McLellan JS, Chen M, Kim A, Yang Y, Graham BS, Kwong PD. 2010. Structural basis of respiratory syncytial virus neutralization by motavizumab. Nat Struct Mol Biol 17:248–250.

65.   Arbiza J, Taylor G, Lopez JA, Furze J, Wyld S, Whyte P, Stott EJ, Wertz G, Sullender W, Trudel M, Melero JA. 1992. Characterization of two antigenic sites recognized by neutralizing monoclonal antibodies directed against the fusion glycoprotein of human respiratory syncytial virus. J Gen Virol 73:2225–2234.

66.   Hall CB, Weinberg GA, Iwane MK, Blumkin AK, Edwards KM, Staat MA, Auinger P, Griffin MR, Poehling KA, Erdman D, Grijalva CG, Zhu Y, Szilagyi P. 2009. The Burden of Respiratory Syncytial Virus Infection in Young Children. N Engl J Med 360:588–598.

67.   Nair H, Nokes DJ, Gessner BD, Dherani M, Madhi SA, Singleton RJ, O'Brien KL, Roca A, Wright PF, Bruce N, Chandran A, Theodoratou E, Sutanto A, Sedyaningsih ER, Ngama M, Munywoki PK, Kartasasmita C, Simões EA, Rudan I, Weber MW, Campbell H. 2010. Global burden of acute lower respiratory infections due to respiratory syncytial virus in young children: a systematic review and meta-analysis. Lancet 375:1545–1555.

68.   Falsey AR, Hennessey PA, Formica MA, Cox C, Walsh EE. 2005. Respiratory Syncytial Virus Infection in Elderly and High-Risk Adults. N Engl J Med 352:1749–1759.

69. Falsey AR, Formica MA, Hennessey PA, Criddle MM, Sullender WM, Walsh EE. 2006. Detection of Respiratory Syncytial Virus in Adults with Chronic Obstructive Pulmonary Disease. Am J Respir Crit Care Med 173:639–643.

70. Walsh EE, Falsey AR. 2012. Respiratory syncytial virus infection in adult populations. Infect Disord Drug Targets 12:98–102.

71. Leader S, Kohlhase K. 2003. Recent trends in severe respiratory syncytial virus (RSV) among US infants, 1997 to 2000. J Pediatr 143:127–132.

72. Rose EB, Wheatley A, Langley G, Gerber S, Haynes A. 2018. Respiratory Syncytial Virus Seasonality — United States, 2014–2017. Morb Mortal Wkly Rep 67:71–76.

73. Amorim-Figueiredo R, Neves R, Simoes J, Simao M, Domingues R, Rocha P, Ferreira S, Perry R, Costa B, MacHado R, Amaral D. 2021. Resurgence of respiratory syncytial virus after COVID-19 pandemics-was there a change in seasonality? Cogent Med.

74. Hodjat P, Christensen PA, Subedi S, Bernard DW, Olsen RJ, Long SW. 2021. The Reemergence of Seasonal Respiratory Viruses in Houston, Texas, after Relaxing COVID-19 Restrictions. Microbiol Spectr 9:e0043021.

75. Bont L, Aalderen WMC van, Kimpen JLL. 2000. Long-term consequences of respiratory syncytial virus (RSV) bronchiolitis. Paediatr Respir Rev 1:221–227.

76. Fujiogi M, Dumas O, Hasegawa K, Jartti T, Camargo CA. 2022. Identifying and predicting severe bronchiolitis profiles at high risk for developing asthma: Analysis of three prospective cohorts. EClinicalMedicine 43:101257.

77. Cai W, Buda S, Schuler E, Hirve S, Zhang W, Haas W. 2020. Risk factors for hospitalized respiratory syncytial virus disease and its severe outcomes. Influenza Other Respir Viruses 14:658–670.

78. Hislop AA. 2002. Airway and blood vessel interaction during lung development. J Anat 201:325–334.

79. Ostadabbas S, Bulach C, Ku DN, Anderson LJ, Ghovanloo M. 2014. A passive quantitative measurement of airway resistance using depth data, p. 5743–5747. *In* 2014 36th Annual International Conference of the IEEE Engineering in Medicine and Biology Society.

80. Glezen WP, Taber LH, Frank AL, Kasel JA. 1986. Risk of primary infection and reinfection with respiratory syncytial virus. Am J Dis Child 1960 140:543–546.

81. Hall CB, Walsh EE, Long CE, Schnabel KC. 1991. Immunity to and frequency of reinfection with respiratory syncytial virus. J Infect Dis 163:693–698.

82. Smith PK, Wang SZ, Dowling KD, Forsyth KD. 2001. Leucocyte populations in respiratory syncytial virus-induced bronchiolitis. J Paediatr Child Health 37:146–151.

83. Everard ML, Swarbrick A, Wrightham M, McIntyre J, Dunkley C, James PD, Sewell HF, Milner AD. 1994. Analysis of cells obtained by bronchial lavage of infants with respiratory syncytial virus infection. Arch Dis Child 71:428–432.

84. Funchal GA, Jaeger N, Czepielewski RS, Machado MS, Muraro SP, Stein RT, Bonorino CBC, Porto BN. 2015. Respiratory syncytial virus fusion protein promotes TLR-4-dependent neutrophil extracellular trap formation by human neutrophils. PloS One 10:e0124082.

85. Oshansky CM, Barber JP, Crabtree J, Tripp RA. 2010. Respiratory Syncytial Virus (RSV) F and G Proteins Induce IL-1α, CC and CXC Chemokine Responses by Normal Human Bronchoepithelial Cells. J Infect Dis 201:1201–1207.

86. Johnson TR, Johnson JE, Roberts SR, Wertz GW, Parker RA, Graham BS. 1998. Priming with Secreted Glycoprotein G of Respiratory Syncytial Virus (RSV) Augments Interleukin-5 Production and Tissue Eosinophilia after RSV Challenge. J Virol 72:2871–2880.

87. Harcourt J, Alvarez R, Jones LP, Henderson C, Anderson LJ, Tripp RA. 2006. Respiratory Syncytial Virus G Protein and G Protein CX3C Motif Adversely Affect CX3CR1 [+] T Cell Responses. J Immunol 176:1600–1608.

88. Cusi MG, Martorelli B, Di Genova G, Terrosi C, Campoccia G, Correale P. 2010. Age related changes in T cell mediated immune response and effector memory to Respiratory Syncytial Virus (RSV) in healthy subjects. Immun Ageing A 7:14.

89. Shinoff JJ, O'Brien KL, Thumar B, Shaw JB, Reid R, Hua W, Santosham M, Karron R. 2008. Young Infants Can Develop Protective Levels of Neutralizing Antibody after Infection with Respiratory Syncytial Virus. J Infect Dis 198:1007–1015.

90. Strannegård Ö, Cello J, Bjarnason R, Sigurbergsson F, Sigurs N. 1997. Association between pronounced IgA response in RSV bronchiolitis and development of allergic sensitization. Pediatr Allergy Immunol 8:1–6.

91. Weibel RE, Stokes J, Leagus MB, Mascoli CC, Tytell AA, Woodhour AF, Vella PP, Hilleman MR. 1967. Respiratory virus vaccines. VII. Field evaluation of respiratory syncytial, parainfluenza 1, 2, 3, and Mycoplasma pneumoniae vaccines, 1965 to 1966. Am Rev Respir Dis 96:724–739.

92. Chin J, Magoffin RL, Shearer LA, Schieble JH, Lennette EH. 1969. Field evaluation of a respiratory syncytial virus vaccine and a trivalent parainfluenza virus vaccine in a pediatric population. Am J Epidemiol 89:449–463.

93. Fulginiti VA, Eller JJ, Sieber OF, Joyner JW, Minamitani M, Meiklejohn G. 1969. Respiratory virus immunization. I. A field trial of two inactivated respiratory virus vaccines; an aqueous trivalent parainfluenza virus vaccine and an alum-precipitated respiratory syncytial virus vaccine. Am J Epidemiol 89:435–448.

94.   Kim HW, Canchola JG, Brandt CD, Pyles G, Chanock RM, Jensen K, Parrott RH. 1969. Respiratory Syncytial Virus Disease in Infants Despite Prior Administration of Antigenic Inactivated Vaccine. Am J Epidemiol 89:422–434.

95.   Waris ME, Tsou C, Erdman DD, Zaki SR, Anderson LJ. 1996. Respiratory synctial virus infection in BALB/c mice previously immunized with formalin-inactivated virus induces enhanced pulmonary inflammatory response with a predominant Th2-like cytokine pattern. J Virol 70:2852–2860.

96.   Power UF, Huss T, Michaud V, Plotnicky-Gilquin H, Bonnefoy JY, Nguyen TN. 2001. Differential histopathology and chemokine gene expression in lung tissues following respiratory syncytial virus (RSV) challenge of formalin-inactivated RSV- or BBG2Na-immunized mice. J Virol 75:12421–12430.

97.   Murphy BR, Walsh EE. 1988. Formalin-inactivated respiratory syncytial virus vaccine induces antibodies to the fusion glycoprotein that are deficient in fusion-inhibiting activity. J Clin Microbiol 26:1595–1597.

98.   Killikelly AM, Kanekiyo M, Graham BS. 2016. Pre-fusion F is absent on the surface of formalin-inactivated respiratory syncytial virus. Sci Rep 6:34108.

99.   Mazur NI, Higgins D, Nunes MC, Melero JA, Langedijk AC, Horsley N, Buchholz UJ, Openshaw PJ, McLellan JS, Englund JA, Mejias A, Karron RA, Simões EA, Knezevic I, Ramilo O, Piedra PA, Chu HY, Falsey AR, Nair H, Kragten-Tabatabaie L, Greenough A, Baraldi E, Papadopoulos NG, Vekemans J, Polack FP, Powell M, Satav A, Walsh EE, Stein RT, Graham BS, Bont LJ. 2018. The respiratory syncytial virus vaccine landscape: lessons from the graveyard and promising candidates. Lancet Infect Dis 18:e295–e311.

100.   Mejias A, Rodríguez-Fernández R, Oliva S, Peeples MarkE, Ramilo O. 2020. The Journey to an RSV Vaccine. Ann Allergy Asthma Immunol Off Publ Am Coll Allergy Asthma Immunol 125:36–46.

101.   van Miert C, Fernandes RM, Eccleson H, Bedson E, Lane S, Peak M, Thorburn K, Compton V, Woolfall K, Lacy D, Williamson P, McNamara PS. 2018. Non-invasive ventilation for the management of children with bronchiolitis (NOVEMBR): a feasibility study and core outcome set development protocol. Trials 19:627.

102.   Franklin D, Dalziel S, Schlapbach LJ, Babl FE, Oakley E, Craig SS, Furyk JS, Neutze J, Sinn K, Whitty JA, Gibbons K, Fraser J, Schibler A, PARIS and PREDICT. 2015. Early high flow nasal cannula therapy in bronchiolitis, a prospective randomised control trial (protocol): A Paediatric Acute Respiratory Intervention Study (PARIS). BMC Pediatr 15:183.

103.   Franklin D, Babl FE, Schlapbach LJ, Oakley E, Craig S, Neutze J, Furyk J, Fraser JF, Jones M, Whitty JA, Dalziel SR, Schibler A. 2018. A Randomized Trial of High-Flow Oxygen Therapy in Infants with Bronchiolitis. N Engl J Med 378:1121–1131.

104. Kepreotes E, Whitehead B, Attia J, Oldmeadow C, Collison A, Searles A, Goddard B, Hilton J, Lee M, Mattes J. 2017. High-flow warm humidified oxygen versus standard low-flow nasal cannula oxygen for moderate bronchiolitis (HFWHO RCT): an open, phase 4, randomised controlled trial. Lancet Lond Engl 389:930–939.

105. Martinón-Torres F. 2012. Noninvasive ventilation with helium-oxygen in children. J Crit Care 27:220.e1–9.

106. Nascimento MS, Santos É, Prado C do. 2018. Helium-oxygen mixture: clinical applicability in an intensive care unit. Einstein Sao Paulo Braz 16:eAO4199.

107. Liet J-M, Ducruet T, Gupta V, Cambonie G. 2015. Heliox inhalation therapy for bronchiolitis in infants. Cochrane Database Syst Rev CD006915.

108. Seliem W, Sultan AM. 2018. Heliox delivered by high flow nasal cannula improves oxygenation in infants with respiratory syncytial virus acute bronchiolitis. J Pediatr (Rio J) 94:56–61.

109. Srikantiah P, Vora P, Klugman KP. 2021. Assessing the Full Burden of Respiratory Syncytial Virus in Young Infants in Low- and Middle-Income Countries: The Importance of Community Mortality Studies. Clin Infect Dis 73:S177–S179.

110. Young M, Smitherman L. 2021. Socioeconomic Impact of RSV Hospitalization. Infect Dis Ther 10:35–45.

111. Han J, Perez J, Schafer A, Cheng H, Peet N, Rong L, Manicassamy B. 2018. Influenza Virus: Small Molecule Therapeutics and Mechanisms of Antiviral Resistance. Curr Med Chem 25:5115–5127.

112. Meert KL, Sarnaik AP, Gelmini MJ, Lieh-Lai MW. 1994. Aerosolized ribavirin in mechanically ventilated children with respiratory syncytial virus lower respiratory tract disease: a prospective, double-blind, randomized trial. Crit Care Med 22:566–572.

113. Moler FW, Steinhart CM, Ohmit SE, Stidham GL. 1996. Effectiveness of ribavirin in otherwise well infants with respiratory syncytial virus-associated respiratory failure. Pediatric Critical Study Group. J Pediatr 128:422–428.

114. Law BJ, Wang EE, MacDonald N, McDonald J, Dobson S, Boucher F, Langley J, Robinson J, Mitchell I, Stephens D. 1997. Does ribavirin impact on the hospital course of children with respiratory syncytial virus (RSV) infection? An analysis using the pediatric investigators collaborative network on infections in Canada (PICNIC) RSV database. Pediatrics 99:E7.

115. Long CE, Voter KZ, Barker WH, Hall CB. 1997. Long term follow-up of children hospitalized with respiratory syncytial virus lower respiratory tract infection and randomly treated with ribavirin or placebo. Pediatr Infect Dis J 16:1023–1028.

116. Guerguerian A-M, Gauthier M, Lebel MH, Farrell CA, Lacroix J. 1999. Ribavirin in Ventilated Respiratory Syncytial Virus Bronchiolitis. Am J Respir Crit Care Med 160:829–834.

117. Simões EAF, Bont L, Manzoni P, Fauroux B, Paes B, Figueras-Aloy J, Checchia PA, Carbonell-Estrany X. 2018. Past, Present and Future Approaches to the Prevention and Treatment of Respiratory Syncytial Virus Infection in Children. Infect Dis Ther 7:87–120.

118. Roymans D, Alnajjar SS, Battles MB, Sitthicharoenchai P, Furmanova-Hollenstein P, Rigaux P, Berg JV den, Kwanten L, Ginderen MV, Verheyen N, Vranckx L, Jaensch S, Arnoult E, Voorzaat R, Gallup JM, Larios-Mora A, Crabbe M, Huntjens D, Raboisson P, Langedijk JP, Ackermann MR, McLellan JS, Vendeville S, Koul A. 2017. Therapeutic efficacy of a respiratory syncytial virus fusion inhibitor. Nat Commun 8:1–15.

119. Janssen Research & Development, LLC. 2022. A Phase 2b Randomized, Double-blind, Placebo-controlled Study to Evaluate the Efficacy and Safety of Rilematovir (JNJ-53718678) in Adult Outpatients With Respiratory Syncytial Virus (RSV) Infection Who Are at High Risk for RSV-related Disease Progression. NCT04978337. Clinical trial registration. clinicaltrials.gov.

120. Sourimant J, Lieber CM, Aggarwal M, Cox RM, Wolf JD, Yoon J-J, Toots M, Ye C, Sticher Z, Kolykhalov AA, Martinez-Sobrido L, Bluemling GR, Natchus MG, Painter GR, Plemper RK. 2022. 4′-Fluorouridine is an oral antiviral that blocks respiratory syncytial virus and SARS-CoV-2 replication. Science 375:161–167.

121. Rhodin MHJ, McAllister NV, Castillo J, Noton SL, Fearns R, Kim IJ, Yu J, Blaisdell TP, Panarese J, Shook BC, Or YS, Goodwin B, Lin K. 2021. EDP-938, a novel nucleoprotein inhibitor of respiratory syncytial virus, demonstrates potent antiviral activities in vitro and in a non-human primate model. PLOS Pathog 17:e1009428.

122. Patel K, Kirkpatrick CM, Nieforth KA, Chanda S, Zhang Q, McClure M, Fry J, Symons JA, Blatt LM, Beigelman L, DeVincenzo JP, Huntjens DR, Smith PF. 2019. Respiratory syncytial virus-A dynamics and the effects of lumicitabine, a nucleoside viral replication inhibitor, in experimentally infected humans. J Antimicrob Chemother 74:442–452.

123. Groothuis JR, Levin MJ, Rodriguez W, Hall CB, Long CE, Kim HW, Lauer BA, Hemming VG. 1991. Use of intravenous gamma globulin to passively immunize high-risk children against respiratory syncytial virus: safety and pharmacokinetics. The RSVIG Study Group. Antimicrob Agents Chemother 35:1469–1473.

124. Groothuis JR, Simoes EA, Levin MJ, Hall CB, Long CE, Rodriguez WJ, Arrobio J, Meissner HC, Fulton DR, Welliver RC. 1993. Prophylactic administration of respiratory syncytial virus immune globulin to high-risk infants and young children. The Respiratory Syncytial Virus Immune Globulin Study Group. N Engl J Med 329:1524–1530.

125. Kwakkenbos MJ, Diehl SA, Yasuda E, Bakker AQ, van Geelen CMM, Lukens MV, van Bleek GM, Widjojoatmodjo MN, Bogers WMJM, Mei H, Radbruch A, Scheeren FA, Spits H, Beaumont T. 2010. Generation of stable monoclonal antibody-producing BCR+ human memory B cells by genetic programming. Nat Med 16:123–128.

126. AstraZeneca. 2021. A Phase 2, Open-label, Uncontrolled, Single-dose Study to Evaluate the Safety and Tolerability, Pharmacokinetics, and Occurrence of Antidrug Antibody for Nirsevimab in Immunocompromised Children ≤ 24 Months of Age. NCT04484935. Clinical trial registration. clinicaltrials.gov.

127. A joint statement with the Fetus and Newborn Committee. 1999. Palivizumab and respiratory syncytial virus immune globulin intravenous for the prophylaxis of respiratory syncytial virus infection in high risk infants. Paediatr Child Health 4:474–480.

128. Markham A. 2018. Ibalizumab: First Global Approval. Drugs 78:781–785.

129. Markham A. 2021. REGN-EB3: First Approval. Drugs 1–4.

130. Baum A, Fulton BO, Wloga E, Copin R, Pascal KE, Russo V, Giordano S, Lanza K, Negron N, Ni M, Wei Y, Atwal GS, Murphy AJ, Stahl N, Yancopoulos GD, Kyratsous CA. 2020. Antibody cocktail to SARS-CoV-2 spike protein prevents rapid mutational escape seen with individual antibodies. Science eabd0831.

131. Dougan M, Nirula A, Azizad M, Mocherla B, Gottlieb RL, Chen P, Hebert C, Perry R, Boscia J, Heller B, Morris J, Crystal C, Igbinadolor A, Huhn G, Cardona J, Shawa I, Kumar P, Adams AC, Van Naarden J, Custer KL, Durante M, Oakley G, Schade AE, Holzer TR, Ebert PJ, Higgs RE, Kallewaard NL, Sabo J, Patel DR, Dabora MC, Klekotka P, Shen L, Skovronsky DM. 2021. Bamlanivimab plus Etesevimab in Mild or Moderate Covid-19. N Engl J Med 385:1382–1392.

132. Gupta A, Gonzalez-Rojas Y, Juarez E, Crespo Casal M, Moya J, Falci DR, Sarkis E, Solis J, Zheng H, Scott N, Cathcart AL, Hebner CM, Sager J, Mogalian E, Tipple C, Peppercorn A, Alexander E, Pang PS, Free A, Brinson C, Aldinger M, Shapiro AE. 2021. Early Treatment for Covid-19 with SARS-CoV-2 Neutralizing Antibody Sotrovimab. N Engl J Med 385:1941–1950.

133. Playford EG, Munro T, Mahler SM, Elliott S, Gerometta M, Hoger KL, Jones ML, Griffin P, Lynch KD, Carroll H, El Saadi D, Gilmour ME, Hughes B, Hughes K, Huang E, de Bakker C, Klein R, Scher MG, Smith IL, Wang L-F, Lambert SB, Dimitrov DS, Gray PP, Broder CC. 2020. Safety, tolerability, pharmacokinetics, and immunogenicity of a human monoclonal antibody targeting the G glycoprotein of henipaviruses in healthy adults: a first-in-human, randomised, controlled, phase 1 study. Lancet Infect Dis 20:445–454.

134. Hershberger E, Sloan S, Narayan K, Hay CA, Smith P, Engler F, Jeeninga R, Smits S, Trevejo J, Shriver Z, Oldach D. 2019. Safety and efficacy of monoclonal antibody VIS410 in adults with uncomplicated influenza A infection: Results from a

randomized, double-blind, phase-2, placebo-controlled study. EBioMedicine 40:574–582.

135. Fresnais M, Longuespée R, Sauter M, Schaller T, Arndt M, Krauss J, Blank A, Haefeli WE, Burhenne J. 2020. Development and Validation of an LC–MS-Based Quantification Assay for New Therapeutic Antibodies: Application to a Novel Therapy against Herpes Simplex Virus. ACS Omega 5:24329–24339.

136. Heidelberg ImmunoTherapeutics GmbH. 2020. A Randomised, Double-Blind Phase II Trial of Topical HDIT101 Versus Placebo in Patients With Chronic Recurrent HSV-1 Infection and Orolabial Lesion. NCT04539483. Clinical trial registration. clinicaltrials.gov.

137. Andreano E, Nicastri E, Paciello I, Pileri P, Manganaro N, Piccini G, Manenti A, Pantano E, Kabanova A, Troisi M, Vacca F, Cardamone D, De Santi C, Torres JL, Ozorowski G, Benincasa L, Jang H, Di Genova C, Depau L, Brunetti J, Agrati C, Capobianchi MR, Castilletti C, Emiliozzi A, Fabbiani M, Montagnani F, Bracci L, Sautto G, Ross TM, Montomoli E, Temperton N, Ward AB, Sala C, Ippolito G, Rappuoli R. 2021. Extremely potent human monoclonal antibodies from COVID-19 convalescent patients. Cell 184:1821-1835.e16.

138. Salazar G, Zhang N, Fu T-M, An Z. 2017. Antibody therapies for the prevention and treatment of viral infections. Npj Vaccines 2:1–12.

139. Resch B. 2017. Product review on the monoclonal antibody palivizumab for prevention of respiratory syncytial virus infection. Hum Vaccines Immunother 13:2138–2149.

140. Wegzyn C, Toh LK, Notario G, Biguenet S, Unnebrink K, Park C, Makari D, Norton M. 2014. Safety and Effectiveness of Palivizumab in Children at High Risk of Serious Disease Due to Respiratory Syncytial Virus Infection: A Systematic Review. Infect Dis Ther 3:133–158.

141. Johnson S, Oliver C, Prince GA, Hemming VG, Pfarr DS, Wang SC, Dormitzer M, O'Grady J, Koenig S, Tamura JK, Woods R, Bansal G, Couchenour D, Tsao E, Hall WC, Young JF. 1997. Development of a humanized monoclonal antibody (MEDI-493) with potent in vitro and in vivo activity against respiratory syncytial virus. J Infect Dis 176:1215–1224.

142. Brady MT, Byington CL, Davies HD, Edwards KM, Jackson MA, Maldonado YA, Murray DL, Orenstein WA, Rathore MH, Sawyer MH, Schutze GE, Willoughby RE, Zaoutis TE, Ralston SL, Lieberthal AS, Meissner HC, Alverson BK, Baley JE, Gadomski AM, Johnson DW, Light MJ, Maraqa NF, Mendonca EA, Phelan KJ, Zorc JJ, Stanko-Lopp D, Hernández-Cancio S. 2014. Updated Guidance for Palivizumab Prophylaxis Among Infants and Young Children at Increased Risk of Hospitalization for Respiratory Syncytial Virus Infection. Pediatrics 134:415–420.

143.　 Updated Guidance: Use of Palivizumab Prophylaxis to Prevent Hospitalization From Severe Respiratory Syncytial Virus Infection During the 2021-2022 RSV Season. https://www.aap.org/en/pages/2019-novel-coronavirus-covid-19-infections/clinical-guidance/interim-guidance-for-use-of-palivizumab-prophylaxis-to-prevent-hospitalization/. Retrieved 7 March 2022.

144.　Wu H, Pfarr DS, Tang Y, An L-L, Patel NK, Watkins JD, Huse WD, Kiener PA, Young JF. 2005. Ultra-potent antibodies against respiratory syncytial virus: effects of binding kinetics and binding valence on viral neutralization. J Mol Biol 350:126–144.

145.　Wu H, Pfarr DS, Johnson S, Brewah YA, Woods RM, Patel NK, White WI, Young JF, Kiener PA. 2007. Development of Motavizumab, an Ultra-potent Antibody for the Prevention of Respiratory Syncytial Virus Infection in the Upper and Lower Respiratory Tract. J Mol Biol 368:652–665.

146.　McLellan JS, Yang Y, Graham BS, Kwong PD. 2011. Structure of Respiratory Syncytial Virus Fusion Glycoprotein in the Postfusion Conformation Reveals Preservation of Neutralizing Epitopes. J Virol 85:7788–7796.

147.　Gilman MSA, Moin SM, Mas V, Chen M, Patel NK, Kramer K, Zhu Q, Kabeche SC, Kumar A, Palomo C, Beaumont T, Baxa U, Ulbrandt ND, Melero JA, Graham BS, McLellan JS. 2015. Characterization of a Prefusion-Specific Antibody That Recognizes a Quaternary, Cleavage-Dependent Epitope on the RSV Fusion Glycoprotein. PLoS Pathog 11:e1005035.

148.　McLellan JS, Chen M, Joyce MG, Sastry M, Stewart-Jones GBE, Yang Y, Zhang B, Chen L, Srivatsan S, Zheng A, Zhou T, Graepel KW, Kumar A, Moin S, Boyington JC, Chuang G-Y, Soto C, Baxa U, Bakker AQ, Spits H, Beaumont T, Zheng Z, Xia N, Ko S-Y, Todd J-P, Rao S, Graham BS, Kwong PD. 2013. Structure-Based Design of a Fusion Glycoprotein Vaccine for Respiratory Syncytial Virus. Science 342:592–598.

149.　Carbonell-Estrany X, Simões EAF, Dagan R, Hall CB, Harris B, Hultquist M, Connor EM, Losonsky GA. 2010. Motavizumab for Prophylaxis of Respiratory Syncytial Virus in High-Risk Children: A Noninferiority Trial. Pediatrics 125:e35–e51.

150.　Feltes TF, Sondheimer HM, Tulloh RMR, Harris BS, Jensen KM, Losonsky GA, Griffin MP. 2011. A Randomized Controlled Trial of Motavizumab Versus Palivizumab for the Prophylaxis of Serious Respiratory Syncytial Virus Disease in Children With Hemodynamically Significant Congenital Heart Disease. 2. Pediatr Res 70:186–191.

151.　Planas D, Veyer D, Baidaliuk A, Staropoli I, Guivel-Benhassine F, Rajah MM, Planchais C, Porrot F, Robillard N, Puech J, Prot M, Gallais F, Gantner P, Velay A, Le Guen J, Kassis-Chikhani N, Edriss D, Belec L, Seve A, Courtellemont L, Péré H, Hocqueloux L, Fafi-Kremer S, Prazuck T, Mouquet H, Bruel T, Simon-Lorière E, Rey FA, Schwartz O. 2021. Reduced sensitivity of SARS-CoV-2 variant Delta to antibody neutralization. 7871. Nature 596:276–280.

152. VanBlargan LA, Errico JM, Halfmann PJ, Zost SJ, Crowe JE, Purcell LA, Kawaoka Y, Corti D, Fremont DH, Diamond MS. 2022. An infectious SARS-CoV-2 B.1.1.529 Omicron virus escapes neutralization by therapeutic monoclonal antibodies. Nat Med 490–495.

153. Peck KM, Lauring AS. Complexities of Viral Mutation Rates. J Virol 92:e01031-17.

154. Gorbalenya AE, Enjuanes L, Ziebuhr J, Snijder EJ. 2006. Nidovirales: Evolving the largest RNA virus genome. Virus Res 117:17–37.

155. Smith DJ, Lapedes AS, de Jong JC, Bestebroer TM, Rimmelzwaan GF, Osterhaus ADME, Fouchier RAM. 2004. Mapping the antigenic and genetic evolution of influenza virus. Science 305:371–376.

156. Kajihara M, Nakayama E, Marzi A, Igarashi M, Feldmann H, Takada A 2013. Novel mutations in Marburg virus glycoprotein associated with viral evasion from antibody mediated immune pressure. J Gen Virol 94:876–883.

157. Geiß Y, Dietrich U. 2015. Catch Me If You Can--The Race Between HIV and Neutralizing Antibodies. AIDS Rev 17:107–113.

158. Schrag SJ, Rota PA, Bellini WJ. 1999. Spontaneous Mutation Rate of Measles Virus: Direct Estimation Based on Mutations Conferring Monoclonal Antibody Resistance. J Virol 73:51–54.

159. López JA, Bustos R, Örvell C, Berois M, Arbiza J, García-Barreno B, Melero JA. 1998. Antigenic Structure of Human Respiratory Syncytial Virus Fusion Glycoprotein. J Virol 72:6922–6928.

160. Crowe JE, Firestone C-Y, Crim R, Beeler JA, Coelingh KL, Barbas CF, Burton DR, Chanock RM, Murphy BR. 1998. Monoclonal Antibody-Resistant Mutants Selected with a Respiratory Syncytial Virus-Neutralizing Human Antibody Fab Fragment (Fab 19) Define a Unique Epitope on the Fusion (F) Glycoprotein. Virology 252:373–375.

161. Zhao X, Chen F-P, Sullender WM. 2004. Respiratory syncytial virus escape mutant derived in vitro resists palivizumab prophylaxis in cotton rats. Virology 318:608–612.

162. Zhao X, Liu E, Chen F-P, Sullender WM. 2006. In Vitro and In Vivo Fitness of Respiratory Syncytial Virus Monoclonal Antibody Escape Mutants. J Virol 80:11651–11657.

163. Zhao X, Chen F-P, Megaw AG, Sullender WM. 2004. Variable resistance to palivizumab in cotton rats by respiratory syncytial virus mutants. J Infect Dis 190:1941–1946.

164. Adams O, Bonzel L, Kovacevic A, Mayatepek E, Hoehn T, Vogel M. 2010. Palivizumab-Resistant Human Respiratory Syncytial Virus Infection in Infancy. Clin Infect Dis 51:185–188.

165. Zhu Q, McAuliffe JM, Patel NK, Palmer-Hill FJ, Yang C, Liang B, Su L, Zhu W, Wachter L, Wilson S, MacGill RS, Krishnan S, McCarthy MP, Losonsky GA, Suzich JA. 2011. Analysis of Respiratory Syncytial Virus Preclinical and Clinical Variants Resistant to Neutralization by Monoclonal Antibodies Palivizumab and/or Motavizumab. J Infect Dis 203:674–682.

166. Zhu Q, Patel NK, McAuliffe JM, Zhu W, Wachter L, McCarthy MP, Suzich JA. 2012. Natural Polymorphisms and Resistance-Associated Mutations in the Fusion Protein of Respiratory Syncytial Virus (RSV): Effects on RSV Susceptibility to Palivizumab. J Infect Dis 205:635–638.

167. Bates JT, Keefer CJ, Slaughter JC, Kulp DW, Schief WR, Crowe JE. 2014. Escape from neutralization by the respiratory syncytial virus-specific neutralizing monoclonal antibody palivizumab is driven by changes in on-rate of binding to the fusion protein. Virology 454–455:139–144.

168. Hashimoto K, Hosoya M. 2017. Neutralizing epitopes of RSV and palivizumab resistance in Japan. Fukushima J Med Sci 63:127–134.

169. Chen X, Xu B, Guo J, Li C, An S, Zhou Y, Chen A, Deng L, Fu Z, Zhu Y, Liu C, Xu L, Wang W, Shen K, Xie Z. 2018. Genetic variations in the fusion protein of respiratory syncytial virus isolated from children hospitalized with community-acquired pneumonia in China. Sci Rep 8:4491.

170. Zhu Q, Lu B, McTamney P, Palaszynski S, Diallo S, Ren K, Ulbrandt ND, Kallewaard N, Wang W, Fernandes F, Wong S, Svabek C, Moldt B, Esser MT, Jing H, Suzich JA. 2018. Prevalence and Significance of Substitutions in the Fusion Protein of Respiratory Syncytial Virus Resulting in Neutralization Escape From Antibody MEDI8897. J Infect Dis 218:572–580.

171. Berman HM, Westbrook J, Feng Z, Gilliland G, Bhat TN, Weissig H, Shindyalov IN, Bourne PE. 2000. The Protein Data Bank. Nucleic Acids Res 28:235–242.

172. Aminpour M, Montemagno C, Tuszynski JA. 2019. An Overview of Molecular Modeling for Drug Discovery with Specific Illustrative Examples of Applications. Molecules 24:1693.

173. Hall DC, Ji H-F. 2020. A search for medications to treat COVID-19 via in silico molecular docking models of the SARS-CoV-2 spike glycoprotein and 3CL protease. Travel Med Infect Dis 35:101646.

174. Basu A, Sarkar A, Maulik U. 2020. Molecular docking study of potential phytochemicals and their effects on the complex of SARS-CoV2 spike protein and human ACE2. 1. Sci Rep 10:17699.

175. Al-Karmalawy AA, Dahab MA, Metwaly AM, Elhady SS, Elkaeed EB, Eissa IH, Darwish KM. 2021. Molecular Docking and Dynamics Simulation Revealed the

Potential Inhibitory Activity of ACEIs Against SARS-CoV-2 Targeting the hACE2 Receptor. Front Chem 9.

176. McCammon JA, Gelin BR, Karplus M. 1977. Dynamics of folded proteins. Nature 267:585–590.

177. Yoshida R, Igarashi M, Ozaki H, Kishida N, Tomabechi D, Kida H, Ito K, Takada A. 2009. Cross-Protective Potential of a Novel Monoclonal Antibody Directed against Antigenic Site B of the Hemagglutinin of Influenza A Viruses. PLOS Pathog 5:e1000350.

178. Roy U. 2020. Structural and molecular analyses of functional epitopes and escape mutants in Japanese encephalitis virus envelope protein domain III. Immunol Res 68:81–89.

179. Park J-K, Xiao Y, Ramuta MD, Rosas LA, Fong S, Matthews AM, Freeman AD, Gouzoulis MA, Batchenkova NA, Yang X, Scherler K, Qi L, Reed S, Athota R, Czajkowski L, Han A, Morens DM, Walters K-A, Memoli MJ, Kash JC, Taubenberger JK. 2020. Pre-existing immunity to influenza virus hemagglutinin stalk might drive selection for antibody-escape mutant viruses in a human challenge model. 8. Nat Med 26:1240–1246.

180. Lusvarghi S, Wang W, Herrup R, Neerukonda SN, Vassell R, Bentley L, Eakin AE, Erlandson KJ, Weiss CD. Key Substitutions in the Spike Protein of SARS-CoV-2 Variants Can Predict Resistance to Monoclonal Antibodies, but Other Substitutions Can Modify the Effects. J Virol 96:e01110-21.

181. Triveri A, Serapian SA, Marchetti F, Doria F, Pavoni S, Cinquini F, Moroni E, Rasola A, Frigerio F, Colombo G. 2021. SARS-CoV-2 Spike Protein Mutations and Escape from Antibodies: A Computational Model of Epitope Loss in Variants of Concern. J Chem Inf Model 61:4687–4700.

182. Hendy M, Kaufman S, Ponga M. 2021. Molecular strategies for antibody binding and escape of SARS-CoV-2 and its mutations. Sci Rep 11:21735.

183. Miller CR, Johnson EL, Burke AZ, Martin KP, Miura TA, Wichman HA, Brown CJ, Ytreberg FM. 2016. Initiating a watch list for Ebola virus antibody escape mutations. PeerJ 4:e1674.

184. Patel JS, Quates CJ, Johnson EL, Ytreberg FM. 2019. Expanding the watch list for potential Ebola virus antibody escape mutations. PLOS ONE 14:e0211093.

185. Hess B, Kutzner C, van der Spoel D, Lindahl E. 2008. GROMACS 4: Algorithms for Highly Efficient, Load-Balanced, and Scalable Molecular Simulation. J Chem Theory Comput 4:435–447.

186. Schymkowitz J, Borg J, Stricher F, Nys R, Rousseau F, Serrano L. 2005. The FoldX web server: an online force field. Nucleic Acids Res 33:W382–W388.

187. Collins PL, Hill MG, Camargo E, Grosfeld H, Chanock RM, Murphy BR. 1995. Production of infectious human respiratory syncytial virus from cloned cDNA confirms an essential role for the transcription elongation factor from the 5' proximal open reading frame of the M2 mRNA in gene expression and provides a capability for vaccine development. Proc Natl Acad Sci U S A 92:11563–11567.

188. Jin H, Zhou H, Cheng X, Tang R, Munoz M, Nguyen N. 2000. Recombinant respiratory syncytial viruses with deletions in the NS1, NS2, SH, and M2-2 genes are attenuated in vitro and in vivo. Virology 273:210–218.

189. Wyss M, Gradauskaite V, Ebert N, Thiel V, Zurbriggen A, Plattet P. 2022. Efficient recovery of attenuated canine distemper virus from cDNA. Virus Res 316:198796.

190. Keep S, Stevenson-Leggett P, Dowgier G, Everest H, Freimanis G, Oade M, Hammond JA, Armesto M, Vila R, Bru T, Geerligs H, Britton P, Bickerton E. 2022. Identification of Amino Acids within Nonstructural Proteins 10 and 14 of the Avian Coronavirus Infectious Bronchitis Virus That Result in Attenuation In Vivo and In Ovo. J Virol 96:e0205921.

191. Racaniello VR, Baltimore D. 1981. Cloned poliovirus complementary DNA is infectious in mammalian cells. Science 214:916–919.

192. Neumann G, Kawaoka Y. 2004. Reverse Genetics Systems for the Generation of Segmented Negative-Sense RNA Viruses Entirely from Cloned cDNA, p. 43–60. *In* Kawaoka, Y (ed.), Biology of Negative Strand RNA Viruses: The Power of Reverse Genetics. Springer Berlin Heidelberg, Berlin, Heidelberg.

193. Schnell MJ, Mebatsion T, Conzelmann KK. 1994. Infectious rabies viruses from cloned cDNA. EMBO J 13:4195–4203.

194. Garcin D, Pelet T, Calain P, Roux L, Curran J, Kolakofsky D. 1995. A highly recombinogenic system for the recovery of infectious Sendai paramyxovirus from cDNA: generation of a novel copy-back nondefective interfering virus. EMBO J 14:6087–6094.

195. Lawson ND, Stillman EA, Whitt MA, Rose JK. 1995. Recombinant vesicular stomatitis viruses from DNA. Proc Natl Acad Sci U S A 92:4477–4481.

196. Radecke F, Spielhofer P, Schneider H, Kaelin K, Huber M, Dötsch C, Christiansen G, Billeter MA. 1995. Rescue of measles viruses from cloned DNA. EMBO J 14:5773–5784.

197. Durbin AP, Hall SL, Siew JW, Whitehead SS, Collins PL, Murphy BR. 1997. Recovery of Infectious Human Parainfluenza Virus Type 3 from cDNA. Virology 235:323–332.

198. Buchholz UJ, Finke S, Conzelmann K-K. 1999. Generation of Bovine Respiratory Syncytial Virus (BRSV) from cDNA: BRSV NS2 Is Not Essential for Virus

Replication in Tissue Culture, and the Human RSV Leader Region Acts as a Functional BRSV Genome Promoter. J Virol 73:251-259.

199. Peeters BPH, de Leeuw OS, Koch G, Gielkens ALJ. 1999. Rescue of Newcastle Disease Virus from Cloned cDNA: Evidence that Cleavability of the Fusion Protein Is a Major Determinant for Virulence. J Virol 73:5001–5009.

200. Gassen U, Collins FM, Duprex WP, Rima BK. 2000. Establishment of a Rescue System for Canine Distemper Virus. J Virol 74:10737–10744.

201. Volchkov VE, Volchkova VA, Mühlberger E, Kolesnikova LV, Weik M, Dolnik O, Klenk H-D. 2001. Recovery of Infectious Ebola Virus from Complementary DNA: RNA Editing of the GP Gene and Viral Cytotoxicity. Science 291:1965–1969.

202. Grosfeld H, Hill MG, Collins PL. 1995. RNA replication by respiratory syncytial virus (RSV) is directed by the N, P, and L proteins; transcription also occurs under these conditions but requires RSV superinfection for efficient synthesis of full-length mRNA. J Virol 69:5677–5686.

203. Hotard AL, Shaikh FY, Lee S, Yan D, Teng MN, Plemper RK, Crowe JE, Moore ML. 2012. A Stabilized Respiratory Syncytial Virus Reverse Genetics System Amenable to Recombination Mediated Mutagenesis. Virology 434:129–136.

204. Shcherbo D, Murphy CS, Ermakova GV, Solovieva EA, Chepurnykh TV, Shcheglov AS, Verkhusha VV, Pletnev VZ, Hazelwood KL, Roche PM, Lukyanov S, Zaraisky AG, Davidson MW, Chudakov DM. 2009. Far-red fluorescent tags for protein imaging in living tissues. Biochem J 418:567–574.

205. Meng J, Lee S, Hotard AL, Moore ML. 2014. Refining the Balance of Attenuation and Immunogenicity of Respiratory Syncytial Virus by Targeted Codon Deoptimization of Virulence Genes. mBio 5.

206. Moore ML, Chi MH, Luongo C, Lukacs NW, Polosukhin VV, Huckabee MM, Newcomb DC, Buchholz UJ, Crowe JE, Goleniewska K, Williams JV, Collins PL, Peebles RS. 2009. A Chimeric A2 Strain of Respiratory Syncytial Virus (RSV) with the Fusion Protein of RSV Strain Line 19 Exhibits Enhanced Viral Load, Mucus, and Airway Dysfunction. J Virol 83:4185–4194.

207. Lemon K, Nguyen DT, Ludlow M, Rennick LJ, Yüksel S, van Amerongen G, McQuaid S, Rima BK, de Swart RL, Duprex WP. 2015. Recombinant subgroup B human respiratory syncytial virus expressing enhanced green fluorescent protein efficiently replicates in primary human cells and is virulent in cotton rats. J Virol 89:2849–2856.

208. Hu B, Jiang J, Zhan J, Li G, Jiang Y, Guan X, Chen Y, Fang Z. 2014. Development of a reverse genetics system for respiratory syncytial virus long strain and an immunogenicity study of the recombinant virus. Virol J 11:142.

209. Jo WK, Schadenhofer A, Habierski A, Kaiser FK, Saletti G, Ganzenmueller T, Hage E, Haid S, Pietschmann T, Hansen G, Schulz TF, Rimmelzwaan GF, Osterhaus ADME, Ludlow M. 2021. Reverse genetics systems for contemporary isolates of respiratory syncytial virus enable rapid evaluation of antibody escape mutants. Proc Natl Acad Sci 118.

210. Domingo E, Holland JJ. 1997. RNA VIRUS MUTATIONS AND FITNESS FOR SURVIVAL. Annu Rev Microbiol 51:151–178.

211. Burrell CJ, Howard CR, Murphy FA. 2017. Virus Replication. Fenner Whites Med Virol 39–55.

212. Drake JW, Holland JJ. 1999. Mutation rates among RNA viruses. Proc Natl Acad Sci USA 96:13910–13913.

213. Drake JW. 1993. Rates of spontaneous mutation among RNA viruses. Proc Natl Acad Sci 90:4171–4175.

214. Malpica JM, Fraile A, Moreno I, Obies CI, Drake JW, García-Arenal F. 2002. The rate and character of spontaneous mutation in an RNA virus. Genetics 162:1505–1511.

215. Moya A, Holmes EC, González-Candelas F. 2004. The population genetics and evolutionary epidemiology of RNA viruses. Nat Rev Microbiol 2:279–288.

216. Eigen M, Schuster P. 1979. The Hypercycle: A Principle of Natural Self-Organization. Springer Berlin Heidelberg.

217. Domingo E, Sheldon J, Perales C. 2012. Viral Quasispecies Evolution. Microbiol Mol Biol Rev MMBR 76:159–216.

218. Domingo E, Escarmís C, Sevilla N, Moya A, Elena SF, Quer J, Novella IS, Holland JJ. 1996. Basic concepts in RNA virus evolution. FASEB J Off Publ Fed Am Soc Exp Biol 10:859–864.

219. Eigen M. 1993. Viral quasispecies. Sci Am 269:42–49.

220. Coffin JM. 1995. HIV population dynamics in vivo: implications for genetic variation, pathogenesis, and therapy. Science 267:483–489.

221. Kimura M. 1968. Evolutionary Rate at the Molecular Level. Nature 217:624–626.

222. Wylie CS, Shakhnovich EI. 2011. A biophysical protein folding model accounts for most mutational fitness effects in viruses. Proc Natl Acad Sci 108:9916–9921.

223. Serohijos AWR, Lee SYR, Shakhnovich EI. 2013. Highly Abundant Proteins Favor More Stable 3D Structures in Yeast. Biophys J 104:L1–L3.

224. Rotem A, Serohijos AWR, Chang CB, Wolfe JT, Fischer AE, Mehoke TS, Zhang H, Tao Y, Lloyd Ung W, Choi J-M, Rodrigues JV, Kolawole AO, Koehler SA, Wu S, Thielen PM, Cui N, Demirev PA, Giacobbi NS, Julian TR, Schwab K, Lin JS, Smith TJ, Pipas JM, Wobus CE, Feldman AB, Weitz DA, Shakhnovich EI. 2018. Evolution on the Biophysical Fitness Landscape of an RNA Virus. Mol Biol Evol 35:2390–2400.

225. Elena SF, González-Candelas F, Novella IS, Duarte EA, Clarke DK, Domingo E, Holland JJ, Moya A. 1996. Evolution of fitness in experimental populations of vesicular stomatitis virus. Genetics 142:673–679.

226. Novella IS, Elena SF, Moya A, Domingo E, Holland JJ. 1995. Size of genetic bottlenecks leading to virus fitness loss is determined by mean initial population fitness. J Virol 69:2869–2872.

227. Rouzine IM, Rodrigo A, Coffin JM. 2001. Transition between Stochastic Evolution and Deterministic Evolution in the Presence of Selection: General Theory and Application to Virology. Microbiol Mol Biol Rev 65:151–185.

228. Gerrish PJ, Lenski RE. 1998. The fate of competing beneficial mutations in an asexual population. Genetica 102–103:127–144.

229. Miralles R, Gerrish PJ, Moya A, Elena SF. 1999. Clonal Interference and the Evolution of RNA Viruses. Science 285:1745–1747.

230. de la Torre JC, Holland JJ. 1990. RNA virus quasispecies populations can suppress vastly superior mutant progeny. J Virol 64:6278–6281.

231. Webb B, Sali A. 2016. Comparative Protein Structure Modeling Using MODELLER. Curr Protoc Bioinforma 54:5.6.1-5.6.37.

232. Aliev AE, Kulke M, Khaneja HS, Chudasama V, Sheppard TD, Lanigan RM. 2014. Motional timescale predictions by molecular dynamics simulations: Case study using proline and hydroxyproline sidechain dynamics. Proteins Struct Funct Bioinforma 82:195–215.

233. Van Der Spoel D, Lindahl E, Hess B, Groenhof G, Mark AE, Berendsen HJC. 2005. GROMACS: Fast, flexible, and free. J Comput Chem 26:1701–1718.

234. Meng J, Hotard AL, Currier MG, Lee S, Stobart CC, Moore ML. 2015. Respiratory Syncytial Virus Attachment Glycoprotein Contribution to Infection Depends on the Specific Fusion Protein. J Virol 90:245–253.

235. McKimm-Breschkin JL. 2004. A simplified plaque assay for respiratory syncytial virus—direct visualization of plaques without immunostaining. J Virol Methods 120:113–117.

236. Reed LJ, Muench H. 1938. A Simple Method of Estimating Fifty Per Cent Endpoints. Am J Epidemiol 27:493–497.

237. McLellan JS, Chen M, Chang J-S, Yang Y, Kim A, Graham BS, Kwong PD. 2010. Structure of a Major Antigenic Site on the Respiratory Syncytial Virus Fusion Glycoprotein in Complex with Neutralizing Antibody 101F. J Virol 84:12236-12244.

238. Chen M, Chang JS, Nason M, Rangel D, Gall JG, Graham BS, Ledgerwood JE. 2010. A flow cytometry-based assay to assess RSV-specific neutralizing antibody is reproducible, efficient and accurate. J Immunol Methods 362:180–184.

239. Morton CJ, Cameron R, Lawrence LJ, Lin B, Lowe M, Luttick A, Mason A, McKimm-Breschkin J, Parker MW, Ryan J, Smout M, Sullivan J, Tucker SP, Young PR. 2003. Structural characterization of respiratory syncytial virus fusion inhibitor escape mutants: homology model of the F protein and a syncytium formation assay. Virology 311:275–288.

240. Katzen F. 2007. Gateway(®) recombinational cloning: a biological operating system. Expert Opin Drug Discov 2:571–589.

241. Langmead B, Salzberg SL. 2012. Fast gapped-read alignment with Bowtie 2. 4. Nat Methods 9:357–359.

242. Li H, Handsaker B, Wysoker A, Fennell T, Ruan J, Homer N, Marth G, Abecasis G, Durbin R, 1000 Genome Project Data Processing Subgroup. 2009. The Sequence Alignment/Map format and SAMtools. Bioinformatics 25:2078–2079.

243. Danecek P, Bonfield JK, Liddle J, Marshall J, Ohan V, Pollard MO, Whitwham A, Keane T, McCarthy SA, Davies RM, Li H. 2021. Twelve years of SAMtools and BCFtools. GigaScience 10:giab008.

244. Rubin AF, Gelman H, Lucas N, Bajjalieh SM, Papenfuss AT, Speed TP, Fowler DM. 2017. A statistical framework for analyzing deep mutational scanning data. Genome Biol 18:150.

245. Leroy EM, Rouquet P, Formenty P, Souquière S, Kilbourne A, Froment J-M, Bermejo M, Smit S, Karesh W, Swanepoel R, Zaki SR, Rollin PE. 2004. Multiple Ebola Virus Transmission Events and Rapid Decline of Central African Wildlife. Science 303:387–390.

246. Kugelman JR, Kugelman-Tonos J, Ladner JT, Pettit J, Keeton CM, Nagle ER, Garcia KY, Froude JW, Kuehne AI, Kuhn JH, Bavari S, Zeitlin L, Dye JM, Olinger GG, Sanchez-Lockhart M, Palacios GF. 2015. Emergence of Ebola Virus Escape Variants in Infected Nonhuman Primates Treated with the MB-003 Antibody Cocktail. Cell Rep 12:2111–2120.

247. Zhao X, Sullender WM. 2005. In Vivo Selection of Respiratory Syncytial Viruses Resistant to Palivizumab. J Virol 79:3962–3968.

248. Papenburg J, Carbonneau J, Hamelin M-È, Isabel S, Bouhy X, Ohoumanne N, Déry P, Paes BA, Corbeil J, Bergeron MG, De Serres G, Boivin G. 2012. Molecular Evolution

of Respiratory Syncytial Virus Fusion Gene, Canada, 2006–2010. Emerg Infect Dis 18:120–124.

249. Boivin G, Caouette G, Frenette L, Carbonneau J, Ouakki M, De Serres G. 2008. Human respiratory syncytial virus and other viral infections in infants receiving palivizumab. J Clin Virol 42:52–57.

250. Copin R, Baum A, Wloga E, Pascal KE, Giordano S, Fulton BO, Zhou A, Negron N, Lanza K, Chan N, Coppola A, Chiu J, Ni M, Wei Y, Atwal GS, Hernandez AR, Saotome K, Zhou Y, Franklin MC, Hooper AT, McCarthy S, Hamon S, Hamilton JD, Staples HM, Alfson K, Carrion R, Ali S, Norton T, Somersan-Karakaya S, Sivapalasingam S, Herman GA, Weinreich DM, Lipsich L, Stahl N, Murphy AJ, Yancopoulos GD, Kyratsous CA. 2021. The monoclonal antibody combination REGEN-COV protects against SARS-CoV-2 mutational escape in preclinical and human studies. Cell 184:3949-3961.e11.

251. Dougan M, Azizad M, Mocherla B, Gottlieb RL, Chen P, Hebert C, Perry R, Boscia J, Heller B, Morris J, Crystal C, Igbinadolor A, Huhn G, Cardona J, Shawa I, Kumar P, Blomkalns A, Adams AC, Van Naarden J, Custer KL, Knorr J, Oakley G, Schade AE, Holzer TR, Ebert PJ, Higgs RE, Sabo J, Patel DR, Dabora MC, Williams M, Klekotka P, Shen L, Skovronsky DM, Nirula A, BLAZE-1 investigators. 2021. A randomized, placebo-controlled clinical trial of bamlanivimab and etesevimab together in high-risk ambulatory patients with COVID-19 and validation of the prognostic value of persistently high viral load. Clin Infect Dis Off Publ Infect Dis Soc Am ciab912.

252. Weinreich DM, Sivapalasingam S, Norton T, Ali S, Gao H, Bhore R, Xiao J, Hooper AT, Hamilton JD, Musser BJ, Rofail D, Hussein M, Im J, Atmodjo DY, Perry C, Pan C, Mahmood A, Hosain R, Davis JD, Turner KC, Baum A, Kyratsous CA, Kim Y, Cook A, Kampman W, Roque-Guerrero L, Acloque G, Aazami H, Cannon K, Simón-Campos JA, Bocchini JA, Kowal B, DiCioccio AT, Soo Y, Geba GP, Stahl N, Lipsich L, Braunstein N, Herman G, Yancopoulos GD, Trial Investigators. 2021. REGEN-COV Antibody Combination and Outcomes in Outpatients with Covid-19. N Engl J Med 385:e81.

253. ANRS, Emerging Infectious Diseases. 2021. Phase IIa Pilot Study Evaluating the Efficacy of a Monoclonal Antibody and Vaccine-based Post-exposure Prophylaxis Strategy in High-risk Contact Cases of Ebola Virus Disease Infection. NCT04822376. Clinical trial registration. clinicaltrials.gov.

254. International AIDS Vaccine Initiative. 2021. A Phase 1/2a Open Label Study of the Safety, Tolerability, Pharmacokinetics and Antiviral Activity of PGT121, VRC07-523LS and PGDM1400 Monoclonal Antibodies in HIV-uninfected and HIV-infected Adults. NCT03721510. Clinical trial registration. clinicaltrials.gov.

255. National Institute of Allergy and Infectious Diseases (NIAID). 2022. VRC 611: A Phase 1 Safety and Pharmacokinetic Study to Evaluate a Human Monoclonal Antibody (mAb) VRC-HIVMAB0102-00-AB (CAP256V2LS) Administered Via

Subcutaneous and Intravenous Injection in Healthy Adults. NCT04408963. Clinical trial registration. clinicaltrials.gov.

256. ViiV Healthcare. 2022. A Phase 2a Multicentre, Randomized, Open-Label, Two-Part Adaptive Design Study to Evaluate the Antiviral Effect, Safety and Tolerability of GSK3810109A, an HIV-1 Specific Broadly Neutralizing Human Monoclonal Antibody in Antiretroviral-naïve HIV-1-Infected Adults. NCT04871113. Clinical trial registration. clinicaltrials.gov.

257. UBP Greater China (Shanghai) Co., Ltd. 2021. A Randomized, Single-blind, Dose-selected Phase II Trial to Evaluate the Safety and Efficacy of UB-621 in Adults With Recurrent Genital HSV-2 Infection. NCT04714060. Clinical trial registration. clinicaltrials.gov.

258. Chao T-Y, Ren S, Shen E, Moore S, Zhang S, Chen L, Rupprecht CE, Tsao E. 2017. SYN023, a novel humanized monoclonal antibody cocktail, for post-exposure prophylaxis of rabies. PLoS Negl Trop Dis 11:e0006133.

259. Synermore Biologics Co., Ltd. 2021. A Phase 2b Randomized Blinded Study to Evaluate SYN023 Compared to Human Rabies Immune Globulin in Post Exposure Prophylaxis of Rabies in Adults With Different Rabies Exposure Risks. NCT03961555. Clinical trial registration. clinicaltrials.gov.

260. 1998. Palivizumab, a humanized respiratory syncytial virus monoclonal antibody, reduces hospitalization from respiratory syncytial virus infection in high-risk infants. The IMpact-RSV Study Group. Pediatrics 102:531–537.

261. Abou-El-Hassan H, Massaad E, Soudani N, Assaf-Casals A, Shaker R, Khoury ML, Ghanem S, Karam M, Andary R, Saito R, Dbaibo G, Zaraket H. 2019. Detection of ON1 and novel genotypes of human respiratory syncytial virus and emergence of palivizumab resistance in Lebanon. PLoS ONE 14:e0212687.

262. Al Aboud D, Al Aboud NM, Al-Malky MIR, Abdel-Moneim AS. 2019. Genotyping of Type A Human Respiratory Syncytial Virus Based on Direct F Gene Sequencing. Medicina (Mex) 55:169.

263. Drake JW, Charlesworth B, Charlesworth D, Crow JF. 1998. Rates of spontaneous mutation. Genetics 148:1667–1686.

264. Bedford T, Riley S, Barr IG, Broor S, Chadha M, Cox NJ, Daniels RS, Gunasekaran CP, Hurt AC, Kelso A, Klimov A, Lewis NS, Li X, McCauley JW, Odagiri T, Potdar V, Rambaut A, Shu Y, Skepner E, Smith DJ, Suchard MA, Tashiro M, Wang D, Xu X, Lemey P, Russell CA. 2015. Global circulation patterns of seasonal influenza viruses vary with antigenic drift. Nature 523:217–220.

265. Novella IS, Ball LA, Wertz GW. 2004. Fitness Analyses of Vesicular Stomatitis Strains with Rearranged Genomes Reveal Replicative Disadvantages. J Virol 78:9837–9841.

266. Holland JJ, de la Torre JC, Clarke DK, Duarte E. 1991. Quantitation of relative fitness and great adaptability of clonal populations of RNA viruses. J Virol 65:2960–2967.

267. Vignuzzi M, Stone JK, Arnold JJ, Cameron CE, Andino R. 2006. Quasispecies diversity determines pathogenesis through cooperative interactions within a viral population. Nature 439:344–348.

268. Sanjuán R, Moya A, Elena SF. 2004. The contribution of epistasis to the architecture of fitness in an RNA virus. Proc Natl Acad Sci 101:15376–15379.

269. Hinkley T, Martins J, Chappey C, Haddad M, Stawiski E, Whitcomb JM, Petropoulos CJ, Bonhoeffer S. 2011. A systems analysis of mutational effects in HIV-1 protease and reverse transcriptase. Nat Genet 43:487–489.

270. Kryazhimskiy S, Dushoff J, Bazykin GA, Plotkin JB. 2011. Prevalence of epistasis in the evolution of influenza A surface proteins. PLoS Genet 7:e1001301.

271. Lara J, Khudyakov Y. 2012. Epistatic connectivity among hepatitis C virus genomic sites as genetic marker of interferon resistance. Antivir Ther 17:1471–1475.

272. Gong LI, Suchard MA, Bloom JD. 2013. Stability-mediated epistasis constrains the evolution of an influenza protein. eLife 2:e00631.

273. Harms MJ, Thornton JW. 2014. Historical contingency and its biophysical basis in glucocorticoid receptor evolution. 7513. Nature 512:203–207.

274. Maynard Smith J. 1970. Natural Selection and the Concept of a Protein Space. 5232. Nature 225:563–564.

275. Malekshahi SS, Razaghipour S, Samieipoor Y, Hashemi FB, Manesh AAR, Izadi A, Faghihloo E, Ghavami N, Mokhtari-Azad T, Salimi V. 2019. Molecular characterization of the glycoprotein and fusion protein in human respiratory syncytial virus subgroup A: Emergence of ON-1 genotype in Iran. Infect Genet Evol J Mol Epidemiol Evol Genet Infect Dis 71:166–178.

276. Otieno JR, Kamau EM, Oketch JW, Ngoi JM, Gichuki AM, Binter Š, Otieno GP, Ngama M, Agoti CN, Cane PA, Kellam P, Cotten M, Lemey P, Nokes DJ. 2018. Whole genome analysis of local Kenyan and global sequences unravels the epidemiological and molecular evolutionary dynamics of RSV genotype ON1 strains. Virus Evol 4:vey027.

277. Trovão NS, Khuri-Bulos N, Tan Y, Puri V, Shilts MH, Halpin RA, Fedorova NB, Nelson MI, Halasa N, Das SRY 2021. Molecular characterization of respiratory syncytial viruses circulating in a paediatric cohort in Amman, Jordan. Microb Genomics 7:000292.

278. Okamoto M, Dapat CP, Sandagon AMD, Batangan-Nacion LP, Lirio IC, Tamaki R, Saito M, Saito-Obata M, Lupisan SP, Oshitani H. 2018. Molecular Characterization of

Respiratory Syncytial Virus in Children With Repeated Infections With Subgroup B in the Philippines. J Infect Dis 218:1045–1053.

279. Malasao R, Furuse Y, Okamoto M, Dapat C, Saito M, Saito-Obata M, Tamaki R, Segubre-Mercado E, Lupisan S, Oshitani H. 2018. Complete Genome Sequences of 13 Human Respiratory Syncytial Virus Subgroup A Strains of Genotypes NA1 and ON1 Isolated in the Philippines. Genome Announc 6:e00151-18.

280. Agoti CN, Otieno JR, Munywoki PK, Mwihuri AG, Cane PA, Nokes DJ, Kellam P, Cotten M. 2015. Local evolutionary patterns of human respiratory syncytial virus derived from whole-genome sequencing. J Virol 89:3444–3454.

281. Agoti CN, Otieno JR, Ngama M, Mwihuri AG, Medley GF, Cane PA, Nokes DJ. 2015. Successive Respiratory Syncytial Virus Epidemics in Local Populations Arise from Multiple Variant Introductions, Providing Insights into Virus Persistence. J Virol 89:11630–11642.

282. Bin Lu, Liu H, Tabor DE, Tovchigrechko A, Qi Y, Ruzin A, Esser MT, Jin H. 2019. Emergence of new antigenic epitopes in the glycoproteins of human respiratory syncytial virus collected from a US surveillance study, 2015–17. 1. Sci Rep 9:3898.

283. Aljabr W, Armstrong S, Rickett NY, Pollakis G, Touzelet O, Cloutman-Green E, Matthews DA, Hiscox JA. 2019. High Resolution Analysis of Respiratory Syncytial Virus Infection In Vivo. Viruses 11:926.